

https://dspace.org/

Thermally and optically stimulated luminescence in synthetic diamond

Araikum, Shawn

2016
http://hdl.handle.net/10539/21357

Downloaded from a DSpace repository. https://dspace.org/

Thermally and Optically Stimulated Luminescence in Synthetic Diamond

Degree awarded with distinction on 8 Dec 1993.

Shawn Araikum

Submitted for the degree of Master of Science

University of the Witwatersrand, Johannesburg, July 1993

Abstract

This study investigated the photo-excitation and thermoluminescence properties of diamonds which were synthesised primarily for thermoluminescence dosimetry.

For investigations of thermally stimulated processes occurring in these crystals an analysis of the thermoluminescence glow spectra and the temperature dependent isothermal decay spectra was undertaken. Optical activation energies were derived by assessing the efficiency with which thermoluminescence charge trapping states were depopulated as a function of excitation wavelength. These activation energies, thermal and optical, were then compared to provide an interpretation of the mechanism of optical excitations. In addition the properties of deep, thermally inaccessible charge trapping states were investigated by a phototransference *cum* thermoluminescence technique.

The established favourable characteristics of the aforementioned charge trapping states motivated an evaluation of a dosimetry system based on the radiophotoluminescence properties of these diamond. Results of post-irradiation phosphorescence decay suggested a further method whereby synthetic diamond could be used for radiation dosimetry.

I declare that this dissertation is my own, unaided work. It is being submitted for the degree of Master of Science in the University of the Witwatersrand, Johannesburg. It has not been submitted before for any degree or examination in any other university.

16th day of July, 1993

To my family, immediate and extended.

CONTENTS

Chapter 1: Introduction

1.1 Historical Background and Motivation for Study 1

Chapter 2: Instrumentation

2.1 Thermoluminescence Measurements 4

2.2 Optical Absorption Measurements 4

2.3 Isothermal Decay Spectra Measurements 5

2.4 Emission Spectra Measurements 10

2.5 Photoluminescence Measurements 16

Chapter 3: Analysis of Results

3.1 Methods of Analysis 25

3.2 Analysis of the Glow Curve Spectra 26

3.3 Analysis of the Isothermal Decay Spectra 28

Chapter 4: Theoretical Background

4.1 Band Structure 31

4.2 The Luminescence Efficiency 33

Chapter 5: Thermoluminescence Analysis of Discrete Trapping States in the Forbidden Gap of Synthetic Diamond

5.1 Glow Curve Spectroscopy 35

5.2 Results and Discussions 39

5.3 Conclusions 47

Chapter 6: Energy Levels in the Forbidden Gap of Synthetic TLD Diamond

6.1 Introduction 49

6.2 Results and Discussions 50

6.3 Conclusions 64

Chapter 7: Phosphorescence Properties of Synthetic TLD Diamond

7.1 Introduction 65

7.2 Exponential Isothermal Decay Spectra 67

7.3 Inverse-time dependent Isothermal Decay Spectra 75

7.4 Conclusions 79

Chapter 8: Radiophotoluminescence Properties of Synthetic TLD Diamond

8.1 Introduction 80

8.2 Preliminary Measurements and Discussions 80

8.3 Results and Discussions 95

8.4 Conclusions 106

Chapter 9: Conclusions

8.1 Summary of Conclusions 107

Appendix I

Non-linear Equations used in Curve Fitting Procedures 111

Appendix II

Optical Absorbance Spectrum of the TLD Diamond 112

Appendix III

The Co-60 Calibration data 113

Appendix IV

Papers, Patents and Conferences 114

References 116

Preface

I would like to take this opportunity to thank all the people who played an instrumental role in making this project a fascinating experience and for making accessible to me the benefit of their expertise and experience.

First and foremost, I would like to thank my supervisor, Dr T. L. Nam, for providing me with the opportunity to work as a researcher in a field which is rightly an extension of the work initiated for the fulfilment of his Ph.D thesis. In particular, thanks are due for the time provided for frequent discussions relating to the direction of this project. The invaluable assistance provided by him in the elements of mechanical design and presentation, which formed an integral component of this educational experience, is also recorded with gratitude. Many thanks are also due to Professor R. J. Keddy, my co-supervisor, who introduced me to the fascinating subject of solid state dosimetry. His constant support and interest in the development of this project have been a source of encouragement throughout. His critical appraisal of the final draft of this dissertation is also acknowledged with appreciation.

The cooperation received from members of De Beers Diamond Research Laboratory (DRL) in providing excellent advice and technical support required for the fulfilment of this project is also mentioned. In particular, appreciation is expressed to Dr R. J. Caveney, Dr R. C. Burns, Dr G. J. Davies and Mrs V. Cvetkovic for the supply and synthesis of the diamonds used in this study. Thanks are also due to Dr C. Levitt for the loan of optical components required for part of this project, and to Mr J. H. Grobbelaar for the help received with the maintenance of the multi-channel analyser used for the thermoluminescence measurements. The invaluable assistance received from Dr C. Wellbourne in obtaining optical absorption spectra of the diamond TLDs used in this study is also recorded with appreciation.

In the course of the experimental part of this project much help was received from the workshop at Schonland Research Centre in the fabrication of the experimental apparatus. For the role played by Mr I. McQueen in supervising the construction of the

final apparatus and for providing many helpful suggestions in the fulfilment thereof many thanks are due. Also to be thanked for the fabrication of the ceramic portion of the high temperature probe and for excellent technical advice is Mr M. Rebak of Schonland Centre. The construction of the apparatus required for the radiophotoluminescence emission spectra determinations is due to the help received from Mr A. Lombard of the Medical Physics Workshop, Hillbrow Hospital. The courtesy accorded by him is greatly appreciated. Thanks are also extended to Professor J. D. Esser of the Department of Nuclear Medicine for the loan of the TLD reader with which ancillary thermoluminescence measurements were effected. For the assistance and advice given in the choice of a paint coating for the interior conical chamber surface, I would like to gratefully acknowledge the role played by Mr C. Masson of AECI (Ltd) in making his facilities available to me and for providing the reflectance spectrum of the paint.

Although the responsibility for any errors in this text are mine, I would like to express sincere thanks to my father, Mr J. E. Arsikum, for painstakingly checking the grammar and spelling of this manuscript. For the readiness in providing his time and for his companionship in the course of the day to day work I would like to make special mention of Mr J. Ramahlo. To all my other friends at the Schonland Centre, I would also like to express my appreciation for making this experience a memorable one.

Finally, thanks are expressed to Mr L. J-M Bancilhon, the Computer Centre Librarian, for the advice given in the finer points of the Document Composition Facility with which this dissertation was compiled.

CHAPTER 1

Introduction

1.1 Historical Background and Motivation for Study

The first scientifically recorded observation of thermoluminescence (TL) was made by Robert Boyle in a report to the Royal Society in 1663. This had reference to the luminescence observed, in the dark, from a natural diamond to which an external source of heat was applied. Early observations of thermoluminescence recorded 'natural' thermoluminescence, i.e. thermoluminescence caused by natural, background radiation. While these studies had shown that heat stimulated the emission of light, and was not its principal cause, it is generally agreed that real progress in the understanding of the thermoluminescence process began in the late nineteenth century with the reports by Wiedemann and Schmidt (1895) and later Curie (1905). These contributions examined the induced thermoluminescent properties of certain materials after an applied exposure to ionising radiation sources.

Rapid development followed with the theoretical formulation of the thermoluminescence process by Randall and Wilkins (1945a) in which the form of the thermoluminescence glow curve was considered when the thermoluminescent sample was heated at a uniform rate. Given the success of this work in detailing the thermoluminescence phenomenon, the use of this technique in radiation dosimetry followed swiftly; motivated by the research of Daniels *et al.* during the 1950s. The principle behind the use of thermoluminescence phenomenon in radiation dosimetry is based on the fact that a number of materials display thermoluminescence glow intensities that are proportional to the radiation dose absorbed by the material. Daniels *et al.* (1953) found LiF to be a particularly good material to use in radiation dosimetry because of its high sensitivity to ionising radiations. This pioneering work precipitated intense research into the develop-

ment of thermoluminescent detectors. The ensuing work embraced technical innovation as well as new physical insights into the process.

Despite the fact that thermoluminescence was first recorded in diamond, it has not been until very recently that the use of synthetic diamond has been seriously considered as a practical, viable sensor for radiation dosimetry. Radiation detectors, of which diamond form the main sensing element, have been shown to exhibit many attractive features (Keddy *et al.*, 1987). They have the added advantage of showing a response to x and γ rays much like that of biological soft tissue ($Z_{eff} = 7.4$) because diamond is carbon ($Z = 6$). Natural diamonds are disadvantaged in particular by their relatively low sensitivities to ionising radiations and the fact that no two stones can be assumed to be alike. As a result, rigorous testing and selection processes are required to find crystals with suitable, similar characteristics. This makes the general application of natural diamond distinctly unattractive when compared to other commercially available radiation detectors. With the advent of improved synthesis techniques however, synthetic diamonds may be 'tailor made' to contain controlled impurity concentrations. In particular, crystals for thermoluminescence dosimetry (TLD) can be synthesised to exhibit properties which respond linearly over a range of radiation doses seldom matched by other commercial phosphors. Their small physical size (~1mm³) make them ideally suitable for monitoring of radiation fields requiring high spatial resolution, e.g. radiotherapy isodose profile determinations. In contrast to the more frequently used TLD materials, such as lithium fluoride and lithium borate notably, diamond is neither toxic if ingested nor hygroscopic and can thus be used *in vivo* with great confidence.

Despite the significant advantages of using diamond as a thermoluminescent detector a number of problems still persist with the thermoluminescence technique. In particular diamond crystal samples, which have no regular geometry, tend to exhibit a noticeably different glow response depending upon their placement and orientation on the heating element. Of paramount importance to the thermoluminescence technique, are the storage and stability properties of the charge trapping states as well as the ef-

fective dose range over which this technique may be applied. With the low paramagnetic nitrogen concentration synthetic diamond, saturation effects set in at relatively low radiation doses, of the order of 10 Gy. Also of concern is the fact that charge trapping states with trapping depths which are expected to guarantee suitable storage properties, exhibit anomalous loss of thermoluminescence signals. To overcome these problems a possible advancement in radiation dosimetry might be a shift from a thermal to an optical activation of the detector. Parallel to the more practical aspects, optical probing of the sample is advantaged by the ability to probe the deeper, more stable, traps which are inaccessible by the thermoluminescence technique, given the useful temperature range of the thermoluminescence technique. Phototransference of the carriers from the deeper traps to the shallower, thermally more accessible traps is a technique in which both optically and thermally stimulated luminescence may be used to a positive advantage and could shed light on the process(es) which give rise to the less than ideal fading properties of the otherwise useful thermoluminescence peaks of these diamonds. This is the motivation for research into the suitability of the synthetic thermoluminescent dosimetry diamonds made by De Beers Diamond Research Laboratory (DRL) for radioluminescent dosimetry applications.

This dissertation reports on:-

(a) The glow curve and optical excitation spectra analysis of synthetic TLD diamond.

(b) The relationship between thermal and optical activation energies which characterise the defect centres in these diamond.

(c) A comparison of thermoluminescence, phosphorescence and radiophotoluminescence radiation dosimetric properties.

CHAPTER 2

Instrumentation

2.1 Thermoluminescence Measurements

All thermoluminescence measurements were performed on a TOLEDO 654 reader, coupled to a SPECTRUM-88 multichannel analyser. The SPECTRUM-88 analyser is a microprocessor based, stand-alone, analyser with 4096 channel background memory for buffer storage. For data acquisition the SPECTRUM-88 analyser was set to operate in the multi-scaling mode. Using this system the glow curves of the TLD diamonds could be stored on 5¼" floppy disks for later analysis and manipulation.

2 Optical Absorption Measurements

The TLD diamond crystals were all mounted in a darkroom using red photographic safe-lights. The samples were mounted in an indium mask whilst being viewed under a microscope. A red filter was superimposed between the sample and the tungsten lamp microscope illumination which was operated at its lowest setting. All optical absorption spectra were acquired by scanning from the long wavelength to the short wavelength end of the optical absorption spectrum. These measurements were performed at room temperature, in the absorbance mode, at 2 nm resolution, using a Perkin-Elmer Lambda 9 double beam spectrophotometer. A pair of 40 mm focal length condensing lenses were placed in the sample beam of the spectrophotometer. A filter change at 379 nm and a lamp change at 319 nm, which were required, produced discontinuities in the data. These discontinuities were removed using the manufacturers baseline correction software.

2.3 Isothermal Decay Measurements

The system which was used for the isothermal decay measurements is shown in figure 2.1. Depicted is a cross-section of a six-port vacuum chamber in which the specimen was housed. The diamond was housed in a conical chamber (A), which was internally coated with a paint having specific reflective characteristics as follows: Figure 2.2 shows these characteristics of the paint as a function of the wavelength. The paint was also chosen to withstand temperatures in excess of 100 °C. This requirement was considered important for high temperature isothermal decay measurements conducted at temperatures in excess of 200 °C. The light emitted from the diamond was reflected as a parallel beam from a concave mirror (B), to pass through the exit, conical chamber aperture (C), onto the photomultiplier tube (D), which was fixed on a specially constructed flange (E). A Hamamatsu model R928 photomultiplier tube, with a maximum detection efficiency in the 400-500 nm region, coupled to a Thorn EMI photon counting unit was used for signal detection. The counting unit was interfaced to a personal computer via the RS-232-port for automated control and data manipulation. Also depicted in figure 2.3, are the reflective characteristics of the mirror, which were chosen to provide good reflection of the light signal at, and above, wavelengths of 200 nm.

For the measurement of the isothermal decay spectra at elevated temperatures, holder K (figure 2.1) was replaced with a specially constructed sample holder. Depicted in figure 2.4 is a cross-section of the holder showing the holder head (A), with feed-through holes (B) for the leads of the super-band heating element (D) and the thermocouple sensor (I). Both the thermocouple and the heating element were connected to an external analogue temperature controller, which maintained the temperature to better than 1%. As the holder head was fabricated from TUFNOL, which has a maximum temperature tolerance of 130 °C, it was thermally insulated from the brass piece (E), which was machined to fit the heating element, by a cylindrical ceramic portion (F). The inset, "VIEW C", shows the thermocouple sensor (I), attached at (J) to the brass block (K). Also depicted is the sample placement (G) on the copper plate (L).

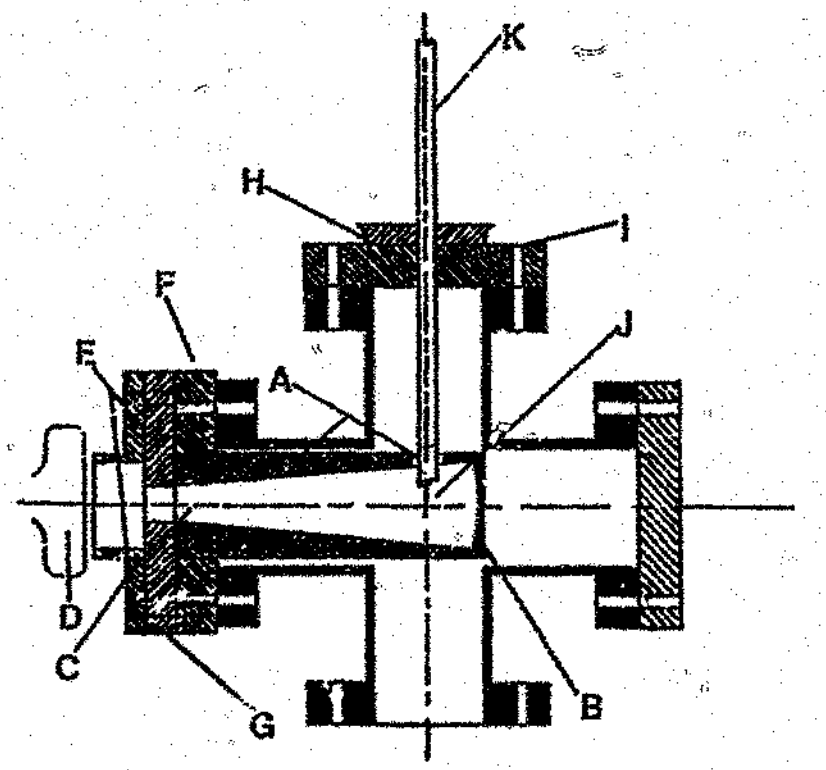

Figure 2.1: A schematic diagram showing the vertical cross-section of the vacuum chamber with the optical cell and sample loader in position.

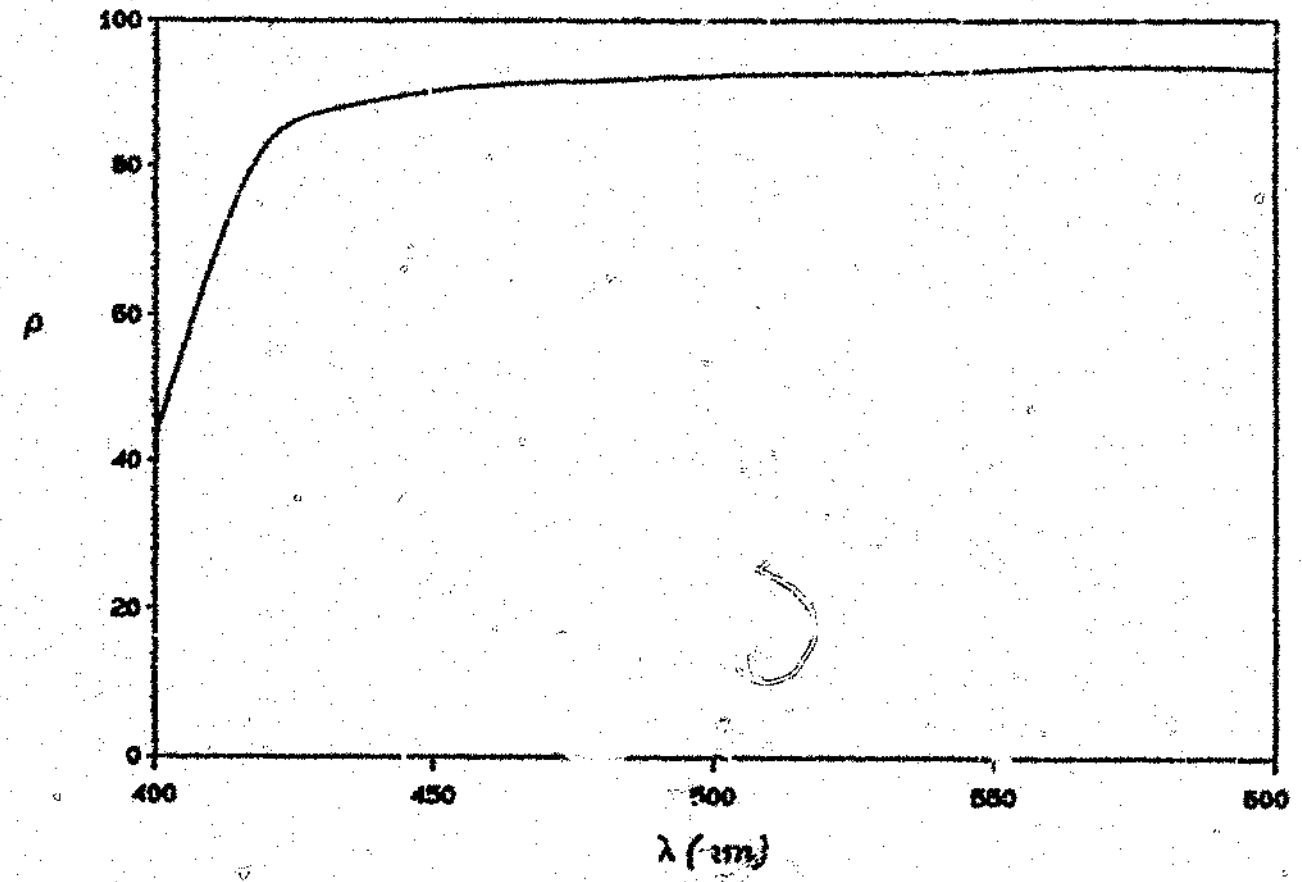

Figure 2.2: The reflective characteristics of the paint used to coat the interior surface of the conical chamber.

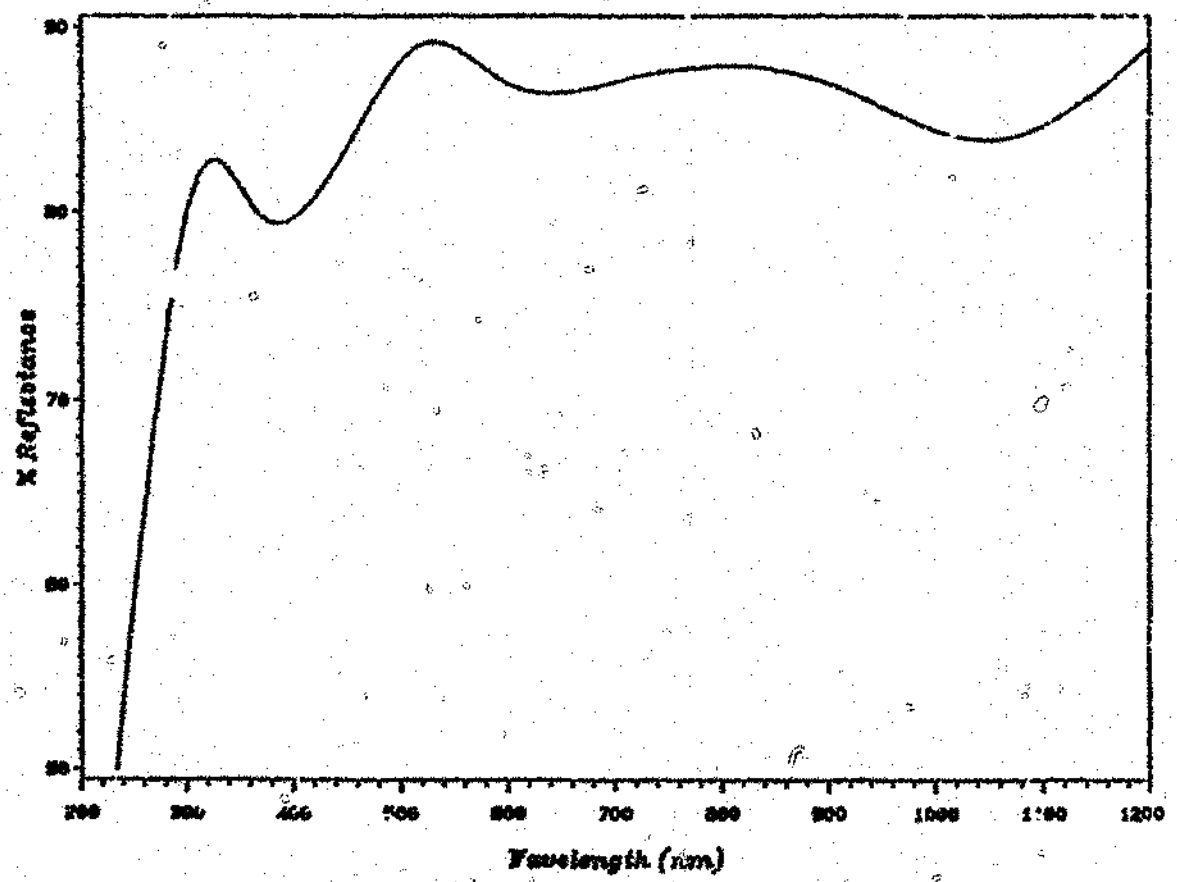

Figure 2.3: The reflective characteristics of the mirror used in the measurement of the radiophotoluminescence and isothermal decay spectra, for the reflection of the light signal from the diamond crystal onto the photomultiplier tube.

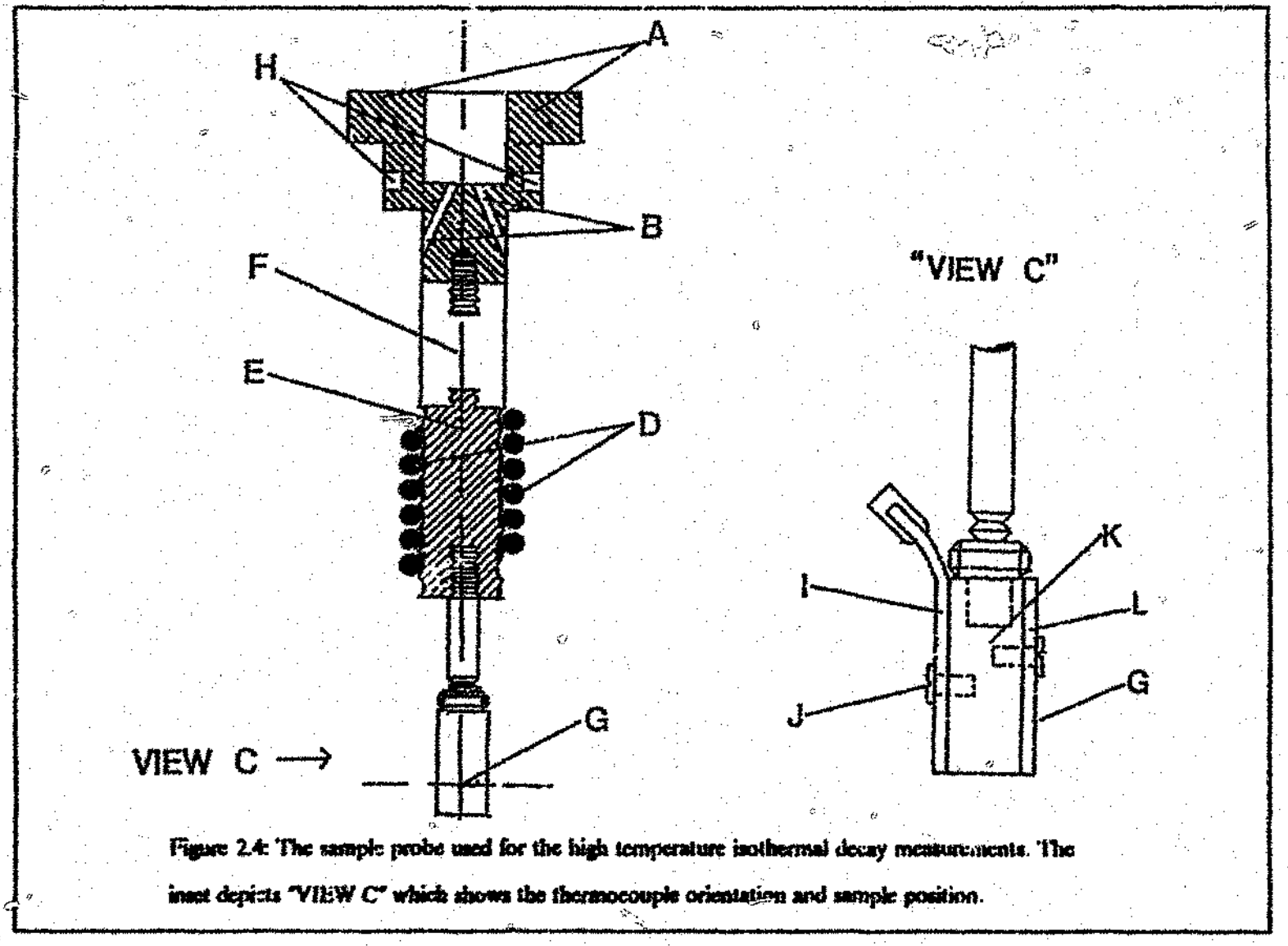

Figure 2.4: The sample probe used for the high temperature isothermal decay measurements. The inset depicts *"VIEW C"* which shows the thermocouple orientation and sample position.

Accurate temperature control at the sample location was achieved by feedback control. The required sample temperature for each isothermal decay experiment was externally set.

2.4 Emission Spectra Measurements

The emission spectra from the diamond crystals of low nitrogen content were measured

- during phosphorescence decay post-excitation with α-particles from an ^{241}Am source and from an ultraviolet light source.
- during excitation with light of the same wavelengths as those used for radiophotoluminescence dosimetry.
- by the cathodoluminescence technique.

(I) The Phosphorescence Emission Spectra

For the measurement of the relaxation spectrum of the diamond crystal during phosphorescence, the vacuum chamber (figure 2.1) was rotated through 90° with respect to its vertical axis, and use was made of the remaining set of ports of a six-port chamber. In this case (cf figure 2.5) a mirror (A) of 50 mm diameter and of 25 mm focal length was housed at one end of one port, and a lens (B) of 250 mm focal length was mounted on a flange which was fixed to the opposite port. The monochromator input (D) was coupled to the exit flange of the vacuum chamber by means of a light-tight arrangement incorporating a set of bellows (C), so that the signal could be detected at the photomultiplier tube (F), which was coupled to the exit of the monochromator slit (E). The concave mirror-lens combination allowed light from the isotropically emitting diamond sample, fixed at the chamber centre to be reflected as a parallel beam toward the focusing lens and onto the monochromator slit 250 mm away, after an initial dosing of

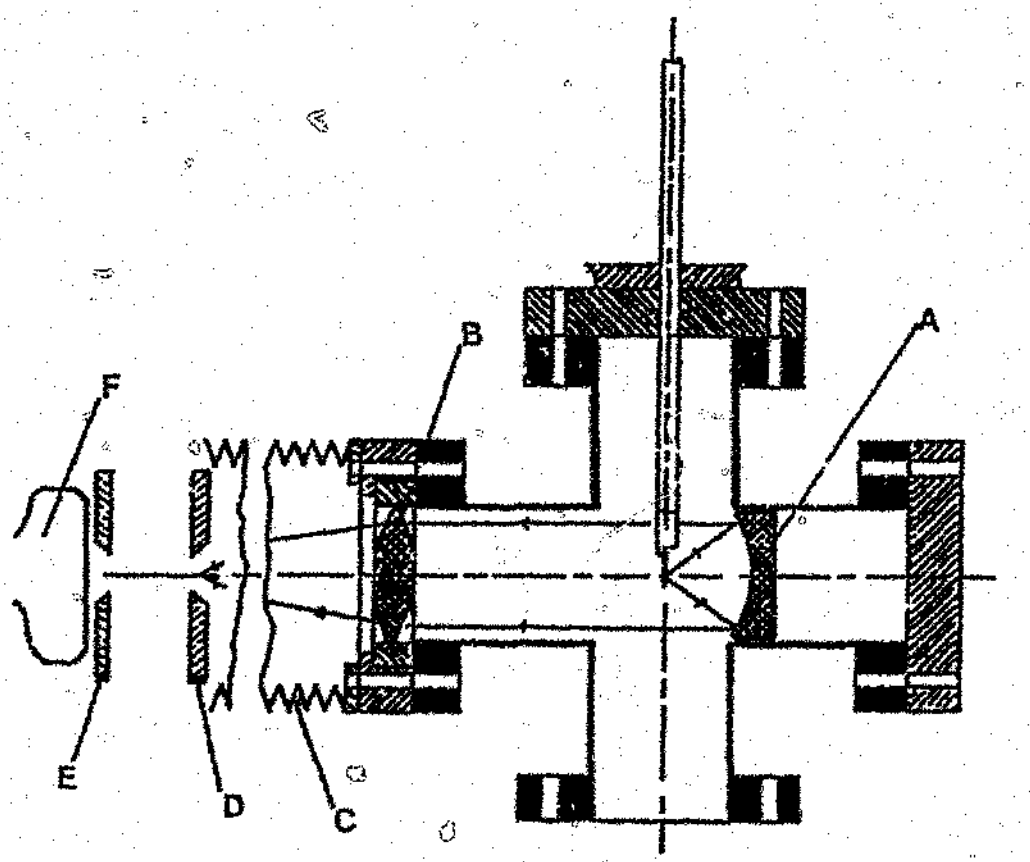

Figure 2.5: The experimental arrangement used in the measurement of the emission spectrum of the synthetic diamond crystals of low nitrogen concentration during phosphorescence.

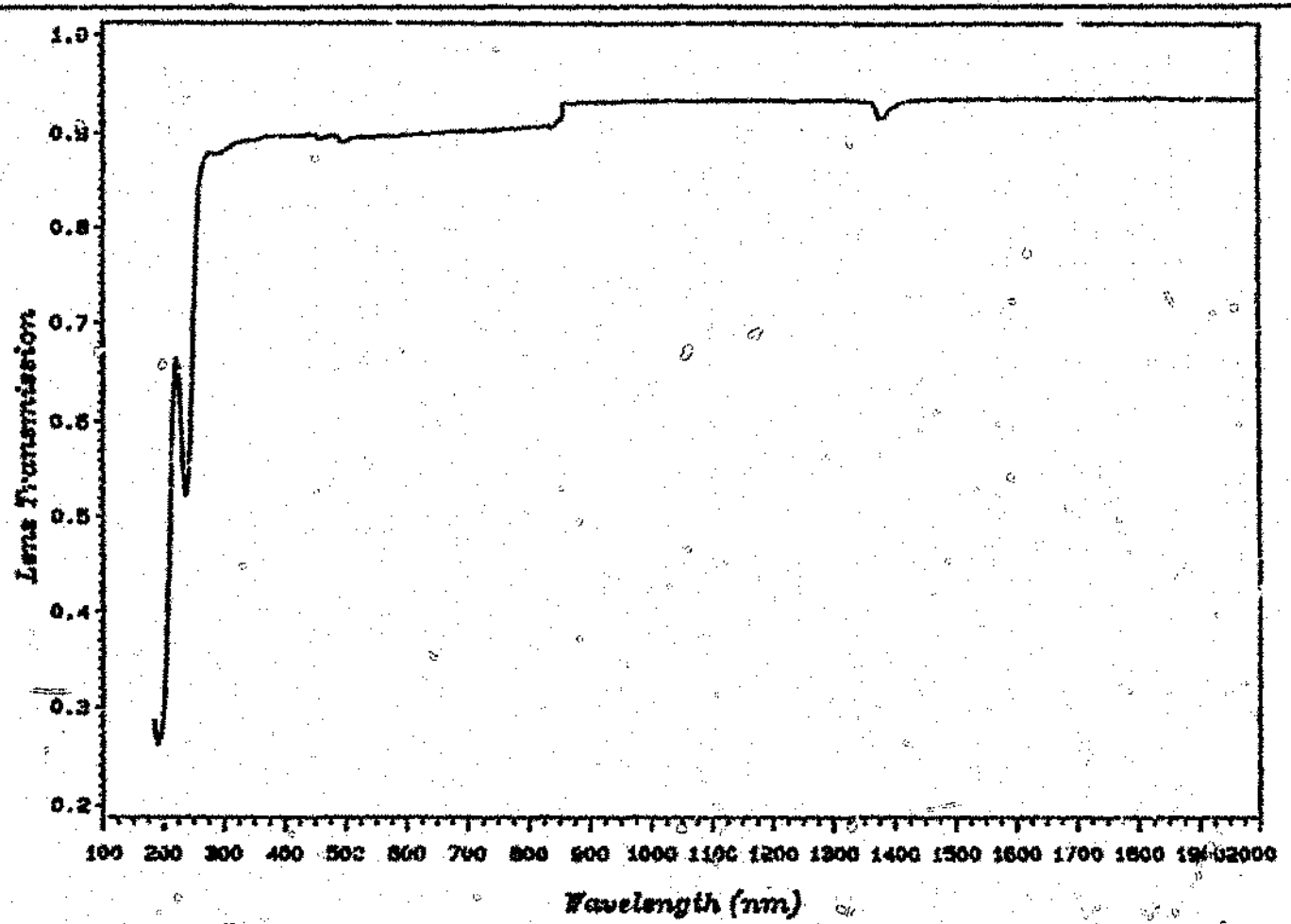

Figure 2.6: The transmission characteristics of the 50 mm diameter lens used for focusing the parallel beam of light from the diamond onto the input slit of the monochromator.

the diamond crystal. The monochromator grating was driven by a stepping motor, controlled by Personal Computer software. Enabling of the required scan, followed the setting of the appropriate scan parameters. The scan speeds could be varied from less than 1 Å s^{-1} to 400 Å s^{-1}. Using this system the relaxation spectra were measured at high monochromator scan speeds.

(ii) The Radiophotoluminescence Spectra

The measurement of the emission spectrum when the diamond crystals were illuminated with excitation light of pre-determined wavelength, was achieved with the experimental instrumentation of figure 2.7. Depicted is a vertical cross-section of an arrangement comprising two filter holders (A & B), a table (C) for sample mounting and optical fibre (D) with "VIEW E" as shown in the inset. The cover-plate could be fixed at the threaded holes labelled H1 and H2 in the inset.

Two light sources were used in the radiophotoluminescence spectra determinations. A 10 W Deuterium light source mounted in the light box and attached at F could be switched on or a 50 W Mercury Pen-Ray lamp could be mounted at location G. Light from either of the sources, pre-selected by the suitable choice of filters, illuminated the diamond crystals on the sample table, enabled the measurement of the emission spectrum from the diamond crystals via the fibre optic to the monochromator input slit, to be made.

(iii) Cathodoluminescence Spectra

The measurement of the cathodoluminescence spectra was effected by means of a custom-built system comprising a Cold Cathode Electron Gun of variable energy settings in the 0-18 keV range, mounted in one of the vacuum chamber ports and a cryostat probe for sample mounting. The electron gun was taken from a model ELM2BX luminoscope and adapted for use with the six-port vacuum chamber system. A cited advantage of using a cold cathode gun over the more conventional heated filament gun, pertains to the positive ions which form part of the cold cathode discharge. These ions

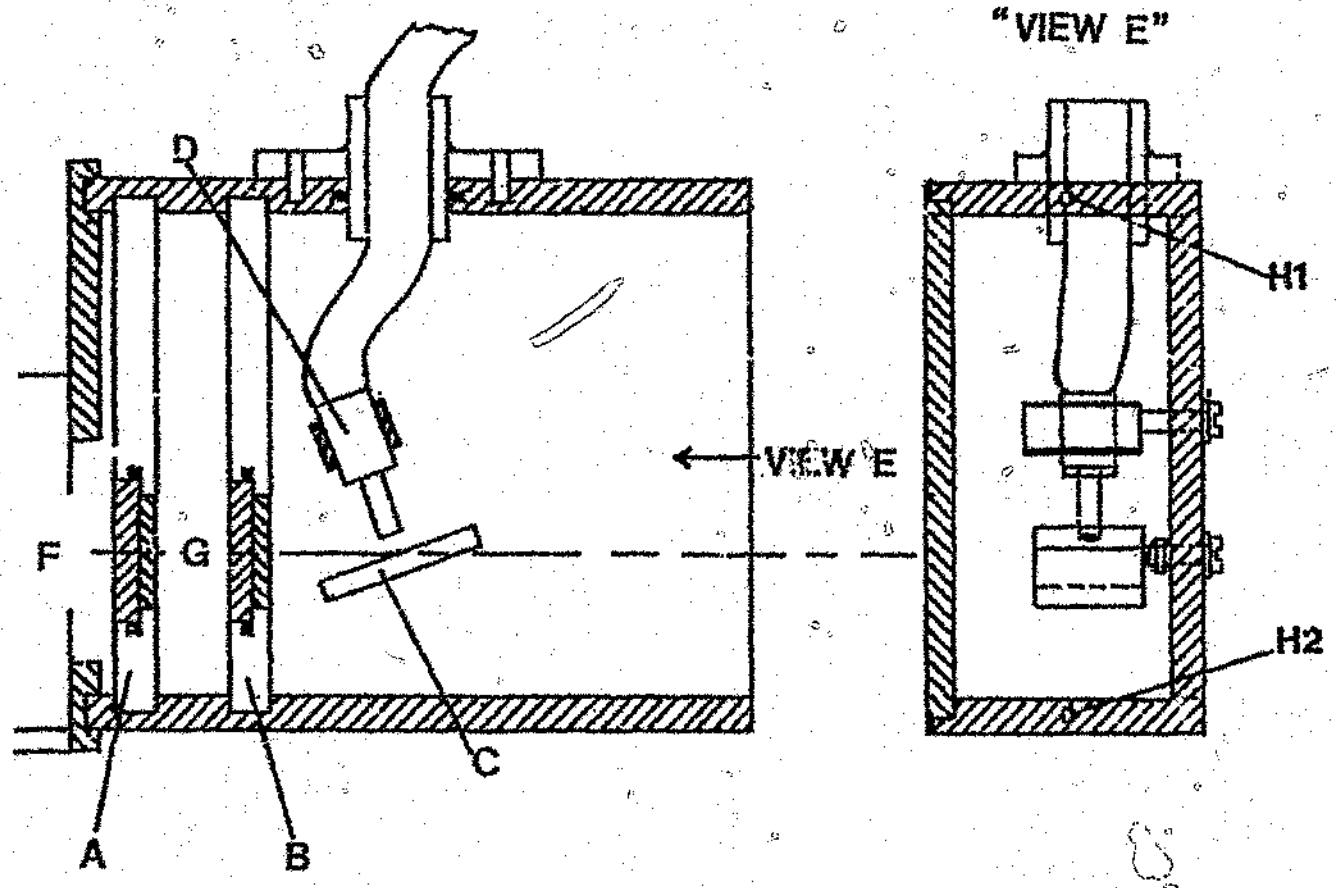

Figure 2.7: The experimental arrangement used for radiophotoluminescence emission spectra determinations.

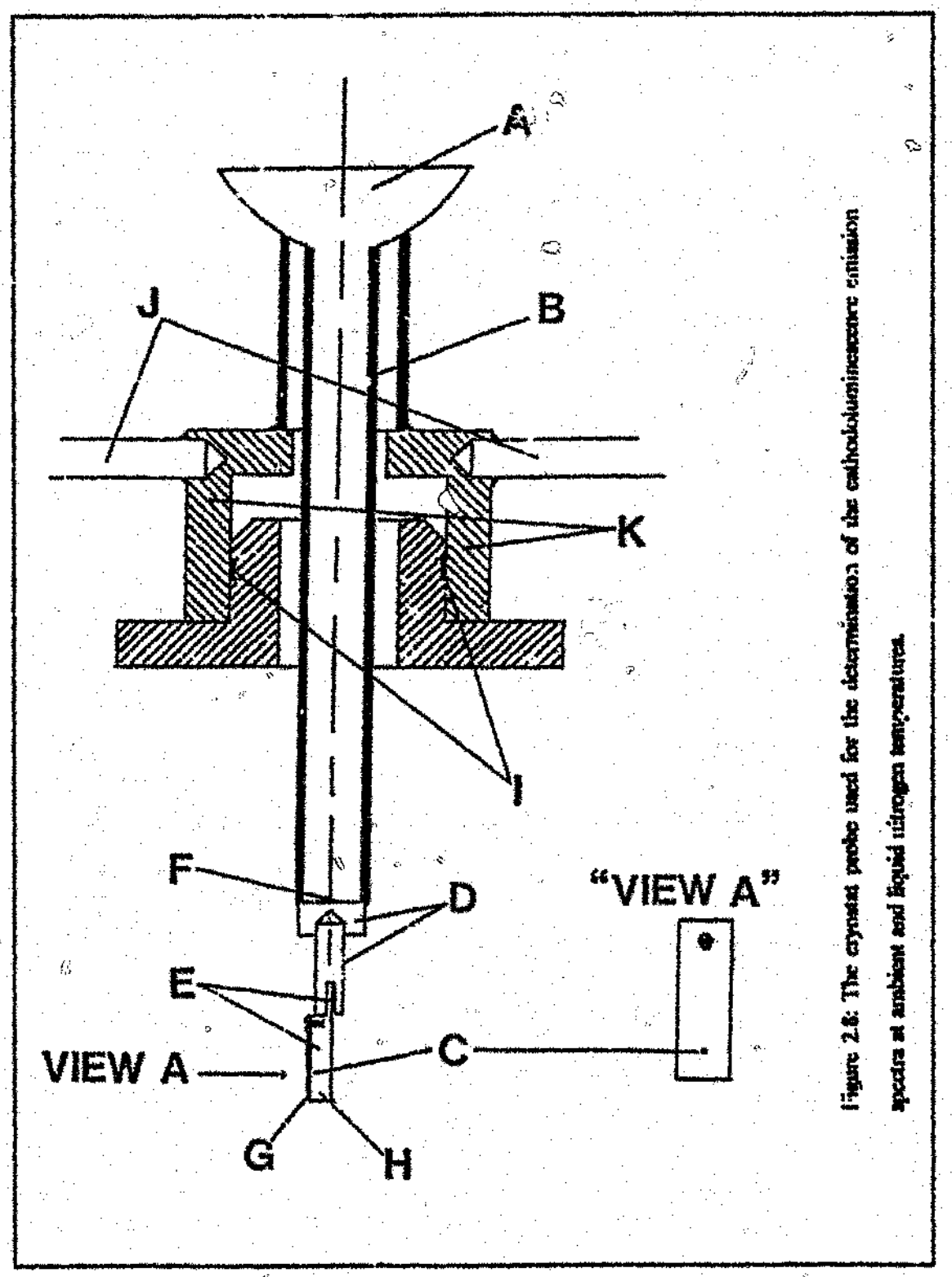

Figure 2.6: The cryostat probe used for the determination of the cathodoluminescence emission spectra at ambient and liquid nitrogen temperatures.

serve to neutralise the build-up of space charge on the sample surface, thereby decreasing the Coulombic repulsion of the incident electron beam from the sample surface.

The lens-mirror arrangement of figure 2.5 was used for the measurement of the cathodoluminescence spectra. For this purpose, the probe depicted in figure 2.8 was mounted to a specially constructed flange to replace the probe shown in figure 2.5. A reservoir (A) consisting of a cylindrical vessel (B) of stainless steel in which the liquid nitrogen could be placed, was used for cooling the sample situated at location C. The copper attachments (D) on which the sample loader (E), also fabricated of copper, could be fitted were soldered to the cylindrical stainless steel vessel (B) with silver solder. The choice of copper and silver, both of which have high thermal conductivities, in the roles described, was made to ensure optimal transfer of heat from the sample to the liquid nitrogen reservoir at the interface labelled F in the diagram. The sample loader consisted of a copper plate (G) attached to a copper block (H) and is shown for clarity as "VIEW A" in the inset of the figure. Both the copper block and the plate on which the sample was mounted were coated with a layer of gold of a few microns thickness to suppress the background signal which would result from the excitation of copper.

For meaningful measurements at liquid nitrogen temperature, the vacuum chamber had to be evacuated to a pressure of 100 millitorr. The O-ring seal which is labelled I in the diagram, was necessary to maintain good vacuum. Also shown are the handles (J) which facilitated the angular orientation of the sample. These handles, which are fixed to the rotatable turret (K) on which the reservoir is soldered, allows reproducible angular settings to be made, enabling reproducible determinations of the cathodoluminescence spectra of the diamond crystals. A thermocouple was incorporated in the construction to measure the equilibrium temperature at the sample position.

2.5 Photoluminescence Measurements

The radiophotoluminescence (RPL) technique involved the initial irradiation of the diamond sensor with γ or β radiation, followed by a subsequent illumination with

excitation light of a specific bandwidth, centred about a given wavelength. The intensity of the emitted light, centred about the principal emission wavelength, was then measured for dose dependence studies using this experimental arrangement. The following measurements were also performed to provide further insight into the physical processes involved:

- the optical bleaching of the thermoluminescence signals as a function of the wavelength of stimulating light.

- the optical bleaching response of the thermoluminescence response as a function of the period of illumination for light of pre-selected wavelength.

- the emission spectra during phosphorescence, cathodoluminescence and during excitation with light of pre-determined wavelength.

Optical bleaching measurements, as well as measurements of the response of the diamond crystals to light in the near ultraviolet (320-400 nm) and actinic (200-320 nm) ranges, were carried out using a Bausch & Loumb high intensity (150 W) Xenon light source, which was attached to a grating-type monochromator unit for operation in the 350-900 nm region. Shorter wavelengths were obtained by exploiting second order diffraction effects in conjunction with the use of suitable bandpass filters. Depicted in figure 2.9 is the spectral emission of the Xenon lamp supplied by the manufacturer (solid line). For the absolute calibration of the radiant power of the Xenon lamp a silicon diode detector, traceable to an absolute radiometer, was used. The monochromator settings were calibrated by adjusting the settings for coincidence with published values for the mercury lines. An uncertainty in the calibration of ±3 nm was attributed to the non-linearity of the monochromator. The radiant power output was measured in the 400-800 nm wavelength region, in steps of 50 nm. Figure 2.10 shows the experimental arrangement used for the measurements. An order-sorting filter (F) was used to eliminate

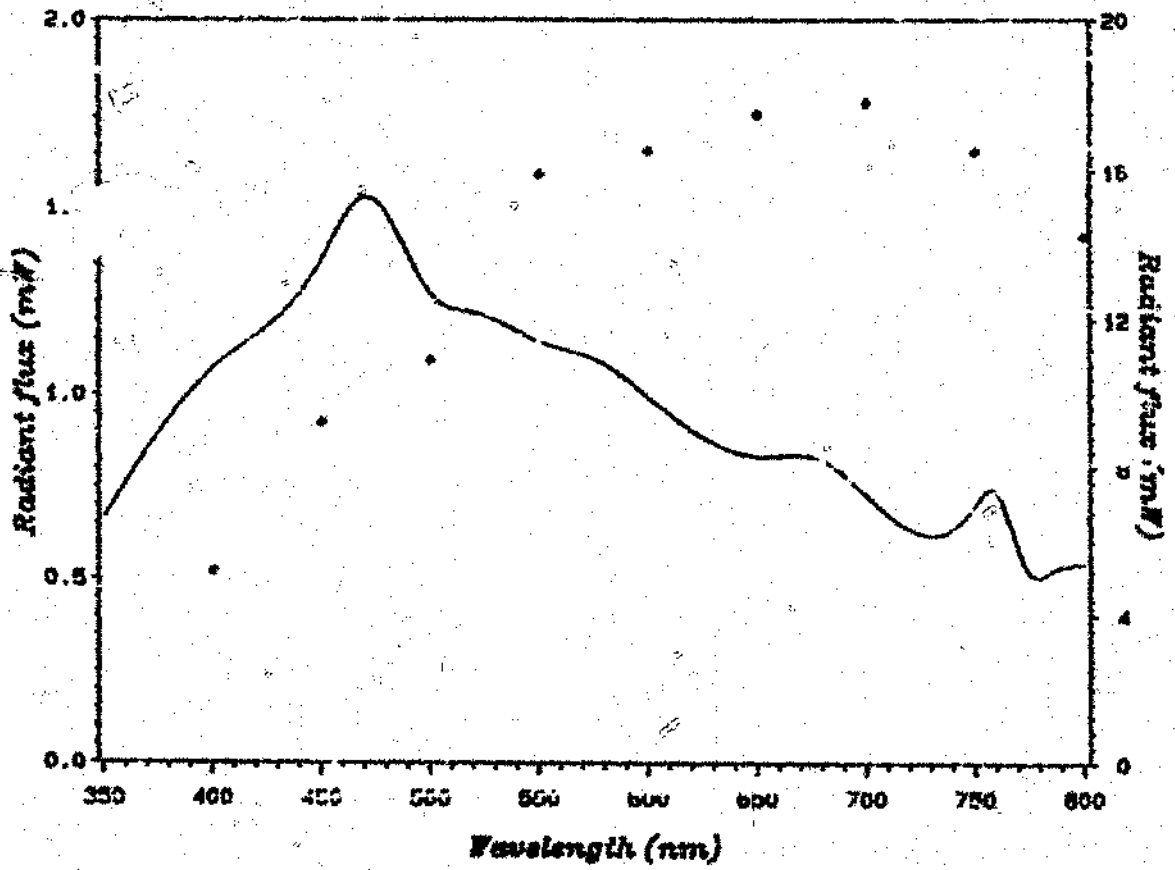

Figure 2.9: The spectral emission of the Xenon lamp. (—), depicts the initial intensity (right vertical axis) and (◇) depicts the intensity at the time of operation (left vertical axis); both represented as a function of the wavelength.

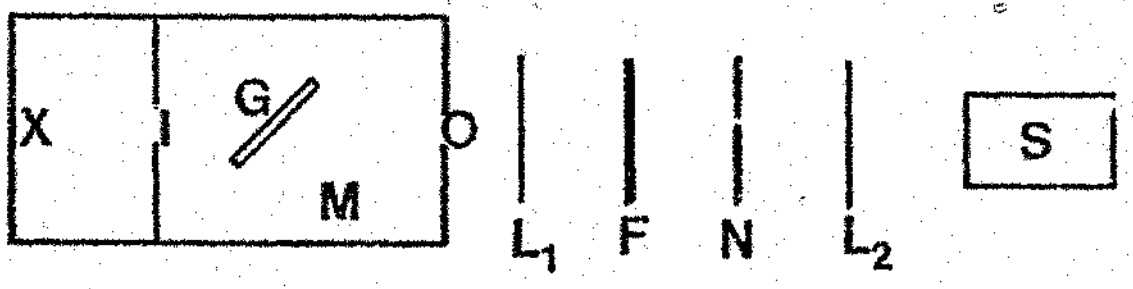

Figure 2.10: The schematic arrangement showing the positions of the monochromator (M), lenses (L_1 and L_2), filters (F,N) and photo-diode (S) used for the calibration of the Xenon lamp.

second order wavelengths at the exit slit of the monochromator. In the 400-650 nm range of wavelengths, the SCHOTT WG345 filter was used, which transmitted 65% of the light of these wavelengths. In the 650-800 nm wavelength region, the SCHOTT OG570 filter was used, which transmitted 91% of the light signal. The neutral density filters (N), were used, in the location shown, to decrease the signal level, thereby inhibiting the overloading of the photo-diode.

All the calibration measurements for the Xenon light source and monochromator assembly system were conducted with an entrance slit width setting of 5.36 mm and an exit slit width setting of 3.00 mm. These were the settings used for the measurement of the optical bleaching spectra. The light emitted from the exit slit of the monochromator was collimated to a parallel beam of 40 mm diameter by the first lens (L_1), which had a focal length of 40 mm. The filtered parallel light from filters F and N (cf figure 2.10) was focused by means of the second lens (L_2) onto the silicon photo-diode (S). The final value for the absolute light intensity was therefore derived from the expression:

$$R_A = \frac{R_D}{T_f \times T_{nd} \times T_l} \tag{2.1}$$

Here R_A is the absolute radiant power, R_D is the radiant power measured at the silicon detector, T_f is the filter transmission factor, T_{nd} is the neutral density filter transmission factor and T_l is the lens transmission factor. Depicted in figure 2.9 is the result of these measurements. What was evident at the outset was the observation that the emission intensity had deteriorated appreciably from the initial intensity. Despite this limitation, the intensity proved adequate for the measurement of the optical bleaching of thermoluminescence signals by the choice of suitable illumination exposures. No attempt was made to calibrate the Xenon lamp in the ultraviolet region absolutely as suitable quartz lenses were unavailable.

The radiophotoluminescence measurements were taken with a specially designed system incorporating the six-port vacuum chamber depicted in figure 2.1. A lens focus-

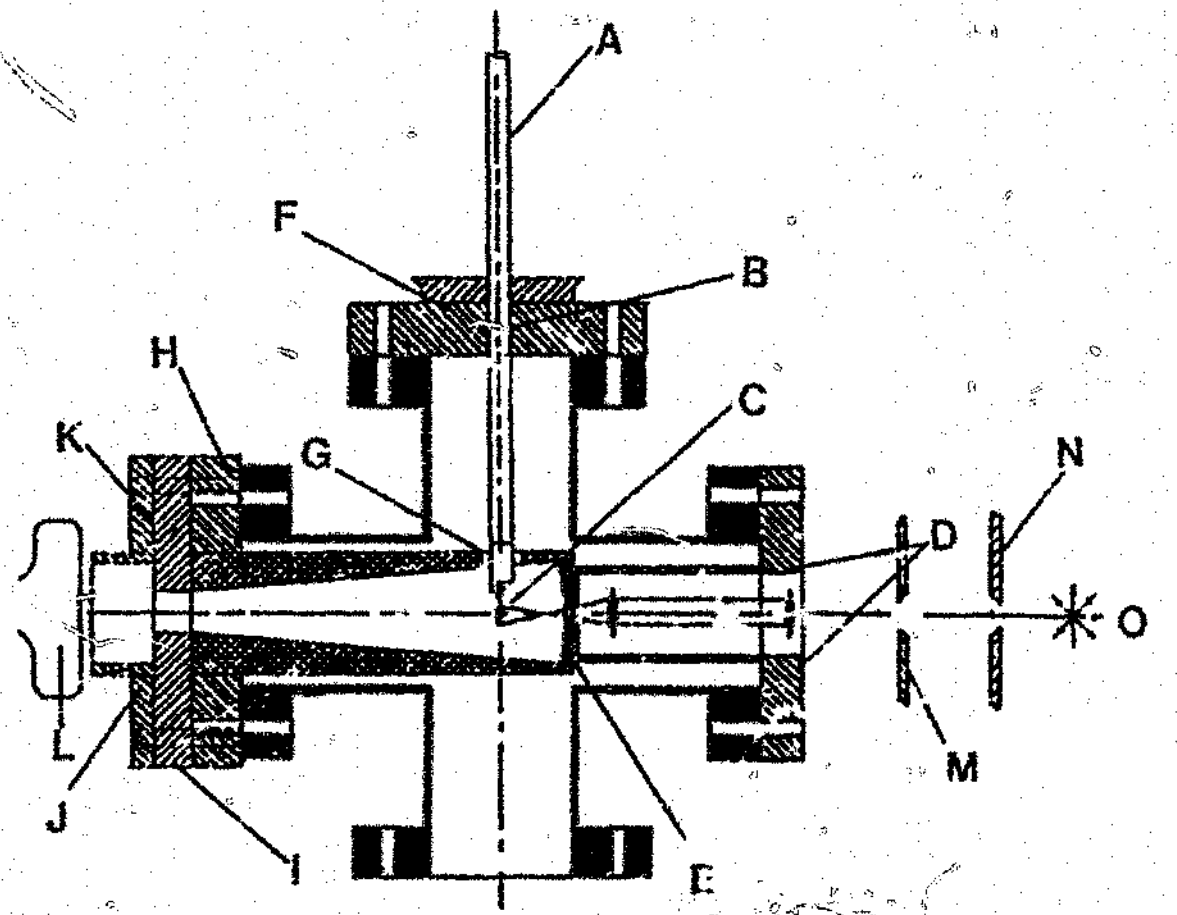

Figure 2.11: Experimental arrangement used for the ... photoluminescence response as a function of the radiation dose imparted to the diamond ...

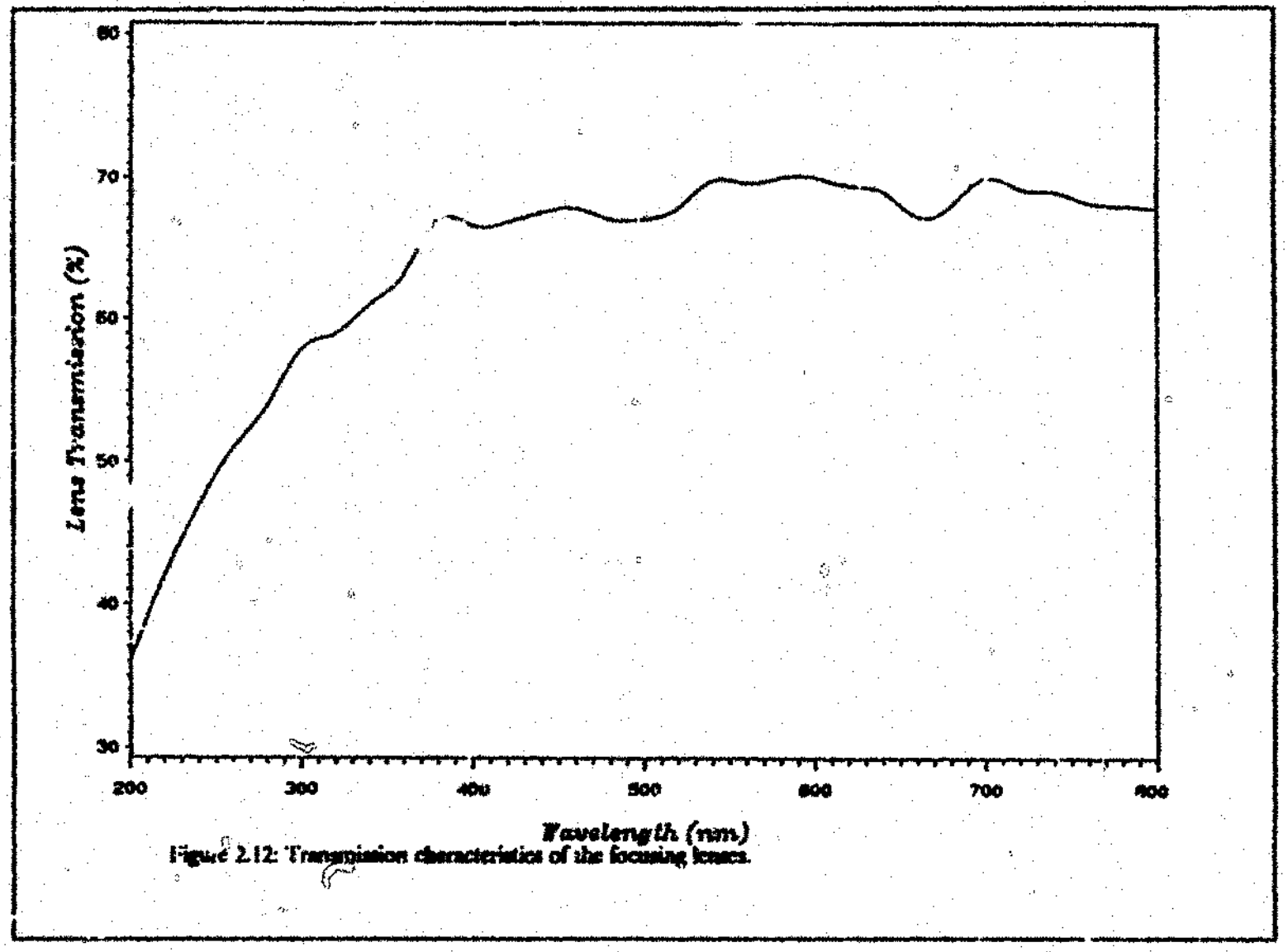

Figure 2.12: Transmission characteristics of the focusing lenses.

ing system, shown in figure 2.11, was accommodated in the port opposite the conical chamber. For the radiophotoluminescence measurements, activating light of fixed wavelength from the exit slit (M_2 of the monochromator was directed onto the diamond sensor which was mounted at the centre of the chamber (C). The diamond crystal was mounted using a top-loading system (A). The light emitted from the diamond was reflected from a specially constructed concave mirror (E) with an axial orifice, and a conical housing chamber (G) internally coated with high reflectivity paint, to pass through a filter (I), mounted on the filter wheel (J), onto a R928 photomultiplier tube (L) which was coupled via the photon counting unit to a Personal Computer. Focusing lenses of quartz were chosen to provide good transmission characteristics (cf figure 2.12) at, and above, 200 nm. The light source used throughout was a 50 W Pen-Ray mercury lamp (O). The photo-excitation wavelength was computer selected on the McPherson model 275 UV-visible scanning monochromator system which was capable of operating in the 185-1000 nm range. The focusing of the incident light onto the sample was based upon the manufacturers specification that the light from the monochromator exit slit is divergent, of 10 mm maximum height and thickness, with a focal distance of approximately 20 mm. This dictated the choice of the focal length of the first lens. The hole size of the mirror was chosen to minimise the solid angle subtended by the focal point of the mirror, where the sample would reside, while allowing the focused beam through. The focal length and the distance of the second lens from the diamond crystal was decided upon using the following expressions for the geometric parameters.

$$f = \frac{x_2 d}{2r_2} \tag{2.2}$$

$$x_2 = \frac{r_c r_2}{r_1 + r_2} \tag{2.3}$$

$$s = f + x_2 \tag{2.4}$$

Here s is the diamond to lens distance, d is the prescribed beam thickness, r_c is the radius of curvature of the mirror, r_1 is the radius of focused beam at the mirror aperture, r_2 is the radius of focused beam at the diamond crystal position, f is the focal length of the second lens and x_2 is the distance from the crystal to the focal point of the second lens. The focal length required was thus calculated. Based on such calculations, a commercially available lens with specifications nearest to the calculated value viz. 20 mm, was chosen for the second lens. The given expressions were then inverted to obtain the correct lens to sample distance.

$$r_2 = \frac{r_c d}{2f - r_1} \tag{2.5}$$

$$x_2 = \frac{r_c r_2}{r_1 + r_2}$$

The final geometrical specifications of $d = 10$ mm, $r_c = 19$ mm, $f = 20$ mm and $r_1 = 2$ mm were similarly obtained. Using such a lens system, the isotropically emitted light from the TLD-diamond sample could be reflected as a parallel beam into the photomultiplier tube. The flux of the parallel beam passing through the concentric area between the exit diameter of the conical housing and the diameter of the mirror was reflected by the specially coated surface into the detector, allowing for minimal loss of emitted light. All the photoluminescence measurements were carried out using this experimental arrangement.

CHAPTER 3

Analysis of Results

3.1 Methods of Analysis

All minimisation procedures for the procuring of parameter estimates were based on the least squares optimisation principal (Marquardt, 1963). The generalised weighted least squares problem can be elaborated on as follows. Let

$$\sum_{i=1}^{N} w_i \left[y_{exp}^{(i)} - y_m^{(i)}(\alpha_j) \right]^2$$

be the quantity to be minimised. Here N is prescribed by the number of data points, w_i is the weighting factor for each data point, $y_{exp}^{(i)}$ is the experimentally measured function value and $y_m^{(i)}$ is the theoretically determined expectation value. The latter is a function of the α_j parameters which define the theoretical expectation. Most commonly w_i is chosen to be unity or $\frac{1}{y_{exp}^{(i)}}$. In the latter instance the quantity being minimised is Chi-squared (χ^2). These minimisations, in practice, tend to weight the data points lowest in value to a greater extent because of their $\frac{1}{y_{exp}^{(i)}}$ dependence. In this study it was found that better minimisations could be achieved by taking $w_i = 1$ i.e. by weighting all the data points equally. The minimisation of the sum of the errors squared for each data point (SSQ) was achieved by finding the solutions for the extrema described by expressions 3.1, i.e. values for α_j for which

$$\frac{\partial}{\partial \alpha_j} \left[\sum_{i=1}^{N} (y_{exp} - y_m(\alpha_j))^2 \right] = 0 \qquad (3.1)$$

is satisfied. This defines a set of j equations for the α_j parameters. In some cases these equations are linear and can be solved in closed form. In other cases a nonlinear set of

equations have to be solved. In this study the nonlinear equations which resulted were solved by either of the Levenburg-Marquardt or the MINUITS algorithms described in the following section.

3.2 Analysis of the Glow Curve Spectra

For the analysis of the glow curves derived in this study, the methods of partial and complete curve fitting were used to derive estimates for the trapping parameters. Both methods required computational analysis. All computation for these purposes was executed in FORTRAN on the IBM VM/XA mainframe system. For the nonlinear regression of the measured glow curve spectra of the Fe-free synthetic diamond sample, to the theoretical form for the glow curve given by Horowitz *et al.* (1986), the Levenburg-Marquardt algorithm (Jorge *et al.*, 1980) was used to solve the system of nonlinear equations presented by this problem. The latter system is derived and given in Appendix I. A FORTRAN program was written which called the external Library function NEQNF (cf IMSL MATH LIBRARY) with an initial guess for the required parameters. The solution vector with the optimised parameters were returned to the main program when the algorithm converged. Applications of this algorithm converged rapidly when reasonable initial guesses were provided.

For the analysis of the general order expression of May and Partridge (1964), applied earlier in a similar form by Halperin *et al.* (1960), the remaining glow ($n(T)$) beyond the temperature T, was derived from the Simpson integration formula. This involved evaluating:

$$n(T) = \frac{1}{\beta}\int_{T}^{\infty} dt\, I(t) \tag{3.2}$$

numerically from the experimental data. Here β is the heating rate, and $I(T)$ is the experimentally measured glow intensity at a temperature T. This numerical integration procedure proved accurate and reliable for this purpose. For the minimisation part of

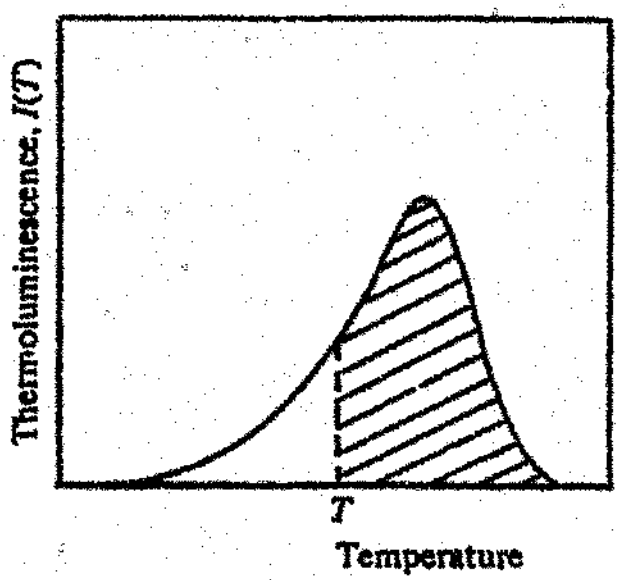

Figure 3.1: The value of $n(T)$ as derived for the determination of the order parameter b. The shaded area under the glow curve beyond the temperature, T, is evaluated as the quantity which is directly proportional to $n(T)$. (After Halperin *et al.*, 1960).

this program, a linear regression of $\ln\left(\frac{I(T)}{n^b}\right)$ vs $\frac{1}{T}$, on a linear grid of b-values between 1 and 2, was performed. For each b-value, the correlation coefficient and SSQ were written to an output file for later comparison and manipulation.

The analysis of the glow spectrum of the Fe-free diamond by the method of complete curve fitting involved the use of the MINUITS search algorithm. A FORTRAN subroutine was written which provided the SSQ, derived from the difference in values obtained from the general order expression of May and Partridge and the experimentally measured data, to the external MINUITS main program for minimisation. The integral

$$\int_{T_0}^{T} d\tau \ \exp(-E/k\tau)$$

with T_s specifying the initial temperature, was evaluated by a Romberg integration subroutine. IMSL library functions were not used explicitly in this minimisation, because of the extended running times involved in calling these external library functions. These library functions were, however, used as separate programs to compare values derived by these routines as opposed to the Romberg routine written for the minimisation subroutine. The values derived from the latter routine were also compared against published theoretical glow curves, such as those provided by Randall and Wilkins (1945a), in particular. Both these consistency checks proved positive, and gave an indication of the high accuracy which the glow curve could be described theoretically.

3.3 Analysis of the Isothermal Decay Spectra

The analysis of the isothermal decay spectra measured, proceeded along two directions dictated by the theoretical form exhibited by the spectra. In this study, the behaviour of these spectra fell into two general groupings, viz. exponential-type decay and the inverse-time (t^{-1}) dependent relationship. For the regression of the experimental data to an assumed sum of exponential components, an algorithm described by Prony (Hildebrand, 1959) and refined by Simon (1970) to account for Poisson noise was utilised. Simon used this method to provide estimates of the exponential factors of multi-compartmental systems which occur in certain physiologic studies. Cited advantages of this method are that no initial guesses are needed for the required parameters and convergence of this algorithm is guaranteed for data containing a Poisson distributed noise component. This afforded a unique method for both the determination number of exponential components as well as the best estimates of such components.

An application of this method involves the initial assumption of the number of exponential components. A search for twice as many components is initiated. From the components derived, only the real-valued solutions are taken i.e the oscillatory solutions which describe the noise are discarded. A possible shortcoming of this method, in general, regards the maximum number of components derivable because the solutions are

obtained numerically from the roots of an nth order polynomial, n being twice the number of required components. The search for such roots numerically, involves polynomial deflation. In practice, this means that the roots of polynomials of order > 10 derived by this technique are prone to be inaccurate and often the search does not converge. In the phosphorescence study a maximum of two exponential components were required to describe the experimental data to very high correlation. Shown in Table 3.1 is a comparison of the exponential factors recovered using the program used throughout this study, in contrast to those derived by Simon (1970). The example in closed form is given by:

$$y = 10 \times 0.2^n + 2 \times 0.7^n + 1 \times 0.94^n = a_1 \times u_1^n + a_2 \times u_2^n + a_3 \times u_3^n$$

Table 3.1

Data Set number	True Values	Reference Article's Values	Values derived by custom software
1	(0.2,0.7,0.94) (10,2,1)	(0.198,0.676,0.934) (9.91,1.98,1.10)	(0.204,0.707,0.940) (10.08,1.93,0.987)
2	" " " " " " " "	(0.177,0.655,0.935) (9.47,2.46,1.08)	(0.213,0.773,0.969) (10.4,2.04,0.60)
3	" " " " " " " "	(0.205,0.715,0.944) (10.1,1.92,0.93)	(0.196,0.704,0.943) (9.96,2.09,0.947)

Data set 1 is derived from the above expression for y and has no noise component. Data sets 2 and 3 both have a component of Poisson distributed noise added to the data set 1. As can be seen, the estimates derived by the software used in this study compares favourably with published values derived independently and in most cases provided bet-

ter estimates. All exponential fitting procedures carried out in this study were therefore derived in this manner.

For the parameter estimation of the isothermal decay spectra showing an inverse time dependence rather than the exponential-type dependence, the MINUIT5 fitting procedures were once again used in the fashion described previously. The subroutine for this minimisation simply involved writing in the expression to be regressed in closed form.

CHAPTER 4

Theoretical Background

4.1 Band Structure

The most rudimentary results describing the energy states of electrons in crystalline solids, viz. the band structure, have been derived from the solution of Schrödinger's equation for a periodically varying potential (cf Kittel, 1986), which characterises the perfect crystal lattice. In the perfect crystal, the potential satisfies the property of invariance under a suitable crystal translation, and models such as the Krönig-Penney model, which assume such a potential to characterise the perfect lattice, reveal that electrons in the perfect crystalline solid can exist in allowed energy states (bands) while other energy values for these electrons constitute forbidden zones (bands).

The occupancy of each electronic band is described by the Fermi-Dirac distribution $f(E)$, in terms of the energy E, which relates the density of energy states, $D(E)$, to the density of available states, $Z(E)$, at any given temperature, T, measured on the absolute scale.

$$D(E) = Z(E)\,f(E) \tag{4.1}$$

$$f(E) = \frac{1}{\exp[(E-\mu)/kT] + 1} \tag{4.2}$$

In expression 4.2, μ refers to the chemical potential of the system and is a function of the temperature and the number of particles in the system. k is the Boltzmann constant. At absolute zero, $\mu = E_f$, where E_f is the Fermi energy level which provides the demarcation level for the occupied and unoccupied energy states. By definition, all energy states below E_f are occupied while all those above E_f are empty at absolute zero. In the high temperature limit where $E - \mu \gg kT$, the Fermi-Dirac distribution reduces to the Maxwell or Boltzmann distribution.

$$f(E) = \exp[-(u - E)/kT] \tag{4.3}$$

For the description of thermally stimulated processes, e.g. thermoluminescence and phosphorescence, the Boltzmann distribution is used in a different form to equation 4.3. What must be considered for the discussion of these processes is the situation in which heat is transferred from a large reservoir to the thermoluminescent phosphor. In this situation it is required to know the probability distribution which describes the likelihood that an electron possesses an energy $E > 0$ commensurate with the energy of a free carrier, at the temperature (T) of interest. If the additional requirement that no transfer of charge particles can take place between the phosphor and the heat reservoir is made, then it can be shown (cf Kittel) that such a distribution is given by:

$$f(E) = \exp(-E/kT) \tag{4.4}$$

Throughout the discussions of thermally stimulated processes in this dissertation the Boltzmann distribution of equation 4.4 is explicitly used and tacitly assumed in situations where the relative population of states, due to a system's thermal energy, is considered. Typical situations include the discussions of the forms of the thermoluminescence glow spectrum as a function of temperature. For the phosphorescence decay from discrete trapping states with time the trivial result in equation 4.5 can be written:

$$i(t) = i_0 e^{-t/\tau} \tag{4.5}$$

where $i(t)$ is the phosphorescence intensity at the time t post-irradiation, i_0 is the initial intensity at the instant irradiation ceases and τ is the characteristic decay constant.

Another factor to be considered in the interpretation of the thermoluminescence and phosphorescence spectra, refers to the situation in which a closely spaced distribution of levels is present. In Chapter 6 the relative energy distribution of states at room temperature is determined experimentally. Such distributions of states have been studied in detail by past researchers. Randall and Wilkins (1945b), for example, have studied the

theoretical implications of exponential, uniform and Gaussian distributions of states on the characteristics of thermoluminescence and isothermal decay spectra. In the case of the thermoluminescence spectra such distributions result in a broad, composite glow spectrum. The most relevant result in the case of the isothermal decay spectra on the other hand, refers to the theoretical form of such spectra. More recent analysis (Medlin, 1961b) showed that the theoretical dependence of luminescence decay from a distribution of states can follow an inverse time dependence. Equation 4.6 describes this dependence identically:

$$i(t) = i_0 \left[\frac{b}{b+t} \right]^m \qquad (4.6)$$

Here $i(t)$, t and i_0 are as described in equation 4.5. The phenomenological parameters b and m have been shown to describe the physical luminescence decay spectrum uniquely.

4.2 The Luminescence Efficiency

Two types of transitions occur between electron states in solids, viz. radiative and non-radiative transitions (Seitz, 1938). The sequential occurrence of these transitions by a charge carrier is generally termed a phonon assisted transition. In order that thermoluminescence be observed in a crystal it is necessary that radiative recombinations of previously trapped charge carriers, at luminescence centres, occurs. In addition, a large number of solids exhibit the presence of centres with which carriers can only recombine non-radiatively. These centres are generally termed *'killer centres'*. The larger the concentration of these centres, the lower the thermoluminescence yield. In the TLD diamonds used in this investigation nitrogen, which is generally accepted to appear in synthetic diamond in dispersed paramagnetic form, is implicated as a radiationless or killer recombination centre for charge carriers (Nam *et al.*, 1991). As can be appreciated from this study, the concentration of paramagnetic nitrogen has a marked effect upon

the sensitivity of the thermoluminescence response of the Fe-based synthetic diamond crystals.

For non-radiative processes involving Coulombic confinement, the luminescence efficiency can be explicitly expressed as (McKeever, 1985):

$$\eta(T) = \frac{1}{1 + c\ \exp(-E_w/kT)} \tag{4.7}$$

Here c is a constant and E_w is the activation energy for the particular non-radiative process which occurs. In the case of thermoluminescence it has been shown (Wintle, 1975) that the shape of the glow curve can be altered by a temperature dependent luminescence efficiency. This effect can be represented by:

$$I'(T) = \eta(T) \times I(T) \tag{4.8}$$

where $I(T)$ is the glow curve resulting from a constant luminescence efficiency, and $I'(T)$ is the glow spectrum resulting from the temperature dependent luminescence efficiency, as given in equation 4.7, for example.

CHAPTER 5

Thermoluminescence Analysis of Discrete Trapping States in the Forbidden Band Gap

5.1 Glow Curve Spectroscopy

Much of the emphasis in theoretical work in the thermoluminescence technique has been placed upon the formulation of models which give the form of the glow curve for a phosphor containing a single trap depth in terms of empirical trapping parameters (Randall and Wilkins, 1945a; Garlick and Gibson, 1948). Given relationships of this nature, methods have been devised to extract the trapping parameters of interest. For dosimetry, an estimate of the trapping parameters, especially the trapping depth and frequency factor, affords a method for the determination of the mean life of the thermoluminescence peak under consideration. From the trapping parameters the degree of stability of the peak can be considered. Since the work of Randall and Wilkins (1945a) which produced the form for the thermoluminescence glow curve due to a first order kinetic process, glow curve analysis has lent itself to partial and complete glow curve fitting, from which estimates of the trapping parameters, viz. E, the trap depth, s, the frequency factor and n_0, the initial trapped charge concentration, can be determined. This model assumes that the luminescence efficiency is unity and that the glow curve is due to a single species of trap.

Garlick and Gibson (1948) considered the case in which re-trapping is non-negligible and derived an expression for the glow spectrum for second order or bimolecular mechanics, when the luminescence efficiency is also assumed to be unity. The distinguishing feature of this work is that *all* empty traps and recombination centres were considered to compete equally for the free charge carriers. The work of Randall and Wilkins (1945a) did not account for the likelihood that traps emptied thermally could re-trap free carri-

ers. The effect of this feature on the shape of the glow curve, is that the region on the higher temperature side of the thermoluminescence peak shows proportionally more luminescence, i.e. the peak broadens. The effect of re-trapping is therefore demonstrated to delay the thermoluminescence (figure 5.1). Such behaviour is believed to be dominant in phosphors in which the mean separation between traps and recombination centres is relatively large. This condition is satisfied when the concentrations of traps and recombination centres are relatively small (cf Avouris and Morgan, 1981, for example), so that the mean free path for the recombination process is relatively large.

Many workers have reported (cf McKeever, 1983) that not all recorded glow curves conform to either of the monomolecular or bimolecular forms given by Randall and Wilkins and Garlick and Gibson, respectively. A further development has been the formulation of expressions for general order kinetics by May and Partridge (1964) and Chen *et al.* (1981a) to account for the fact that the capture cross-sections of the electron and hole centres for the recombination of free charge carriers need not be identical. Equations 5.1 and 5.2 given by May and Partridge give the integral form and the integrated out form of the general order expression, respectively.

$$I(T) = (n^b s'/N)\exp(-E/kT) \tag{5.1}$$

In expression 5.1 $n = n(T)$, is the trapped charge concentration remaining at temperature T, b is the order parameter which can take on values ranging between 1.0 to 2.0, and N is the total concentration charge trapping states, and k is the Boltzmann constant.

$$I(T) = \frac{n_0^b s'' \exp(-E/kT)}{\left[1 + (n_0 s''/\beta)\int_{T_0}^{T} d\tau \ \exp(-E/k\tau)\right]^{b/(b-1)}} \tag{5.2}$$

In equation 5.2 $s'' = (s/N)n^{b-1}$ and β is the heating rate at which the temperature of the sample is ramped from the initial temperature T_0 to the final temperature T.

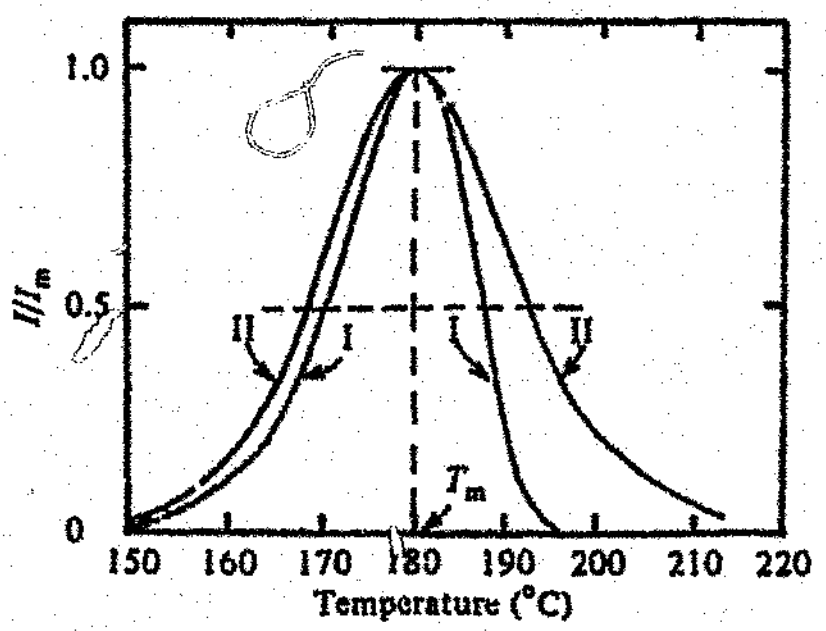

Figure 5.1: Computed thermoluminescence peaks for (I) first- and (II) second-order kinetics for $E = 0.42$ eV, $s = 10^{12}$ s^{-1}. (After Chen and Kirsch, 1981)

In addition, the shape of the glow curve can be affected by other physical processes such as thermal and impurity quenching, and tunnelling phenomena which could manifest themselves in a number of ways (Johnson and Williams, 1952; Wintle, 1975; Fillard *et al.*, 1978; Sunta and Bapat, 1982). In the approximation $T \sim T_m$, all the expressions for the glow curve spectrum, regardless of the kinetic order, are amenable to partial curve analysis, in which the initial rise portion of the glow curve is accurately represented by an expression of the form

$$I(T) = constant \times \exp(-E/kT) \qquad (5.3)$$

from which an estimate of the trapping depth E is readily arrived at from a plot of $\ln|I(T)|$ vs $1/T$. On the other hand, the analysis of the whole glow curve requires the

computationally more tedious approach of curve fitting procedures. The advantage of whole curve analysis concerns the physical interpretation of the glow curve. By use of error minimisation procedures it is possible to objectively determine the kinetics of the thermoluminescence process by finding the best minimisation of the first, second and general order expressions. In this process other glow parameters (E and s) can also be determined which render the glow curve more amenable to physical interpretation. A possible shortcoming of thermoluminescence analysis when utilised in isolation, as noted by a number of researchers (cf McKeever, 1985), is that only three glow parameters can be determined at most. If the rate equations for the emptying and filling of defect centres are considered, as done by Adirowitch (1963) for example, then it becomes apparent that the dependence of the form of the glow curve on the three parameters (E, s, and b) can be derived via simplifying assumptions from rate equations involving the total trap concentration, the concentration of holes in the recombination centres, the transition coefficient for electrons in the conduction band becoming trapped at electron trapping centres, and the recombination transition coefficient for electrons in the conduction band with holes in luminescence centres.

Other useful methods for glow curve parameter estimation involve utilising two or three points on the glow curve which characterise the shape of the curve. As can be appreciated from the variation in the shapes of the first and second order glow curves (cf figure 5.1), the order of the kinetic process can appreciably alter the shape of the glow spectrum. As a result, analytical methods have been derived which give parameter estimates based upon the shape of such glow spectra. The temperature of the peak maximum, as well as the low- and high-temperature half heights, are the points on the glow spectrum most often used. Such methods allow a reasonably reliable estimate of the glow parameters to be arrived at, by a technique which also takes into account the kinetic order of the process and the heating rate used to obtain the glow spectra. In this manner glow curve parameter estimates can be arrived at which are comparable to the methods of complete curve fitting. Two peak shape methods given in the literature

which prove useful are given by Chen (1969a) and Horowitz *et al.* (1986). Chen's technique is based upon the numerical evaluation of the mixed-order expression, derived by him to describe the glow curve in terms of the semi-empirical shape parameters defined by Halperin and Braner (1960). The technique proposed by Horowitz and co-workers also makes use of a semi-empirical relationship based on these shape factors for the description of the glow spectrum of commercial LiF TLDs, in particular. Both these techniques, as well as the technique of complete curve fitting, were used in this research to derive unique and reliable estimates for the trapping parameters of the glow spectrum obtained from the Fe-free synthetic diamond sample.

5.2 Results and Discussions

The glow curve of the Fe-free synthetic diamond was analysed by a number of techniques in order to gain reliable estimates for the glow spectrum parameters. This glow spectrum was arrived at by ramping the diamond samples at 16°C s^{-1} from room temperature to 450°C. Single Fe-free diamond crystals showed a low sensitivity to ionising radiations. The glow curve analysed in this experiment was obtained from a collection of such crystals subjected to an initial radiation treatment with the ^{90}Sr β-source. The initial rise portion of the glow curve was regressed to equation 5.3. The result of this regression gave an estimate of 1.38 eV for the activation energy. The best regression in terms of the correlation coefficient took into account a background subtraction, which was applied to give the best fit.

The peak shape method of Horowitz *et al.* (1986) was used as a consistency check, so that the value of the energy depth derived from the initial rise analysis could be confirmed. This method, which has been applied for dosimetry, using LiF in particular, comprises the approximation of an isolated glow peak, P, by the following expressions:

$$P = I_m \exp\left[1 + \frac{\Delta T}{T_m}\,\frac{E}{kT_m} - \exp\left(\frac{\Delta T}{T_m}\,\frac{E}{kT_m}\right)\right] \qquad (5.4a)$$

$$P(x) = I_m \exp[1 + W(x - x_0) - \exp(W(x - x_0))] \qquad (5.4b)$$

The first expression 5.4a describes the glow curve in terms of the peak height, I_m, the temperature at which the peak maximum occurs, T_m, and the activation energy, E, for the glow peak. ΔT is equal to $T - T_m$ where T is the sample temperature and k is the Boltzmann constant. The equivalent expression 5.4b gives the explicit dependence of P on the width parameter W and the independent variable, x, which is representative of the sample temperature in this study. The temperature at which the peak maximum occurs is given by x_0. The geometrical factors viz. ω, τ and δ, are related to the width parameter W by the following relationships:

$$\omega = \frac{2.44}{W}, \qquad \delta = \frac{0.982}{W}, \qquad \tau = \frac{1.46}{W} \qquad (5.5)$$

FORTRAN-based software was written to find the trapping depth, as described in Chapter 3 (§3.2). Shown in figure 5.2 is the result of the minimisation procedure, which yielded an activation energy of 1.68 eV. As can be seen from the fit shown in this figure, a significant deviation of the fitted values (the solid line) from the experimentally determined data (diamonds), is a characteristic feature. This feature is due to the non-first order form of the experimentally measured glow curve. This fact becomes immediately apparent on the comparison of this curve with the shape of the second order glow curve shown in figure 5.1. The shape of the glow curve described by equations 5.4 and 5.5, on the other hand conforms more to the first order form for a hypothetical glow curve. As can be seen from the diagram, this factor alone resulted in a less than desirable fit to the experimental data. It can also be concluded on the basis of this fit that the energy depths derived by the method of Horowitz *et al.* are prone to give erroneous results if the shape of the glow curve deviates appreciably from the shape of first order glow curves.

In an effort to improve on the estimate of the activation energy, as derived by the method of Horowitz and co-workers, partial curve analysis, as developed by

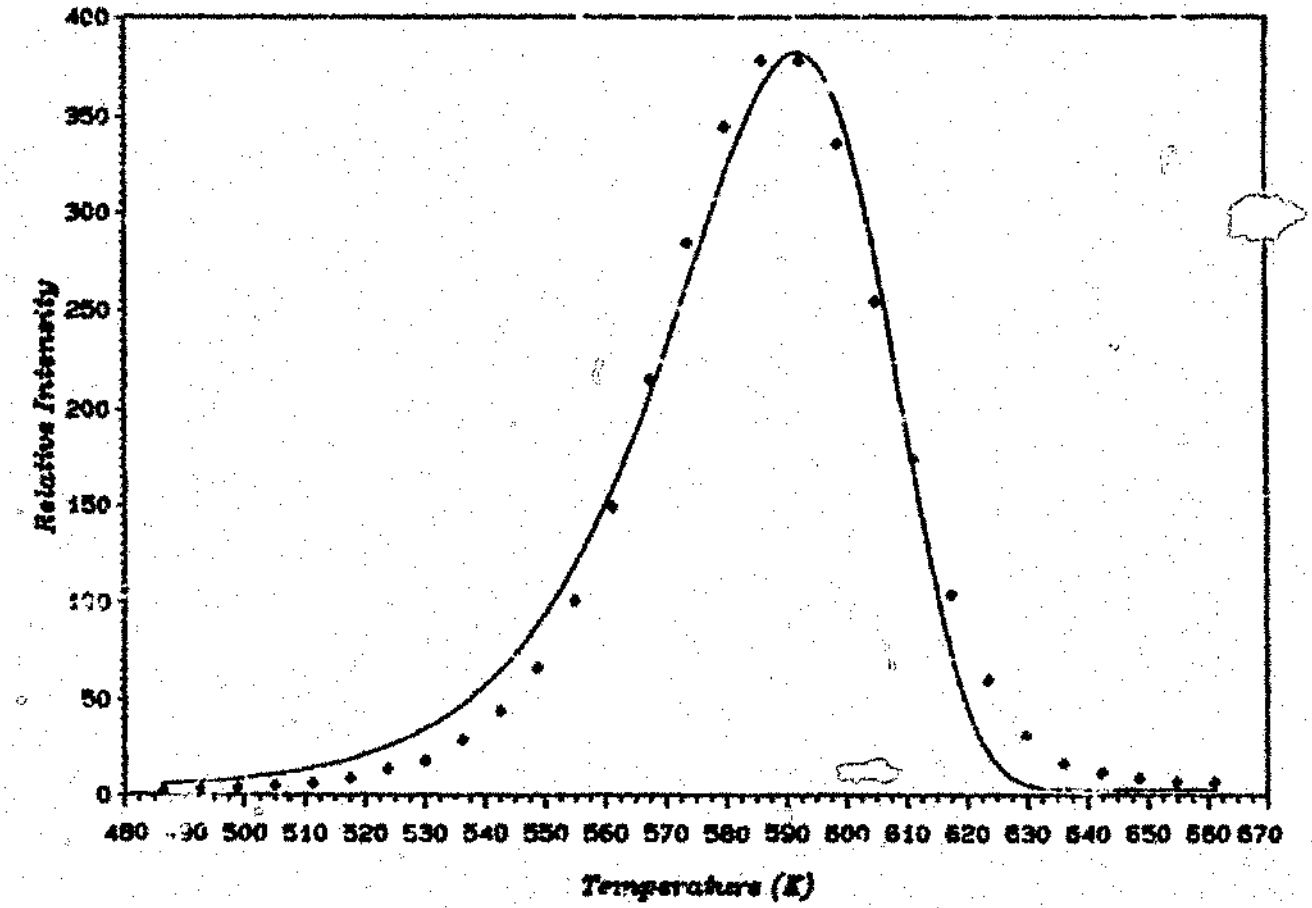

Figure 5.2: The result of the regression of expression 5.4 to the experimentally determined glow spectrum of the Fe-free diamond. The fitted parameters describing the theoretical curve are given by $I_m = 379.4$, $T_m = 319.2$°C, $E = 1.68$ eV and the background correction factor was 3.0.

Chen (1969a,b) for general order kinetics, was applied. A general formula for the trap depth (E) was derived by Chen in terms of the shape parameters. Equation 5.6 gives a less general form written in terms of the shape parameter δ.

$$E = C_\delta \left(\frac{kT_m^2}{\delta} \right) \tag{5.6}$$

$$\text{with} \quad C_\delta = 0.976 + 7.3\,(\mu_g - 0.42)$$

Furthermore, values for the shape parameter, $\mu_g = \frac{\delta}{\omega}$, defined by Halperin and Braner (1960), were numerically derived by Chen as a function of the order parameter, b. When the order parameter is determined μ_g can be determined from Chen's published values of μ_g as a function of b. In order to arrive at an estimate of the energy depth from equation 5.6 it was therefore necessary to find a reliable value for the order parameter. This was achieved in the following manner. For this part of the study the general order expression, written in terms of the temperature as the independent variable, was applied in the method similar to that used by Halperin *et al.* (1960):

$$I(T) = \frac{n^b s'}{\beta} \exp(-E/kT) \tag{5.7}$$

Inspection of this relationship reveals that a plot of $\ln |I(T)/n^b|$ vs $\frac{1}{T}$ gives a straight line with a slope $(-E/k)$ and an intercept of $\ln(s'/\beta)$ when the correct value of b is used. Software was written which regressed the experimental data on an equally spaced, linear grid of b-values. The best fit was decided upon by a least squares fitting procedure, and extracting also a maximum correlation coefficient, applied for each b-value. Figure 5.3 shows the result of the fitting procedure applied for values of b between 1.0 and 2.0, i.e. for first order kinetics ($b = 1$), general order kinetics ($1 < b < 2$) and second order kinetics ($b = 2$). On the left vertical axis the correlation coefficient x 100% is given (κ), while the SSQ (ε) is shown on the right vertical axis, with the order parameter (b) given as the independent ordinate. The minimum SSQ, which can be read off figure 5.3, occurs at a

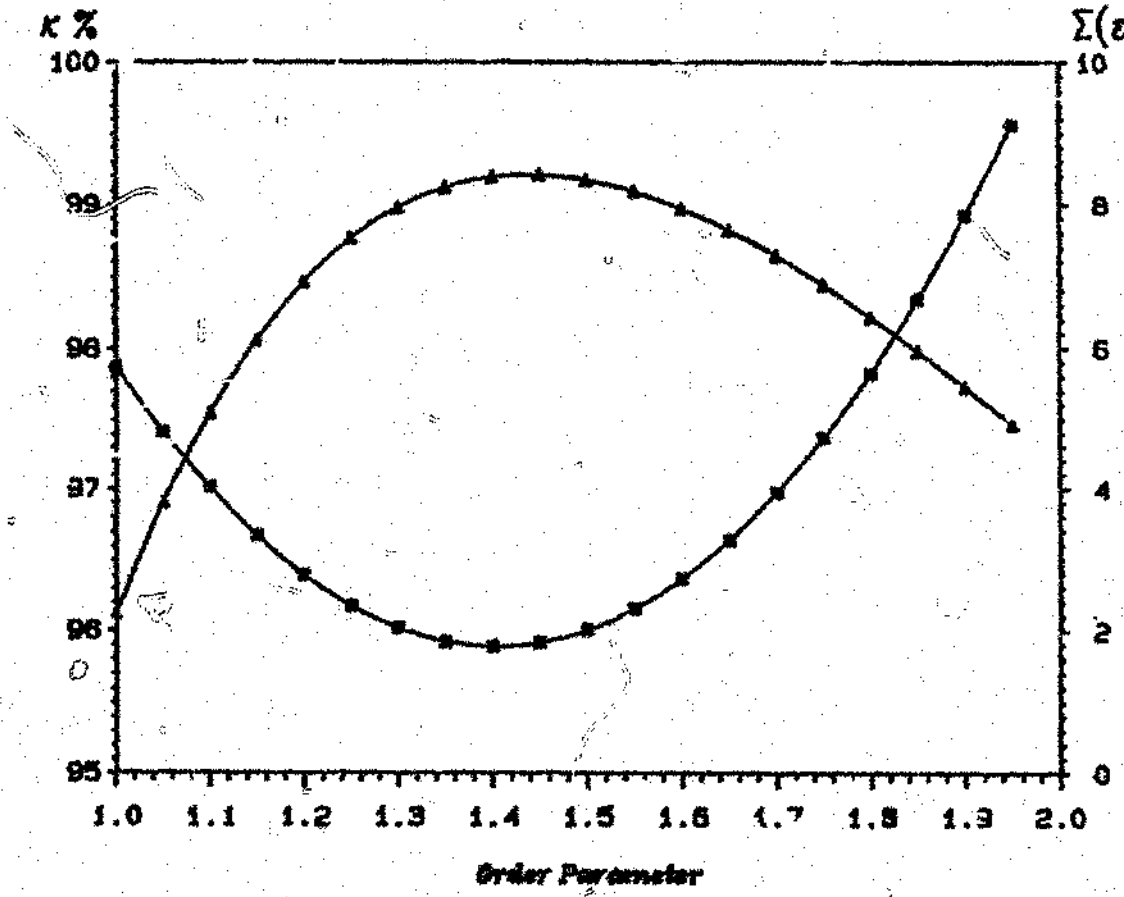

Figure 3.3: The SSQ (#) and correlation (A) computed from the general order expression, expressed as a function of the order parameter.

value for b of approximately 1.40. The maximum correlation which can be determined from the figure, on the other hand, occurs at a value for b of 1.45. For this study, both of these b-values derived were used to obtain values of μ_g, from which the activation energy, E, could be derived. Table 5.1 shows the values derived by this method. The values of E listed in Table 5.1 were derived from equation 5.6 with $T_m = 390$ K and $\delta = 21.43$ K. These geometrical factors were derived from the experimentally measured glow curve in figure 5.2. Criticisms of this method centre upon the fact that the estimate of the energy parameter depends solely on a few experimental points on the glow curve; in this case only two data points were required. This can lead to appreciable errors in the estimation of the energy depth, especially in cases where other processes which affect the shape of the glow curve, e.g. thermal and impurity quenching (Sunta and Bapat, 1982; McKeever, 1985), may be prevalent. A quoted error in the estimation (Shenker and Chen, 1972; Kivits and Hagebeuk, 1977) places the accuracy of this method at approximately 5 %. An error of this order of magnitude gives an estimate of the trap depth of 1.90±0.05 eV.

Table 5.1

b	1.40	1.45
μ_g	0.470	0.475
C_b	1.341	1.378
E (eV)	1.877	1.929
mean energy, $\bar{E}$ = 1.90±0.02 eV (using equation 5.6, cf text)		

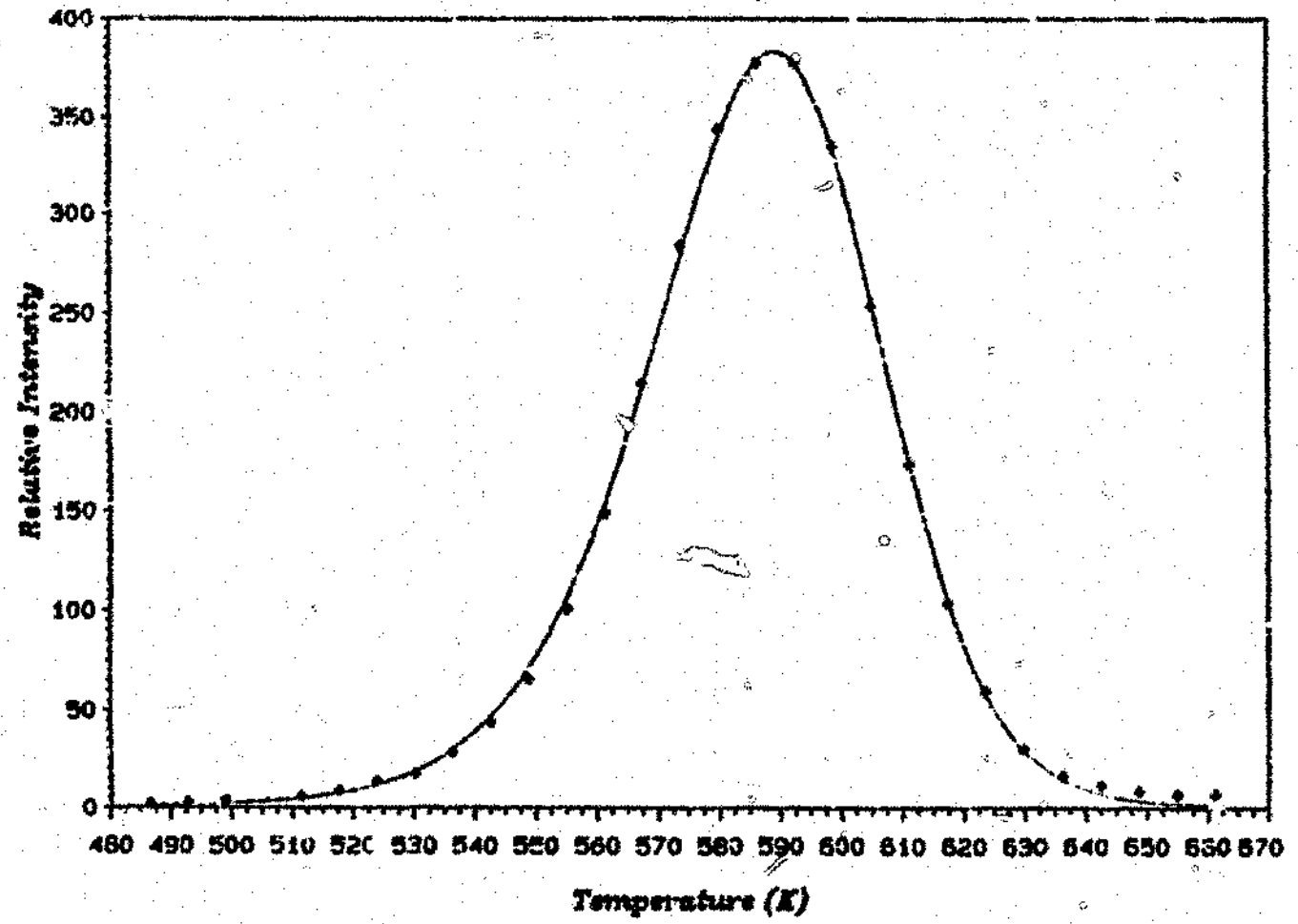

Figure 5.4: The least squares regression fit of the experimentally derived Fe-free synthetic diamond glow spectrum (○) to the general order expression given by May and Partridge (1964).

Finally, a method which made use of complete glow curve fitting was applied in order to arrive at estimates of the trapping parameters. In this analysis, the general order expression of May and Partridge, equation 5.2, was used for the regression of the experimentally measured data. For this purpose the MINUITS package was used, as described in §3.2 of Chapter 3. Depicted in figure 5.4 is the resultant fit. This minimisation procedure provided estimates as follows: $E = 1.872$ eV, $s' = 10^{15}$ and $b = 1.39$. The error estimates derived from the MINUITS minimisation for E, b and s' are given by 8.0×10^{-4} eV, 2.2×10^{-3} and 1.0, respectively. These errors clearly are negligibly small. It can also be seen from the fit in figure 5.4 that the experimental data is described excellently by the theoretically determined fit, represented by the solid line. The value for the energy depth and the order parameter derived by this method are also in excellent agreement with the values derived earlier by the partial curve analysis of Chen.

It has already been shown why the method of Horowitz and co-workers does not provide reliable estimates for the activation energy (E) from the glow curve of the Fe-free synthetic diamond. The estimate for E derived by the method of the initial rise also deviates appreciably from the values determined by partial and complete curve analysis. The theoretical form and significance of the luminescence efficiency has been described previously. It has been shown by Wintle (1975) that when the luminescence efficiency is temperature dependent, the initial rise portion of the glow curve can be described by:

$$I(T) \sim constant \times n(T) \times \exp(-E/kT)$$

In the limit where $c \times \exp(-E_w/kT) \gg 1$ the expression for the luminescence efficiency (equation 4.7) reduces to:

$$\eta(T) \sim c^{-1} \exp(E_w/kT) \qquad (5.8)$$

so that the initial rise portion of the glow curve can be written as:

$$I(T) \sim constant \times \exp[-(E - E_w)/kT]$$

This means that an application of the initial rise technique, in a situation where the luminescence efficiency is temperature dependent, will provide an estimate of $(E - E_a)$, rather than E. This effect has been extensively dealt with by Wintle in the analysis of activation energies of lunar material to assess the effects of these estimates on the archeologic dating of such materials. The values of $(E - E_a)$ derived from the initial rise portions of the glow curve were found to give anomalously low values for the lifetimes of such glow peaks.

This effect could provide a possible explanation for the difference in activation energies derived from the thermoluminescence glow spectrum of the Fe-free synthetic diamond by the method of the initial rise (1.38 eV) and the methods of complete and partial curve fitting (1.90 eV). This difference yields a value of approximately 0.52 eV for E_a. In this interpretation of the experimental results, a luminescence quenching mechanism, with an activation energy of 0.52 eV could explain the experimentally measured results. In order to clarify the actual nature of the quenching process postulated for the Fe-free diamond crystals, further studies beyond the scope of this dissertation, are needed. Photo-Hall mobility measurements at liquid nitrogen and liquid helium temperatures could prove useful.

5.3 Conclusions

It has been demonstrated that complete glow curve fitting can provide parameter estimates which are physically meaningful and accurate to a very high degree. It is also evident from the analysis presented in this chapter, that the fitting of glow spectra, without due care being exercised to account for phenomena such as thermal and impurity quenching, can lead to erroneous estimates of the trapping parameters. This can also lead to an erroneous interpretation of the physical processes occurring in the given phosphor under consideration. Even an analysis of single, isolated glow peaks can, due to occurrence of such processes, present a non-trivial task. However, it can be concluded, on the basis of the curve fitting methods applied (Chen, 1969a,b; May and

Partridge, 1964) that the glow spectrum of the Fe-free synthetic diamond is due to discrete charge trapping states in the forbidden gap of these diamond, with an activation energy of 1.90 eV. In addition, a non-radiative process which has an activation energy of 0.52 eV is postulated to explain the quenching of luminescence observed.

In the context of this dissertation, a method which has been demonstrated to be reliable in providing estimates of activation energies for levels in the forbidden gap of synthetic diamond has been developed viz. the complete curve fitting to the general order expression for the glow spectrum. This method is used in a complementary role with initial rise analysis, taking cognizance of the quenching mechanisms which can occur in the resolution of the broad, composite thermoluminescence spectrum exhibited by the low nitrogen concentration TLD diamond and to estimate thermal activation energies within the crystals.

CHAPTER 6

Energy Levels in the Forbidden Band Gap of the Synthetic TLD Diamond

6.1 Introduction

This chapter presents the experimental measurement of the relative density of energy states in the forbidden gap of the synthetic diamond crystals containing paramagnetic nitrogen concentrations typically lower than 20 ppm. These crystals were specially synthesised for a sensitive thermoluminescence dosimetry response and have a high luminescence efficiency as compared to synthetic diamond crystals of higher paramagnetic nitrogen concentrations. The thermoluminescence glow curve, of which the most distinctive feature is the broad, composite peak structure in the temperature range which varies from room temperature to 450°C, has been reported previously. Bands of energy states have been postulated to be responsible for such thermoluminescence glow spectra. Examples of phosphors displaying glow spectra characterised by bands of thermoluminescence states have been reported by Bull and Garlick (1950), where the thermoluminescence glow of natural diamond samples was discussed, and Avouris and Morgan (1981) for the case of Zn_2SiO_4:Mn. Such phosphors containing quasi-continua of states in the forbidden band gap have demonstrably large full widths at half the glow maxima (FWHM) and exhibit characteristic displacement of the glow peak maximum with pre-heating cycles of increasing maximum temperature. These characteristics cannot be reconciled with the behaviour of isolated glow curves resulting from the presence of first order, second order or general order kinetic processes, exclusively. The analysis of this chapter shows that this behaviour is also typical of the TLD diamond crystals. Having demonstrated that the glow spectrum of these crystals is more adequately described by a distribution of charge trapping states, quantitative estimates of the empirical glow parameters are presented by analytical methods discussed

in Chapters 3 and 5. Also given is the relative density of thermoluminescence states estimated by the fractional glow technique (Gobrecht and Hofmann, 1966).

6.2 Results and Discussions

6.2.1 Preliminary Thermoluminescence Analysis

Initially, the behaviour of the thermoluminescence glow curve was studied when successive pre-heating cycles of increasing maximum readout temperatures were used. The following experimental procedure was employed for data acquisition:

- The TLD diamond was subjected to a 3 Gy gamma cycle dose using a ^{90}Sr source. This dose was chosen to ensure that the resultant thermoluminescence response obtained is sufficient for low statistical error.

- A pre-cleaning cycle was then initiated in which the temperature of the diamond sample was ramped at 16°C s^{-1} to a pre-determined maximum temperature. This step is varied to obtain each of the curves shown in figure 6.1.

- A glow curve readout procedure, in which the temperature of the TLD diamond was ramped at 16°C s^{-1} from 50°C to 400°C, was then initiated.

- Finally, the blackbody signal from the diamond and the heating element were measured. This was achieved by initiating a second readout cycle identical to the previous, in which the sample placement was maintained identically. Subtraction of such a spectrum from the total response allowed correction for background signal contribution.

For each of the cleaning cycles selected the sample was loaded once only, ensuring an identical sample positioning on the heating element. This procedure was considered necessary as individual diamond TLDs subjected to identical radiation treatment but

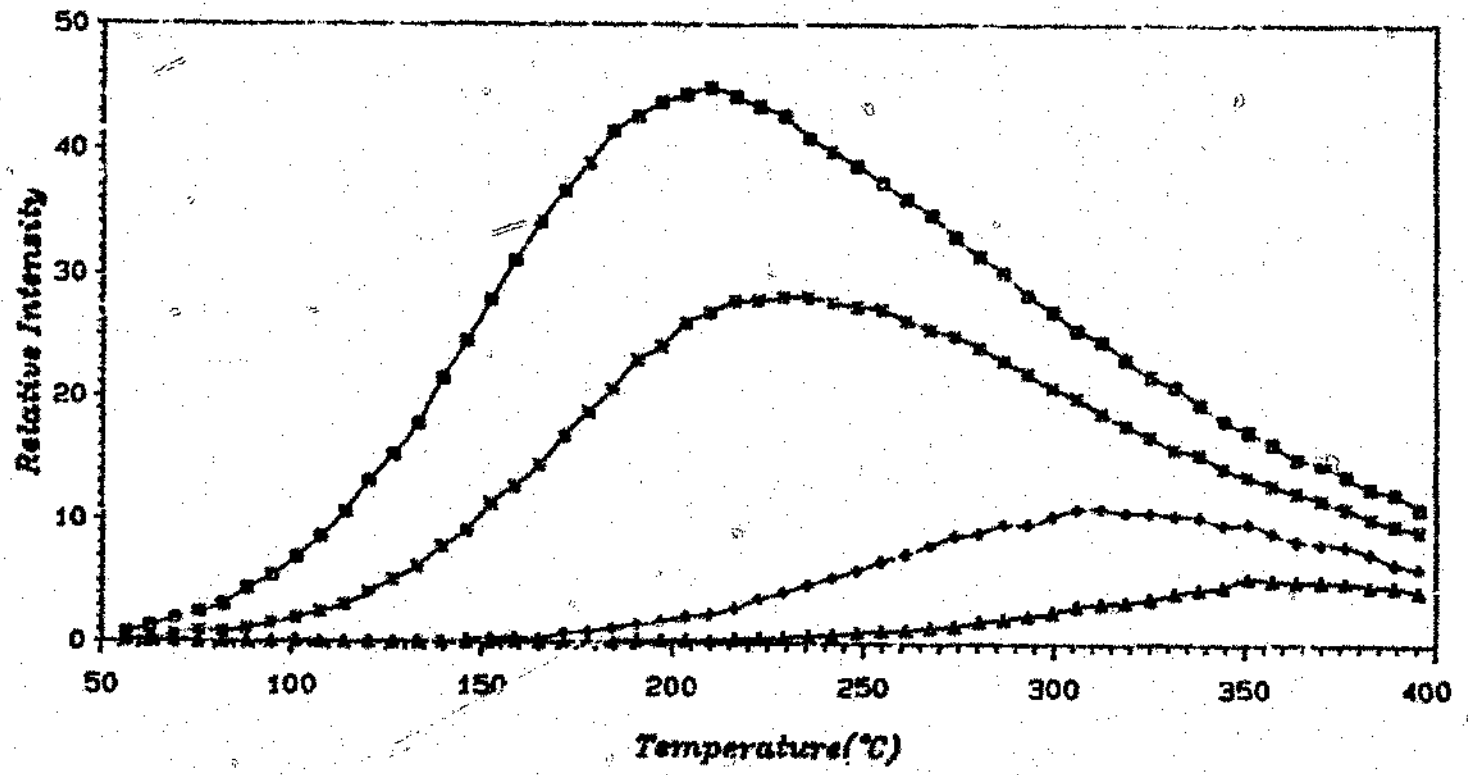

Figure 6.1: The effect of successive cleaning cycles of increasingly higher maximum temperature on the thermoluminescence glow spectrum of the TLD diamond.

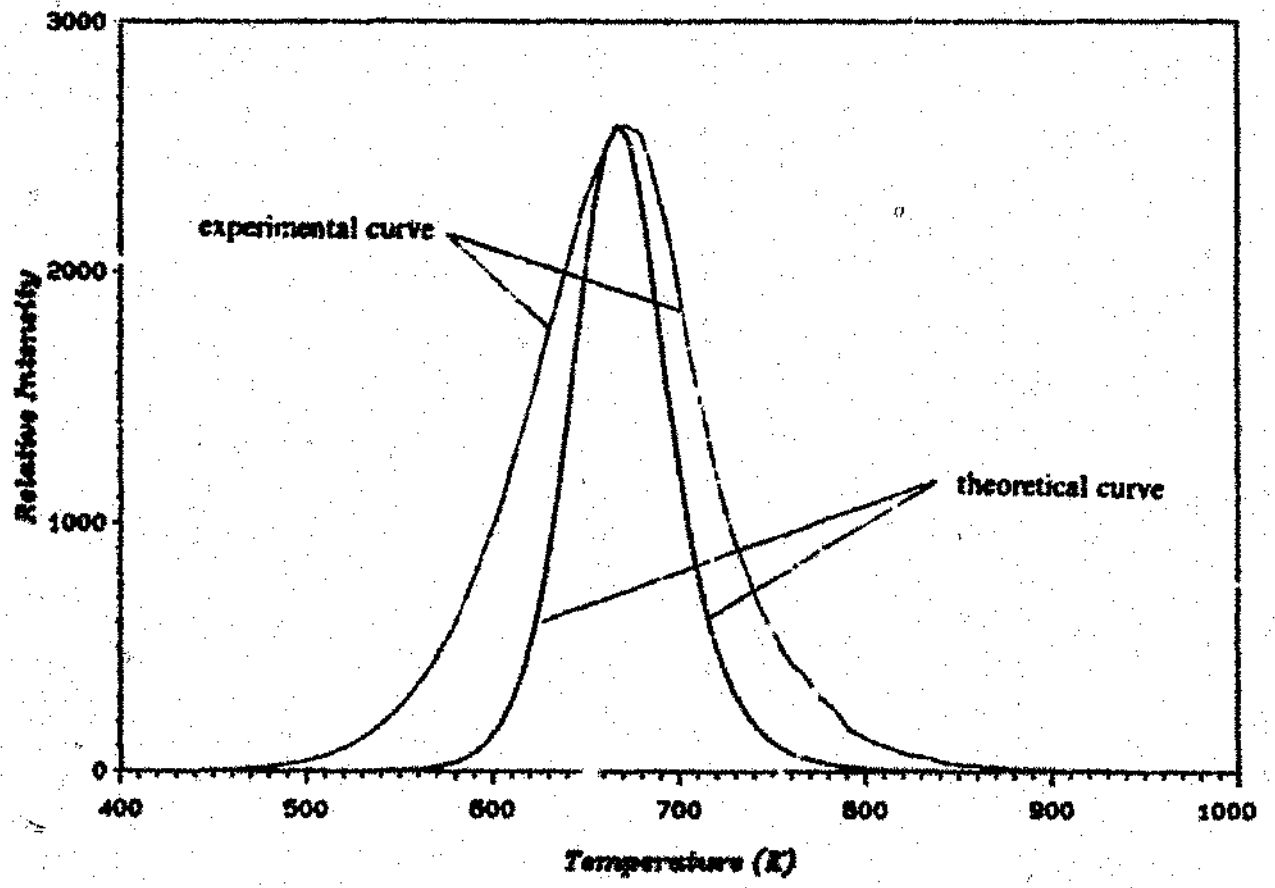

Figure 6.2: The comparative result of an attempted fit of the general order expression (May and Partridge, 1964) to the pre-cleaned thermoluminescence spectrum of the TLD diamond.

placed at different positions on the heating element have been found to give rise to significant standard deviations in thermoluminescence readings. Shown in figure 6.1 are the thermoluminescence glow spectra which were obtained without and with pre-cleaning cycles and with maximum readout temperatures set at 150°C, 260°C, and 320°C. This movement of the glow maximum can be explained by either of two situations. The first refers to the case in which thermoluminescence results from a population of states which follows a non-first order kinetic process. For a hypothetical phosphor in which second order recombination kinetics takes place it has been demonstrated (Levy, 1979) that the position of the glow maximum is dependent upon the fractional population of the charge trapping states. The second situation, which in the case of the TLD diamond is more likely, occurs when the glow spectrum is due to the superposition of a number of charge trapping states having activation energies closely spaced in magnitude. From the glow curve of a TLD diamond which has not been subjected to a pre-heating cycle, it can be inferred that the FWHM of this glow spectrum is too large to correspond to the situation in which a population of discrete charge trapping states of single-valued activation energy is the source of the thermoluminescence spectrum. A possibility which cannot be excluded is the likelihood of a closely spaced distribution of charge trapping states which could follow non-first order recombination kinetics.

A further indication that a more sophisticated approach in the analysis of the thermoluminescence spectrum than was applied in Chapter 5 is necessary, is given in figure 6.2. Depicted here is the attempted fit of the glow curve of the diamond TLD to the general order expression of May and Partridge (1964). The experimentally measured glow curve was derived similarly to the spectra derived in figure 6.1 with the exception of the maximum temperature of the pre-cleaning cycle, which was selected at 280°C. This procedure resulted in the emptying of the shallower charge trapping states as depicted. The glow curve parameters derived from the regression of the experimentally determined glow spectrum yielded: $E = 2.05$ eV, $s' = 10^{16}$ and $b = 2.0$ for the the trap depth, amended frequency factor and kinetic order, respectively. These values describe a glow curve with a maximum in the position shown and having charge trapping states with discrete-valued

activation energy. As can be appreciated from a superficial inspection of this fit, the experimentally determined glow spectrum is not adequately described by the theoretical fit. This further supports the postulate that portions of the glow spectrum of the TLD diamond are not amenable to isolated glow thermoluminescence spectroscopy. The experimentally derived glow curve of figure 6.2 describes approximately 10% of the total thermoluminescence glow. This preliminary analysis demonstrates conclusively that a distribution of closely spaced, overlapping states could describe this spectrum more adequately.

6.2.2 The Relative Distribution of States

The discussion of the previous section underscored the need for an analysis which gives a more detailed picture, and hence a better understanding, of the energy structure of states responsible for the composite thermoluminescence glow spectrum of the synthetic TLD diamond. A survey of the literature has shown that a reliable method for the measurement of the distribution of states has been given by Gobrecht and Hofmann (1966). The relative distribution of states derived in this study was determined by a technique analogous to the method applied by these researchers. The experimental method proposed by Gobrecht and Hofmann centres on the use of several oscillations of glow curve readout cycles. In each subsequent oscillation the phosphor is ramped to an increasingly higher temperature and subsequently cooled at a rapid rate to the initial, room temperature. The glow curve for each of these cycles is then recorded for the analysis of the trap depths by the initial rise technique.

In this study initial rise analysis of the fractional glow spectra, measured in the manner to be described below, was also applied to obtain estimates of the activation energies of the distribution of charge trapping states. In order to derive estimates which could be compared to these values the clean ascending portions of the glow curve were analysed by the method first advocated by Nicholas and Woods (1964). This method proposes the use of the clean ascending portion of the thermoluminescence glow curve in a regression to the theoretical form of a hypothetical single, isolated glow spectrum.

In this study the general order expression (equation 5.2) used in the analysis of the Fe-free synthetic diamond, was utilised for this purpose. The experimental procedure adopted for these measurements was as follows:

- The diamond TLD was irradiated to a β particle dose of 3 Gy.
- The first ramping cycle was initiated 10 minutes post-irradiation. In this cycle the diamond TLD was ramped at 16°C s^{-1} from room temperature to T_{stop}, wher T_{stop} ranges in value in steps of 32°C beyond room temperature.
- Each of these glow spectra was stored for subsequent analysis by fractional glow analysis.

In a single set of measurements, the sample was loaded once so that the sample position was identical for each successive readout cycle. The experimental difficulties of this technique are primarily those which are usually encountered with the thermoluminescence technique. These include the ensuring of accurate temperature control and transfer of heat from the heating element to the phosphor, as well as problems associated with the thermal quenching of luminescence which could be dominant in certain heating regimes of some phosphors, as discussed in Chapter 5. It is this latter mentioned difficulty which prompted the use of the analysis presented by Nicholas and Woods (1964) in this part of this study as an additional step to initial rise analysis, in order that a more complete interpretation of the experimental results may be provided.

Listed in Table 6.1 are values of the activation energies, E_g and E_i derived by the general order method and the method of the initial rise respectively, the initial trapped charge concentration, n_0, the order parameter, b, and the amended frequency factor in the convenient form given by $\log_{10}s'$, derived from the previously discussed expression (equation 5.2). From this Table it can be seen that the analysis of the initial rise portion of the same data set gave values for the activation energy which are in reasonable agreement with the analysis based on the general order expression for the glow curve for

Table 6.1

cycle #	E_{go} (eV)	n_o	b	$\log_{10} s'$	E_{av} (eV)
1	0.52	1086	1.74	6.13	0.52
2	0.56	1336	1.06	6.68	0.56
3	0.71	5864	1.08	8.00	0.68
4	0.73	22168	1.05	7.50	0.72
5	0.77	17721	1.05	7.70	0.73
6	0.82	19223	1.40	7.10	0.77
7	0.85	1[illegible]30	1.16	7.50	0.84
8	0.90	12220	1.46	7.48	0.90
9	0.96	8270	1.48	7.53	0.94
10	1.07	4728	1.61	8.06	0.96
11	1.38	1831	2.00	10.4	1.15
12	1.49	1353	2.00	10.5	1.03
13	2.08	984	1.24	14.3	1.52

the cleaning cycles having lower maximum readout temperatures. One such example, depicted in figure 6.3 gives the graphical representation of data set 3 with the respective fitted curves when (a) the general order expression was used and (b) the method of the initial rise was applied. This example is one in which both methods concur in the esti-

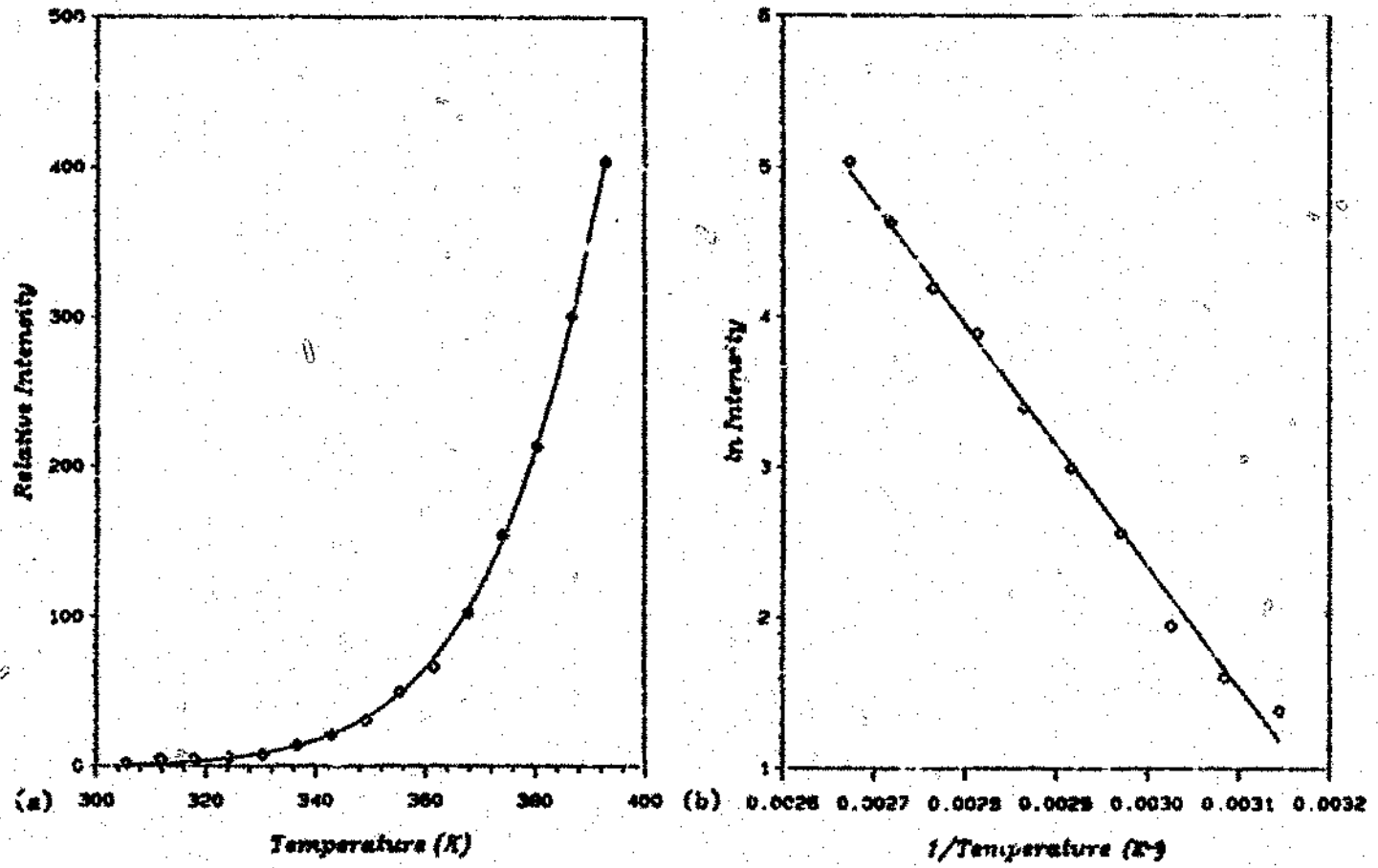

Figure 6.3: (a) The result of the regression to the general order expression of data set 3, $E_{act} = 0.71$ eV. (b) The result of the analysis of the same data set by the method of the initial rise, $E_{act} = 0.68$ eV.

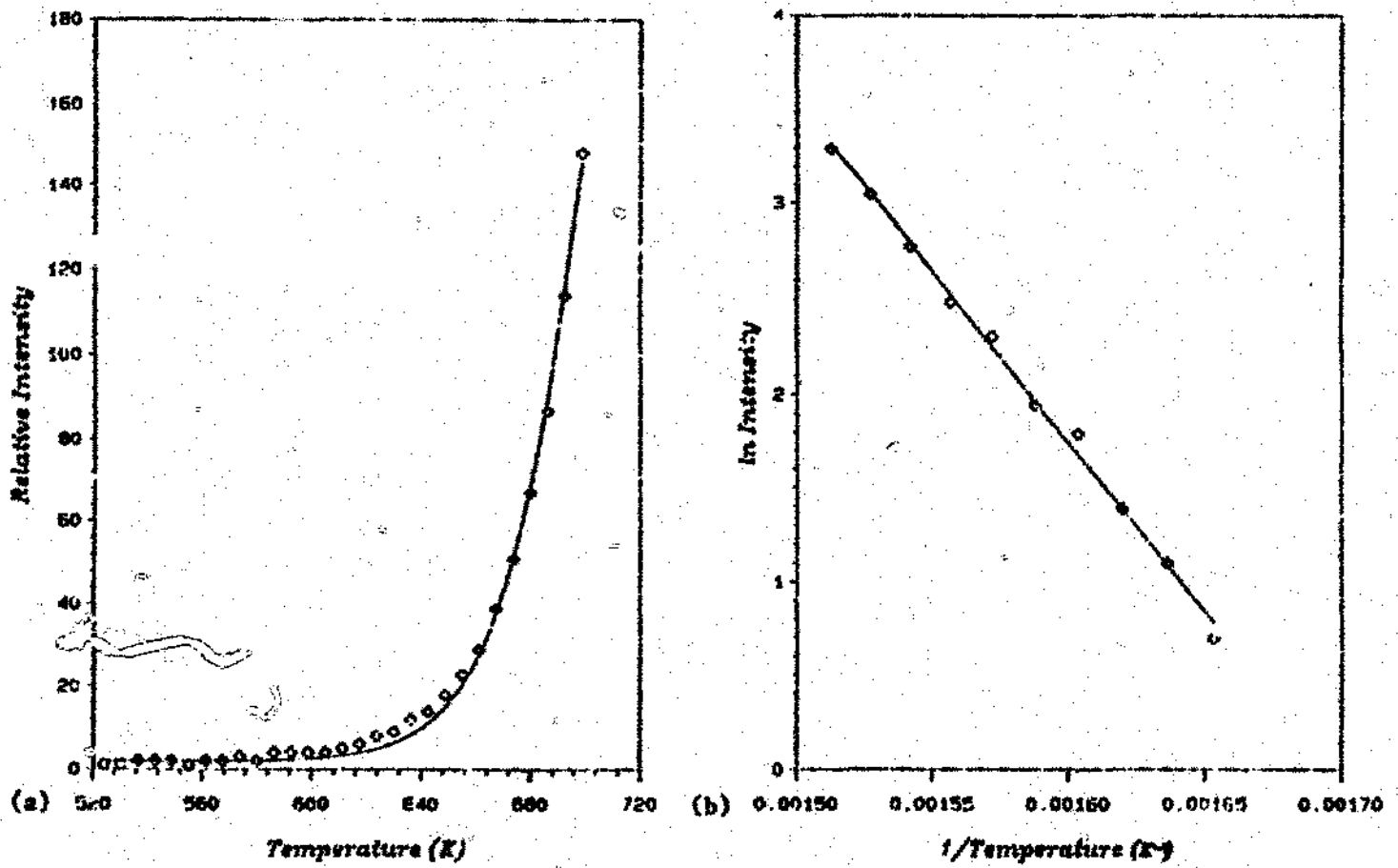

Figure 6.4: (a) The result of the regression to the general order expression of data set 13, E_{go} = 2.08 eV. (b) The result of the analysis of the same data set by the method of the initial rise, E_{ir} = 1.52 eV.

mation of the activation energy. An example, depicted in figure 6.4, where a discrepancy between the values derived by the two methods is conspicuous, is also given. It is postulated that, in an analogous manner to the glow curve of Chapter 5, a thermal quenching mechanism plays a role in the quenching of luminescence which is observed in the glow spectrum of the Fe-based crystals. The results suggest that the activation energy for the quenching process occurring in these diamond is approximately 0.56 eV. It can be concluded that, given the presence of a thermal quenching mechanism, the activation energies derived by the method of the initial rise are influenced (cf Chapter 5) by the presence of non-radiative processes, whereas estimates derived by regression analysis to the general order expression, as given by equation 5.2, more adequately describes the trapping states involved in the radiative portion of the process responsible for the resultant composite thermoluminescence glow spectrum. As the radiophotoluminescence method is unaffected by thermal quenching effects (cf McKeever, 1985), the general order expression rather than the initial rise technique is utilised for the determination of the relative density of states (Table 6.1) for later comparison (Chapter 6) with the optical activation energies of these charge trapping states.

Figure 6.5 (a) gives the graphical representation of the relative density of states using the estimates given in Table 6.1. Depicted on the left vertical axis is the range of values n_0 (in arbitrary units), which is proportional to the area under the glow curve, can take on as a function of the activation energies (in eV) derived. The error in n_0 is given by the vertical error bars in the figure. These values for the glow (n_0) which prescribe the measurement of the relative density of states $N(E_{av})$ say, are not expected be very accurate for activation energies less than 0.70 eV, as these states are thermally unstable at room temperature. The experimental procedure described earlier deliberately allowed for the isothermal decay of the shallow, unstable states in the delay of the fractional cleaning cycles by a period of 10 minutes post-irradiation. The omission of the unstable states was deemed necessary in this study as the lapse in time between the acquisition of subsequent fractional glow cycles can result in the loss of signal by phosphorescence decay.

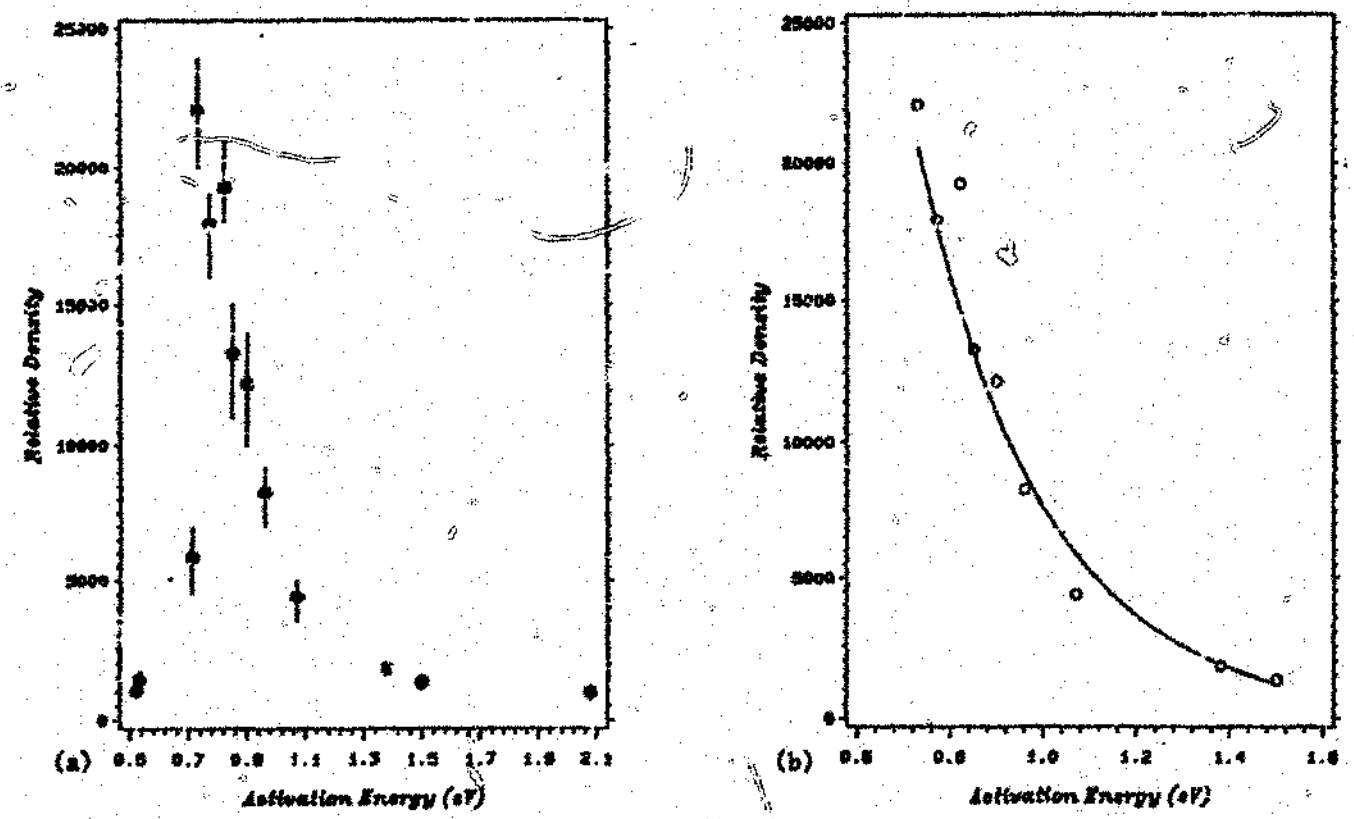

Figure 6.5: (a) The relative density of thermoluminescence states $N(E_m)$ at room temperature. (b) The exponential dependence of these states in the energy range from 0.7 eV to 1.5 eV. The theoretical curve is depicted by the solid line (—) while the experimental points are represented by the open circles (o).

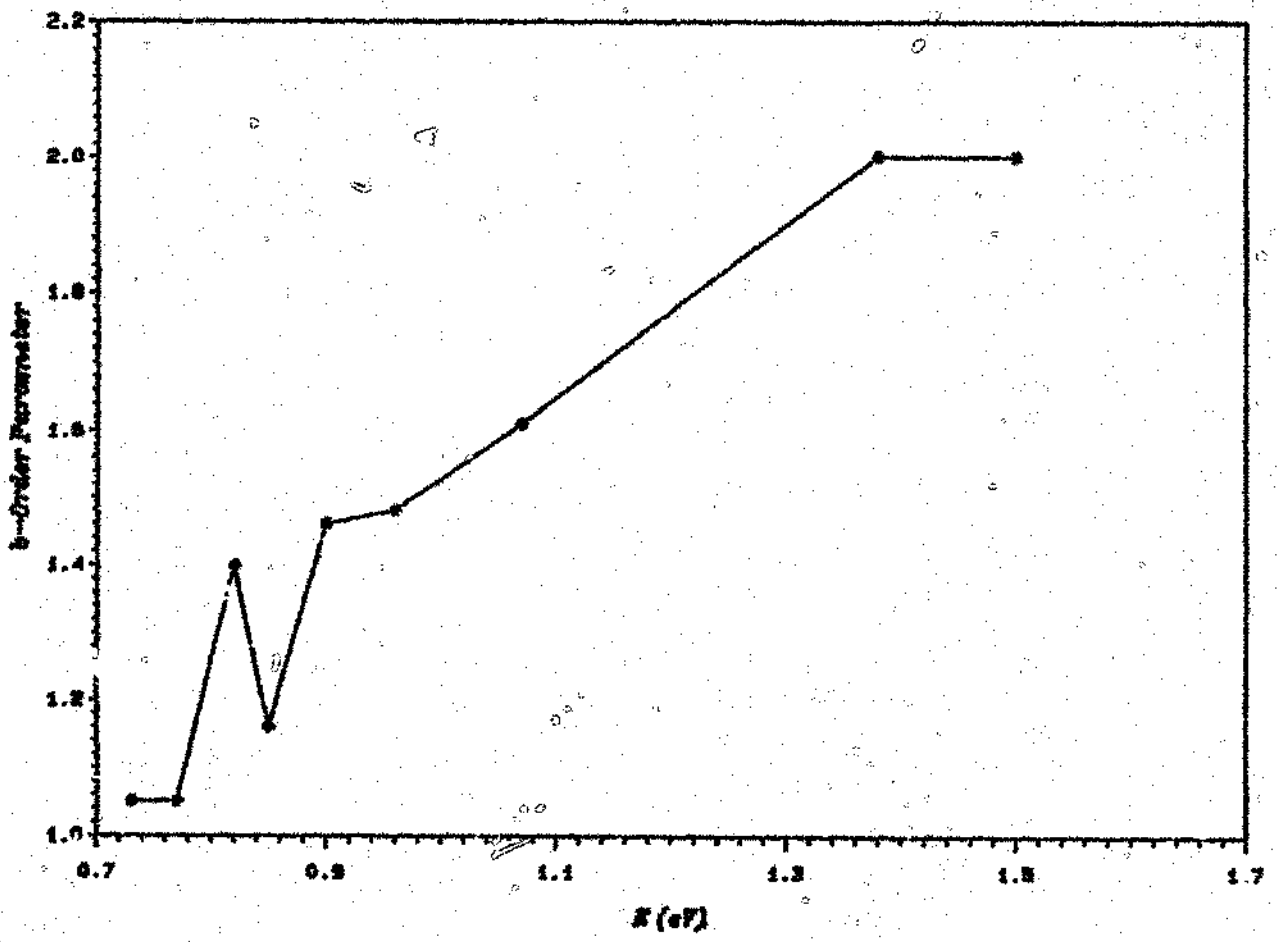

Figure 6.6: The behaviour of the order parameter (b) with the variation in thermoluminescence activation energies for the distribution of figure 6.5 (b).

thus introducing inaccuracies into the method. The exponential description of the density of states given in figure 6.5 (b) was derived by regression analysis which yielded a correlation coefficient of 98 % for the mono-exponential description of the experimental data. The following expression gives the result of this fitting procedure:

$$N(E_{ac}) = 3.02 \times 10^{2}\, e^{-3.64E_{ac}}$$

Such distributions of states have been postulated by Randall and Wilkins (1945b) and studied theoretically by Gobrecht and Hofmann (1966) to describe the thermoluminescence glow spectra observed from certain phosphors. An interesting property of this exponential distribution (figure 6.5 (b)) refers to the variation of the order parameter with activation energy, which is depicted in figure 6.6. A trend in which the order parameter increases with activation energy can be seen. Accepted interpretations (cf Chapter 5) associate order parameters greater than unity with the relative concentrations of activated recombination and trapping centres. In phosphors where the relative density of trapping and recombination centres is small, the mean free path for the radiative recombinations of charge carriers is larger, thus resulting in spectra with broader, non-first order glow spectra. In the example of the TLD diamond this trend is reflected by the fact that recombination and trapping centres are deactivated with each subsequent fractional glow cycle. The result is that the mean free path for recombination becomes progressively larger with increasing activation energy for this distribution.

The final characteristic of the thermoluminescence spectrum of the TLD diamond reported in this chapter refers to the variation of activation energy with the maximum temperatures of the fractional glow cycles used in this analysis. Figure 6.7 shows an increase in the activation energy with an increase in the maximum fractional glow temperature. This result is also in keeping with the trend displayed by a large class of phosphors (McKeever, 1985).

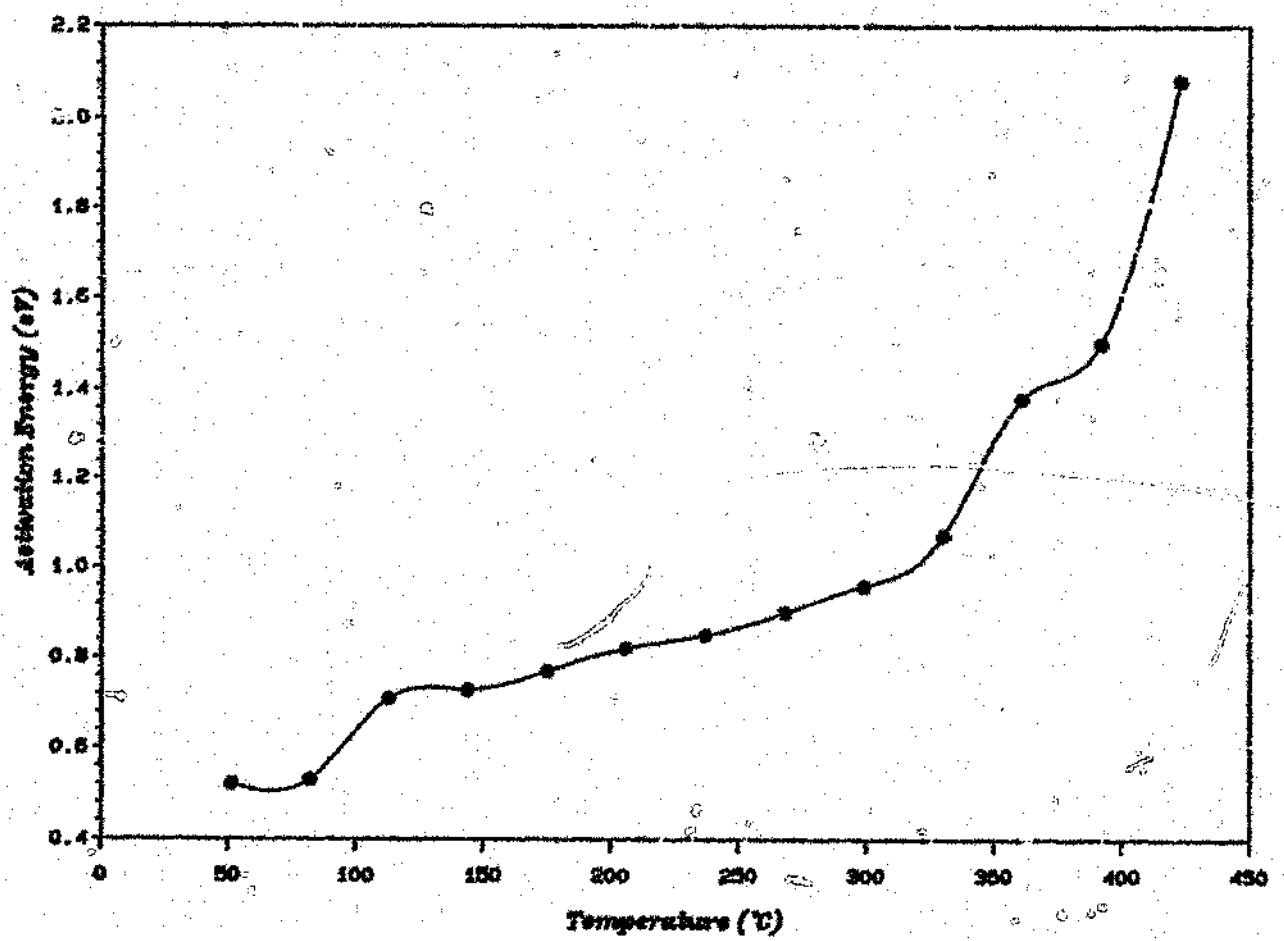

Figure 6.7: The dependence of the activation energy (E_m) with the variation in the maximum temperature of the fractional glow cycles.

6.3 Conclusions

The distribution of thermoluminescence states has been resolved by the technique of the fractional glow. Charge trapping states with activation energies ranging in value from 0.50 to 2.10 eV have been shown to be responsible for the thermoluminescence spectrum of the TLD diamond crystals. These estimates are utilised in the preliminary study of the radiophotoluminescence properties (to follow), where the ratio of optical to thermal activation energies are needed to provide an interpretation of the mechanism of optical excitations.

CHAPTER 7

Phosphorescence Properties of the Synthetic TLD Diamond

7.1 Introduction

A survey of the literature to date has shown that no analysis of the phosphorescence from the synthetic diamond TLDs of low paramagnetic nitrogen concentrations has been reported for application in radiation dosimetry. This chapter presents some of the isothermal decay characteristics of Fe-based synthetic diamond crystals, of low nitrogen concentration, as being favourable for application in *in vivo* radiation dosimetry. These synthetic diamond samples have been shown (Nam *et al.*, 1991) to have enhanced thermoluminescence responses due to an increased luminescence efficiency. This increased luminescence efficiency, resulting from a relatively smaller concentration of killer centres and a proportionally increased number of available charge trapping states, is exploited in this study of the phosphorescence response to varying β doses and dose rates.

Of equal importance to this dissertation is the physical interpretation and the implications of the isothermal decay spectra which have been included in the analysis presented in sections 7.2 and 7.3 of this chapter. Much effort has been devoted to the isothermal decay properties of phosphorescent materials by past researchers. In particular, the time dependence of the isothermal decay spectra measured has been used as a tool in the clarification of the processes occurring in such phosphors. Examples of such research can be found in the studies undertaken by Randall and Wilkins (1945), Medlin (1961a,b), Halperin and Chen (1966) and Avouris and Morgan (1981), among others. A classification of the observed isothermal decay measurements divides the characteristic luminescence decay from phosphors into two general groupings, viz. those exhibiting exponential luminescence decay characteristics and those exhibiting t^{-1} luminescence

decay characteristics. This study shows that a useful decay mechanism for radiation dosimetry, which is also a characteristic of these diamond crystals, is the exponential-type decay which results from a first order kinetic process. In this case the dependence of the luminescence intensity at a given delay time, subsequent to an initial irradiation treatment, is demonstrated to be linearly dependent on the applied radiation doses and dose-rates. The t^{-1} luminescence decay process has, however, been reported to occur under a given number of physical situations. Medlin (1961a) attempted to establish as the source of the t^{-1} dependence, the postulated occurrence of a radiative recombination process following a second order kinetic process. Subsequent analysis and experimental work (Medlin, 1961b) provided greater evidence for the t^{-1} luminescence decay, from the particular phosphors investigated, being a result of the first order recombination from a quasi-continuous distribution of charge trapping states with independent luminescence centres. Recently however, a mechanism for an inverse time dependence for the luminescence decay, was advanced by Avouris and Morgan (1981) wherein the type of luminescence decay was attributed to trapped charge carriers recombining at available recombination centres by a tunnelling mechanism.

What is however clear from the analysis (to be presented), is that the simplest and most useful process to utilize for radiation dosimetry, is one in which a first order kinetic process, from energy states having discrete, single-valued activation energies is prevalent. In the case of the synthetic diamond such states, which are thermally unstable at room temperature and occur in relatively high densities in these crystals, are demonstrated by this study to exist, thereby facilitating an easy readout process. The decay of luminescence at an elevated temperature of 40°C was also measured from the same diamond crystal and the characteristic decay rate compared to the value obtained when a similar measurement was performed at ambient temperatures. This was done to give an indication of the stability of the technique with an accompanied variation in temperature and hence the suitability of this method for dosimetry. The main motivation for the choice of the elevated temperature of 40°C for the comparison of the decay constants, lies in the fact that temperatures in excess of this value are known to result in a risk of

tissue damage in humans (Thorn *et al.*, 1973). At core body temperatures, below 32°C, loss of consciousness can occur. It is therefore expected that applied radiation procedures performed on human subjects will always be undertaken at temperatures below 40°C and above 32°C.

The radiophosphorescence technique, as applied, comprised an initial irradiation, the dose of which was to be determined, of the diamond sensor with β radiation from a ^{90}Sr source. The phosphorescence yield, at a given delay time post-irradiation, due to the total emission of all wavelengths, was then measured as the phosphorescence response.

7.2 Exponential Isothermal Decay Spectra

The measurement of the isothermal decay spectra was performed at room temperature and elevated temperatures, with the experimental arrangement described in §2.3. After an initial exposure of the TLD diamond to ionising radiations, the subsequent luminescence decay with time was measured and stored on a Personal Computer for further analysis and data manipulation. Excitation of luminescence was achieved with β, α and ultraviolet radiation sources. Shown in figure 7.1 is the luminescence decay measured at room temperature after an initial excitation with an ^{241}Am alpha particle source of 14.8 MBq cm^{-2} specific activity. The data was acquired at a resolution of 20 seconds. All measurements were corrected for background noise. The solid line passing through the data points represents the theoretical description of the data set. For diamond crystals with luminescence decay resulting from a single species of charge trapping state, following a first order kinetic process, the luminescence decay is expected to follow the form given in expression 4.5. In the case where a number (N) of such charge trapping states are present and all follow a first order kinetic process, the luminescence is expected to be a linear superposition of decaying states, given by:

$$I(t) = \sum_{n=1}^{N} i_n(t_0) \times \exp(-t/\tau_n) \qquad (7.1)$$

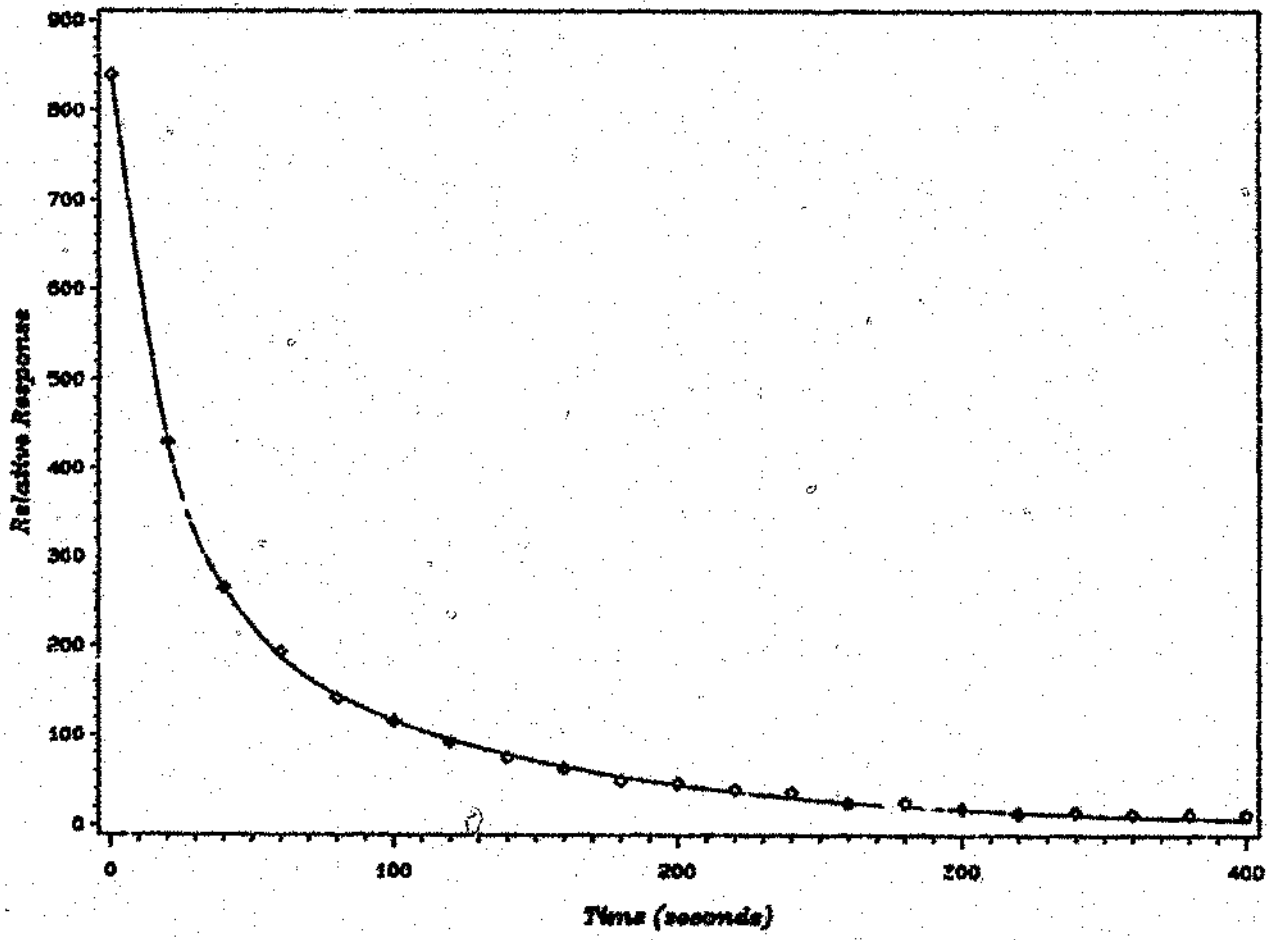

Figure 7.1: The isothermal decay of luminescence at room temperature after an excitation with an ^{241}Am alpha source.

The algorithm used to generate the fit of figure 7.1 has been described in §3.3. Twice the number of components ($2N$) were assumed for each application of this algorithm. The choice of N which minimised the sum of the error squared for each data point (SSQ) was taken to be indicative of the number of phosphorescence components. In this procedure, the number of components for the uncorrected data (no background correction) was fitted to an optimum of three components, one of which had a rate constant $\frac{1}{\tau} \approx 1$, and an amplitude which agreed excellently with the measured background signal. The values of the two other components were then stored for subsequent comparison. The background correction was applied and the procedure for determining the optimum fit was repeated. Subsequent fits, which converged at optimal solutions for two exponential components, were compared to previous values obtained for consistency. Tabulated values of the amplitudes (relative strengths) for each component with the corresponding characteristic rate ($k = 1/\tau$) can be found in Table 7.1.

Table 7.1

n	$L(k)$ (arbitrary units)	k_n (s^{-1})
1	288.8	0.009
2	551.0	0.053

Excitation of luminescence with the α-source resulted in the components listed above. When excitation was effected with β and UV sources, however, the rapidly decaying component (k_2) was not detected. The presence of component (k_1) with the slower characteristic decay rate, was in all the measured spectra and was established to be independent of the type of excitation. Similar measurements of the characteristic decay rates, performed on different diamond crystals, at room temperature, under ultraviolet and β excitation, yielded decay rates of the order of 0.013 ± 0.002 s^{-1}. The accuracy to which these components could be measured, was affected by such factors as the back-

ground noise which had to be corrected for, the resolution with which the luminescence intensity was measured as well as the marginal differences in sensitivity which occurred from crystal to crystal. Of significance to the physical interpretation of the data is the fact that isothermal spectra with an exponential-type dependence implies that the decay rate is independent of the radiation dose. In particular,

$$I(t_0) = C n_0 s e^{-E/kT} = C n_0 \tau^{-1} \qquad (7.2)$$

so that the characteristic decay constant is now defined in terms of the activation energy (E) and frequency factor (s) of the charge trapping states under consideration. Here C is an arbitrary normalisation constant and n_0 is the initial trapped charge concentration. For a given diamond crystal at a fixed temperature, the characteristic decay parameters (τ's) in equation 7.1 are constants because the frequency factors (s) and the trapping depths (E) are dependent on the nature of the defects responsible for the trapping states. The latter are clearly fixed for a given diamond crystal at a given temperature. The $I(t_0)$'s described by expression 7.2 are therefore directly proportional to the initial trapped charge concentrations (n_0's) and hence the incident radiation dose. This predicted behaviour has been verified by the measurement of the luminescence intensity as a function of the incident radiation β dose. Depicted in figure 7.2 is the result of these measurements. The linear form provides further evidence for the postulated existence of a first order kinetic process due to discrete charge trapping states in the forbidden gap of these diamond. The experimental procedure used to derive this data involved irradiating the diamond TLD with the ^{90}Sr source, while already mounted in the copper strip, and then loading the sample in the arrangement shown (figure 2.1). The luminescence yield was then measured at 60 seconds post-irradiation. To return the sample to the virgin state, the diamond TLD was annealed, while mounted in the copper strip at 400°C for 10 minutes. In this way the effect of differences in sample geometry was eliminated. As can be seen, a linear dependence of the luminescence intensity on the radiation dose up to 3 Gy was achieved. The saturation effect is interpreted as a limita-

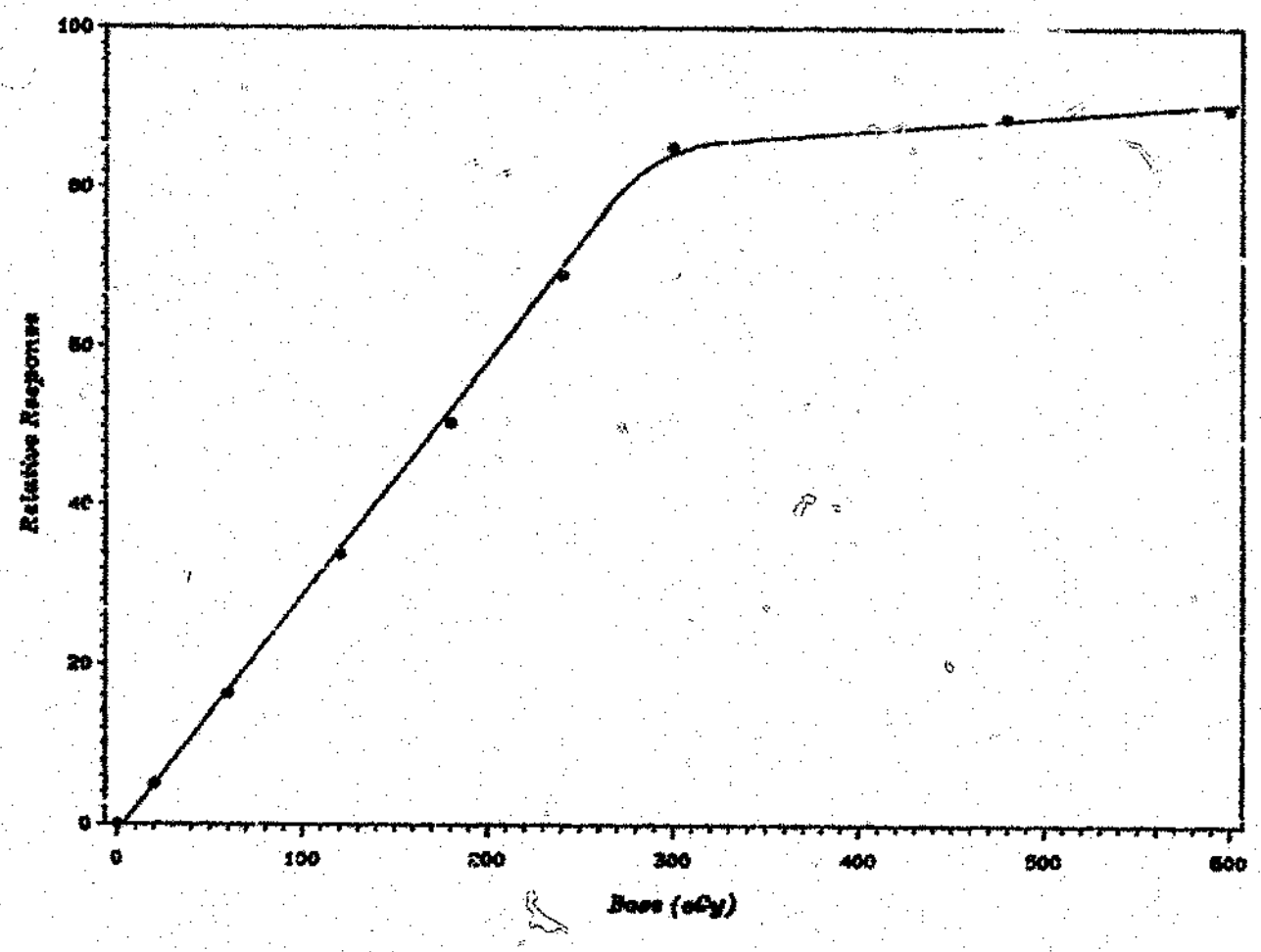

Figure 7.2: The phosphorescence response as a function of β dose from a 10 mCi ^{90}Sr source.

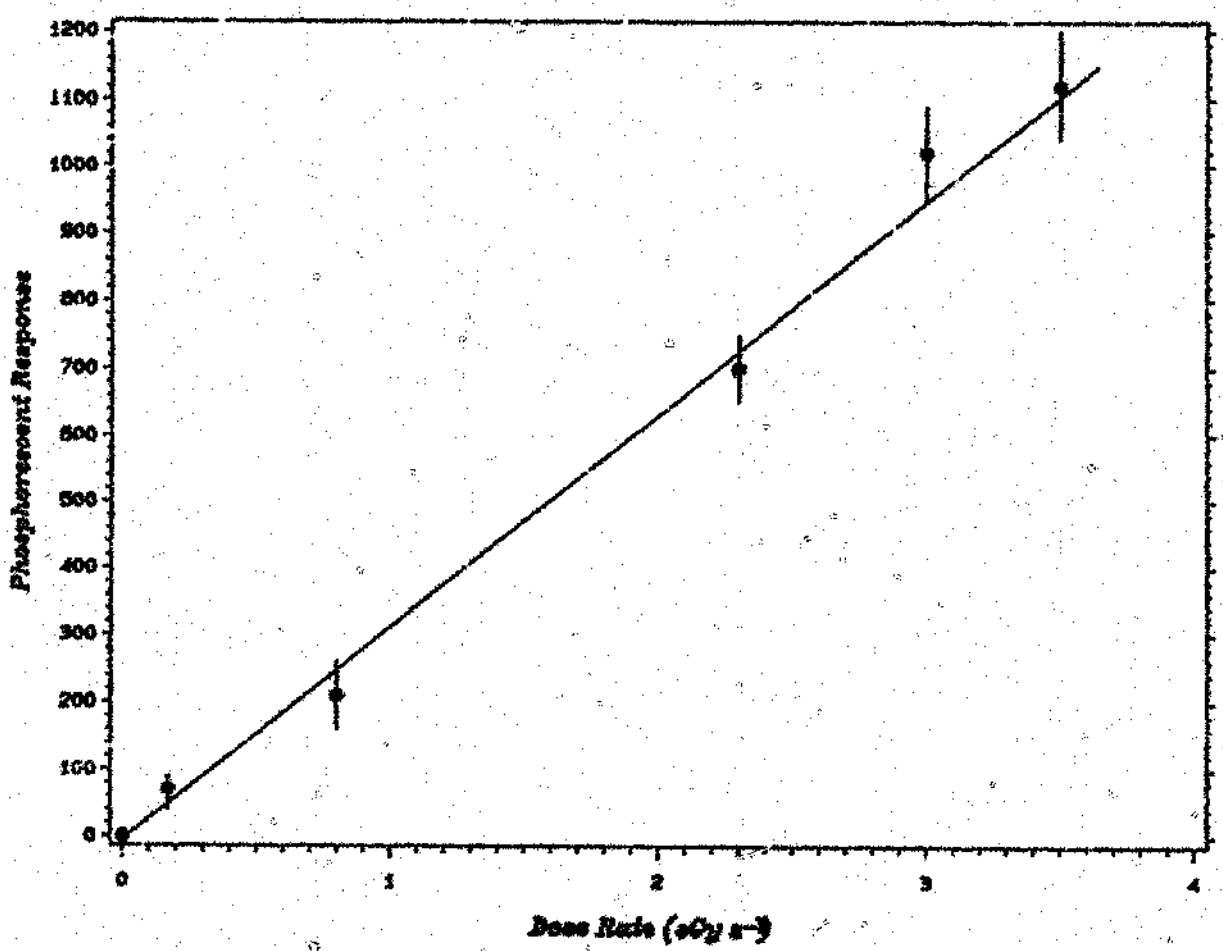

Figure 7.3: The phosphorescence response as a function of the β dose rate from a 10 mCi ^{90}Sr source.

tion of the total concentration of shallow charge trapping states responsible for the measured luminescence decay.

The result of a similar experiment in which the diamond TLD was subjected to β dose rates below 4 cGy s^{-1}, is given in figure 7.3. These measurements were effected by placing the diamond crystal at different distances from the ^{90}Sr source for 30 seconds, and then measuring the phosphorescence response at a fixed interval post-irradiation. The linear form of this result also attests to the first order nature of the recombination process.

In order to assess the effect of a change in temperature upon the change in magnitude of the characteristic decay lifetime of the shallow charge trapping states, these lifetimes were measured for a given crystal at room temperature and 40°C for comparison. Figure 7.4 gives the result of this measurement in which the same diamond crystal was given different UV radiant exposures at 20°C and 40°C. The fitted values for the decay lifetimes show a difference in value of 2 %. The relative change in the phosphorescence intensity resulting from this 2 % change in the decay lifetime, can be shown to be of the following form:

$$\frac{\Delta I(t)}{I(t)} \sim \Delta\tau \left[-\frac{1}{\tau} + \frac{1}{\tau^2} \right] \qquad (7.3)$$

A consideration of the first order approximation in $k = 1/\tau$ (i.e. if all the terms containing factors of the form $(1/\tau)^n$, with $n > 1$ are discarded) reveals the following simple form for the maximum relative change in the phosphorescence intensity due to the corresponding relative change in the characteristic lifetime (τ):

$$\left| \frac{\Delta I(t)}{I(t)} \right|_{max} \sim \left| \frac{\Delta\tau}{\tau} \right| = \left| \frac{\Delta k}{k} \right| \qquad (7.4)$$

This means that the change in 2 % in the decay rate (k) gives a corresponding change of 2 % in the relative change in intensity at a given time (t). These excellent stability

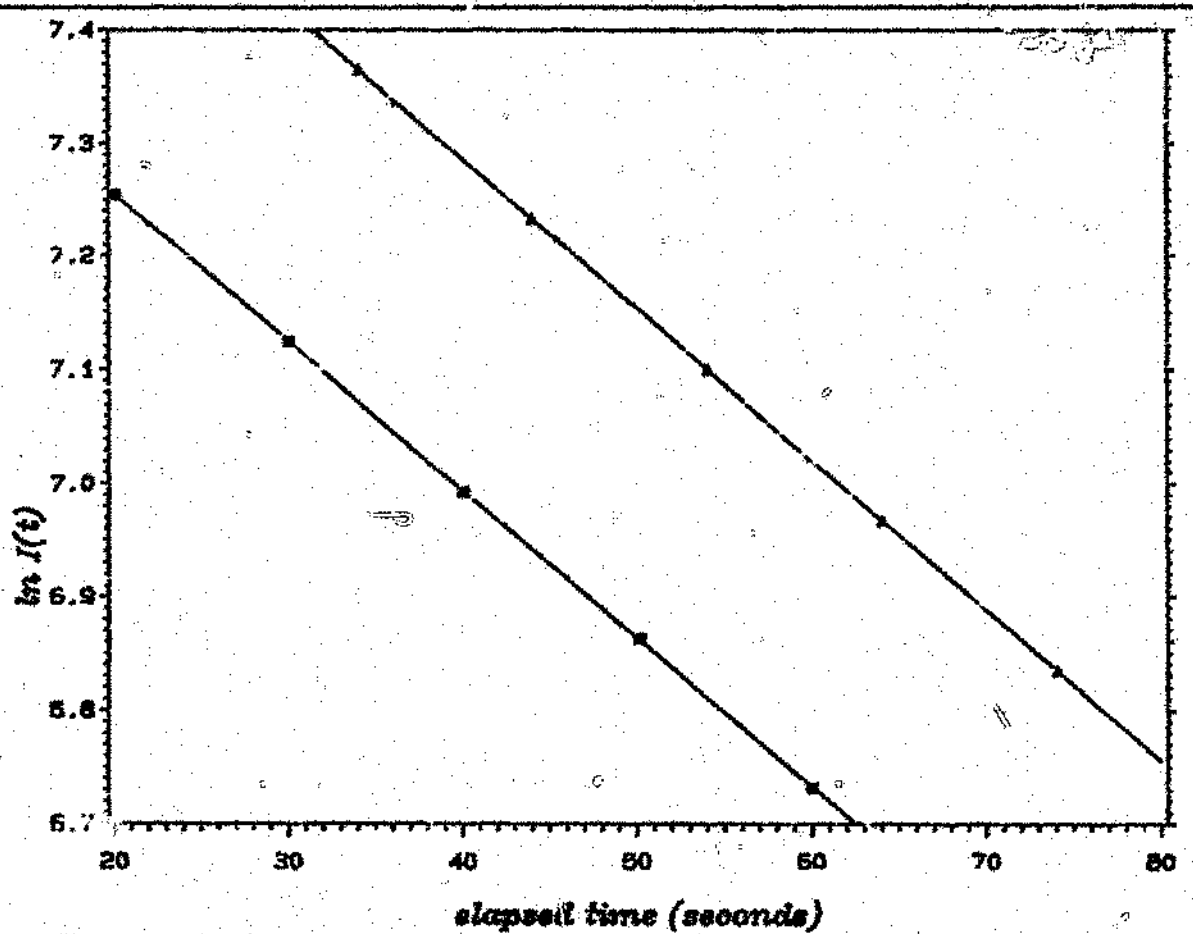

Figure 7.4: The phosphorescence response as a function of the sample temperature. The solid lines represent the fitted curves. The data set represented by the boxes (■) was acquired at 40°C while those acquired at 20°C are represented by triangles (▲).

characteristics ensure a uniform response to incident radiation at temperatures in the range of values from room temperature to 40°C.

7.3 Inverse-time dependent Isothermal Decay Spectra

Unlike phosphorescence decay spectra conducted at room temperature, the luminescence decay of the TLD diamond undertaken at higher temperatures (> 100°C) does not display a simple exponential dependence. When attempted fits of the experimentally measured data to a series of 1 to 10 exponential components was made, the correlation coefficient derived was unacceptably low for each of the respective attempts. However, fitting procedures which performed a parameter minimisation by the MINUITS search algorithm, using expression 4.6, was found to provide more reliable descriptions of the experimental data. Such an expression has been successfully applied to situations in which the observed luminescence has been assumed to be due to first order decay from a distribution of trapping states (Medlin, 1961b).

Shown in figures 7.5, 7.6 and 7.7 are the experimentally determined luminescence spectra obtained at sample temperatures of 150°C, 200°C and 220°C, respectively. These measurements were also performed using the experimental arrangement of figure 2.1. Table 7.2 contains the values of parameters obtained from the fitting procedure. The quantitative interpretation of these parameters is made difficult by the interference of luminescence from overlapping charge trapping states and the variation in the luminescence spectra observed with different UV radiant exposures of particular diamond crystals at identical temperatures. In cases where the relative distribution of charge trapping states varies over an appreciable range of energy values (Medlin, 1961b), the former effect can be serious. Nevertheless, it can be concluded that the analysis of the distribution of charge trapping states of the previous chapter, and evidence of

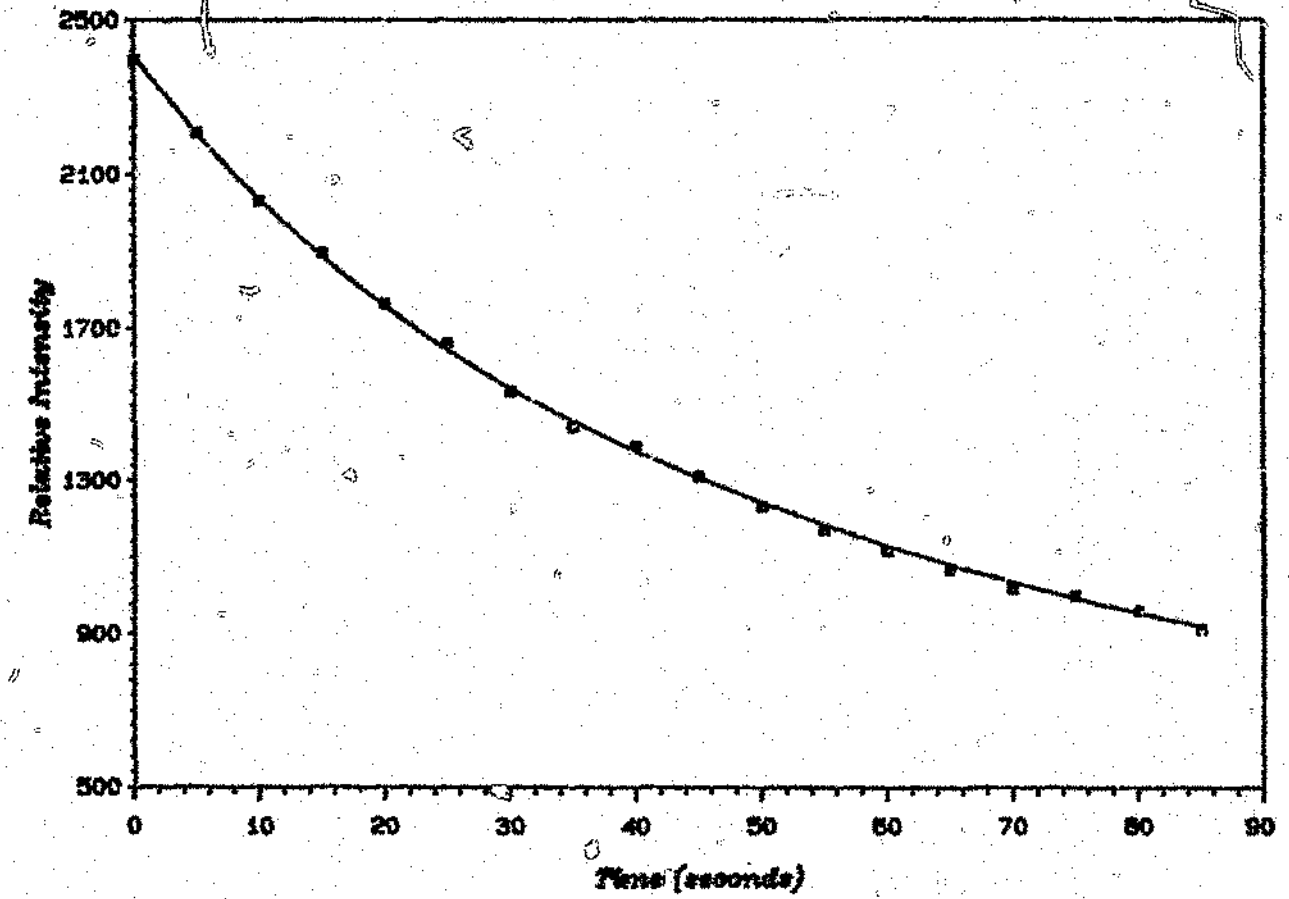

Figure 7.5: The isothermal decay spectrum measured at a sample temperature of 150°C. The solid line represents the fitted curve.

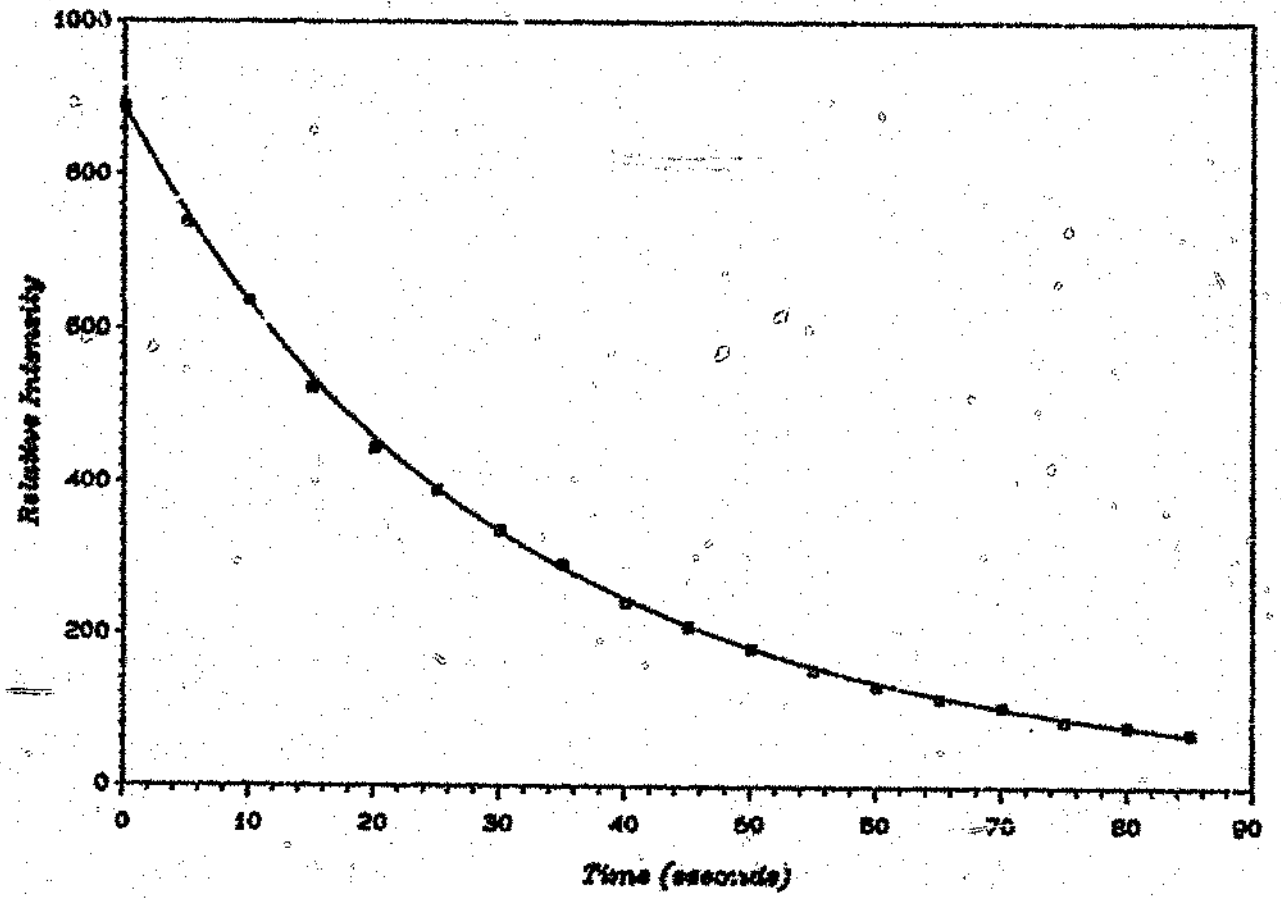

Figure 7.6: The isothermal decay spectrum measured at a sample temperature of 200°C. The solid line represents the fitted curve.

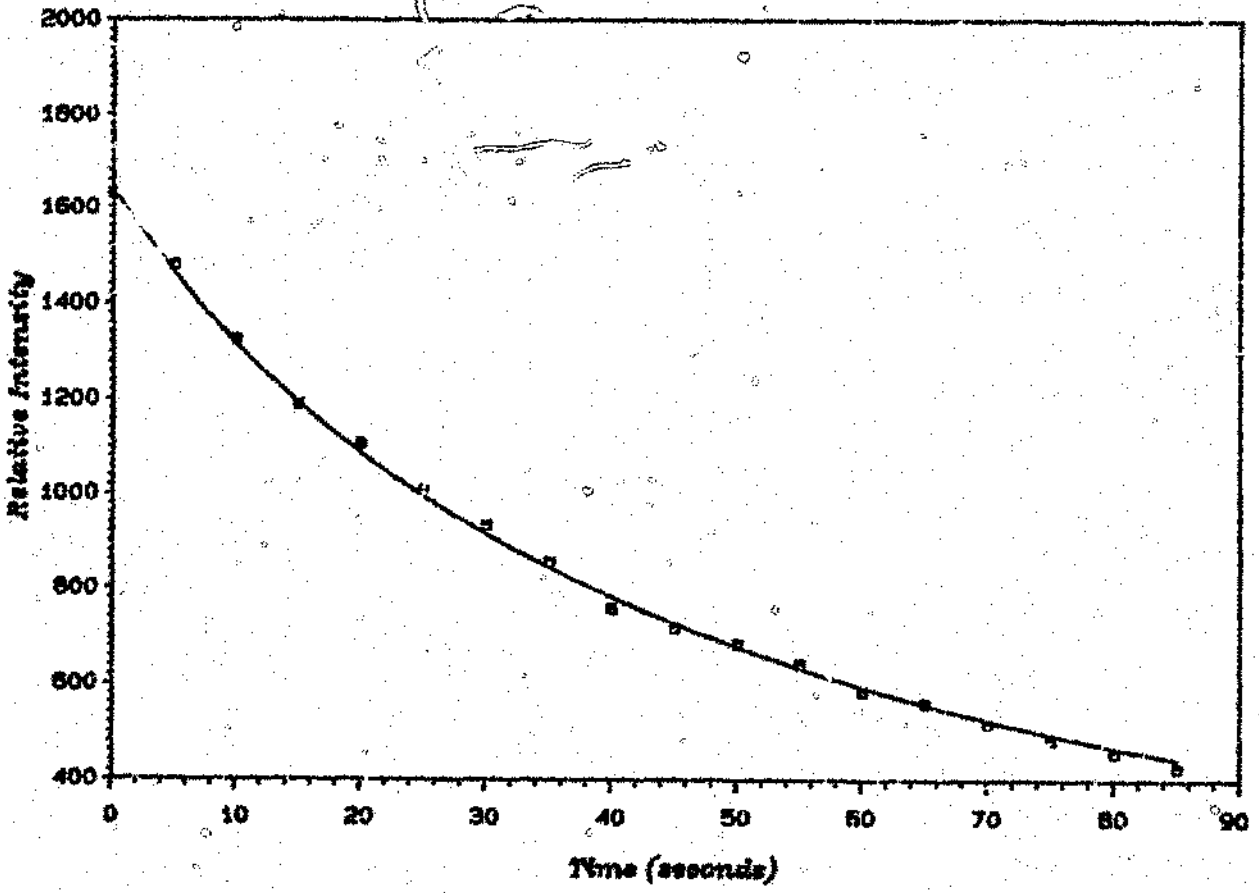

Figure 7.7: The isothermal decay spectrum measured at a sample temperature of 220°C. The solid line represents the fitted curve.

Table 7.2

Temperature (°C)	I_0 (arbitrary units)	t_c (seconds)	m
150	2411	58.6	1.02
200	888	330	11.2
220	1635	73.7	

inverse-time dependence of the luminescence spectra observed at elevated temperatures presented in this chapter provide support for the postulate that the inverse-time dependent decay is the result of a distribution of trapping levels in these synthetic diamond crystals.

7.4 Conclusions

The results presented in this chapter show that shallow charge trapping states in the forbidden gap of the TLD diamond crystals can give rise to crystals with characteristic radiophosphorescence presenting favourable dosimetry properties over the temperature range from 20°C to 40°C. An important requirement, which these diamond fulfil for phosphorescence dosimetry, is the presence of charge trapping states having discrete, single-valued activation energies which are also thermally unstable at room temperature. Linearity and stability of response (±2 %) as a function of the incident dose rate at temperatures ranging in magnitude from room temperature to the maximum temperature sustainable by the human body, and the feasibility of a thin probe with a 1 mm³ diamond at one end of an optical fibre, are features which could make these diamond particularly attractive for application in *in vivo* and *in situ* dosimetry applications; an evaluation of which is beyond the scope of this dissertation.

CHAPTER 8

Radiophotoluminescence Properties of Synthetic TLD Diamond

8.1 Introduction

For this part of the study the RPL properties of the diamond crystals were investigated. The radiophotoluminescence technique, as applied, comprises an initial irradiation of the diamond sensor with γ or β radiation. The sensor is then exposed to light of pre-selected bandpass wavelength. The intensity of the resulting emitted light, centred about the principal emission wavelength, is then measured as the RPL response. The work reported in this chapter focuses on the variation of the radiophotoluminescence signal with time and with the irradiation dose, in particular. In order to gain an understanding of the kinetics of radiophotoluminescence, the optical excitation properties of these diamond crystals were initially probed in the preliminary part of the study. In this way cognizance of the superposition of the effects of optical stimulation upon the RPL-signal were accounted for.

8.2 Preliminary Measurements and Discussions

8.2.1 The Optical Bleaching Measurements

A Bausch & Loumb high intensity Xenon light source with an attached monochromator assembly unit (§ 2.5) for operation in the 350-900 nm wavelength region was used to effect all optical bleaching measurements. The term bleaching is understood to mean the process of depopulation of all traps throughout the discussions of the measurements. For the pre-heating cycle the sample was ramped at a rate of 16°C s^{-1} from room temperature to a maximum readout temperature of 280°C.

For the measurements, the diamond crystal was given a 3 Gy β particle dose, then illuminated after a time delay of two minutes post-irradiation, for a period of three

minutes with light of pre-selected wavelength. A subsequent thermoluminescence read-out process which involved ramping the temperature of the diamond TLD at 16°C s^{-1} from room temperature to a maximum readout temperature of 450°C was initiated after a further delay of two minutes post-illumination. This use of a fixed time cycle allowed a correction for the loss of thermoluminescence signal, due to the liberation of charge carriers by thermal means, to be made. The difference between the integral thermoluminescence glow with the sample not having been illuminated, and defined here as I_{nb}, and when the sample was illuminated with light of pre-selected wavelength, denoted I_b, was taken to be the optical bleaching response of the specimen at that wavelength (λ). This procedure was carried out at a number of wavelengths with results as depicted in figures 8.1 and 8.2 which show the optical bleaching spectrum of the thermoluminescence glow curve obtained without (figure 8.1) and with pre-heating (figure 8.2). The percentage bleaching was derived using the following relationship which expresses the optical bleaching response $R(\lambda)$ in terms of I_{nb} and I_b as well as a lamp correction factor, L_λ, (see § 2.5) used to account for the non-uniform spectral response of the Xenon lamp.

$$R(\lambda) = L_\lambda \left(\frac{I_{nb} - I_b}{I_{nb}} \right) \qquad (8.1)$$

These measurements gave an indication of the effectiveness with which light of a given wavelength depopulated the thermally accessible charge trapping states in these diamond crystals. The optical bleaching spectra of the figures 8.1 and 8.2 also reflect the composite nature of the thermoluminescence spectrum. As can be seen the response as depicted in figure 8.1 exhibits no distinct peaks. Figure 8.2 on the other hand shows the result of pre-cleaning, which has the effect of shifting the bleaching band edge to the shorter wavelengths. The approximate excitation energy at which this band edge occurs

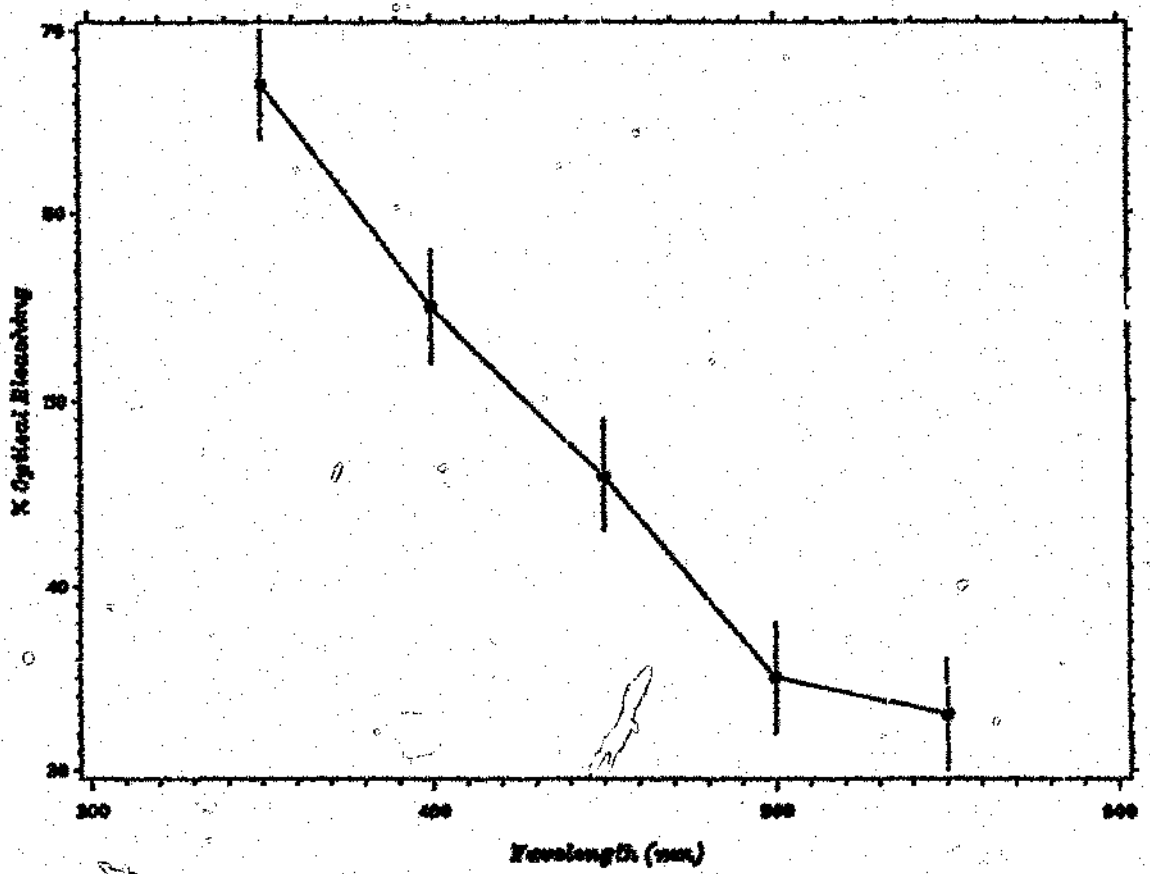

Figure 8.1: The optical bleaching response of the thermoluminescence curve obtained when no pre-cleaning cycle was utilised.

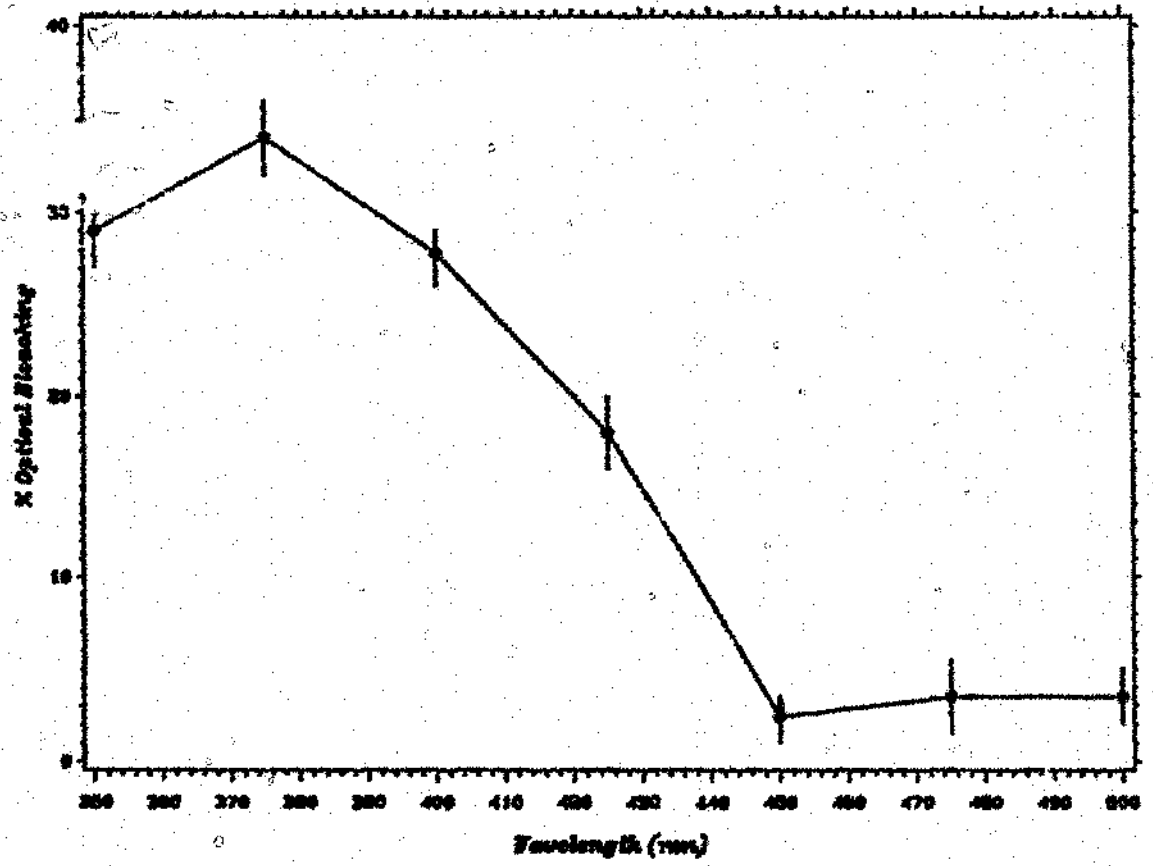

Figure 8.2: The optical bleaching response of the thermoluminescence curve obtained when a pre-cleaning cycle in which the temperature of the diamond crystal was ramped from room temperature to 280°C at 16°C s^{-1} was utilised.

is 3.0 eV. The result of these measurements show that radiophotoluminescence is in principal achievable by the use of light of sufficiently high intensity. The pre-cleaned thermoluminescence glow curve has been found, by the analysis of Chapter 6, to be the result of glow from a distribution of charge trapping states having thermal activation energies (E_{trap}) in the 1.6 eV-2.1 eV range, with a dominant contribution from trapping levels having a mean activation energy of approximately 2.0±0.2 eV. In addition, the optical excitation process for a given trap depth, is expected to have a characteristic bandwidth due to the vibrational degree of freedom of the complex (/defect centre) giving rise to that defect level. The ratio of E_{trap}/E_{trap} for the charge trapping states responsible for the pre-cleaned glow curve is approximately 1.5. Ratios of this nature have been determined by Nahum *et al.* (1963) in an analogous manner for natural diamonds of Type I. Values ranging from 1.5 to 2.5 have been cited. The figure of 1.5 determined in this study suggests that the mechanism as depicted in figure 8.3, and applicable to Stokes-type phosphors, is also applicable to these diamond crystals at ambient temperatures.

8.2.2 The Optical Bleaching Exposure Response at 375 nm

Taking cognizance of the large optical bleaching response of the pre-cleaned thermoluminescence spectrum at 375 nm, the optical bleaching response at this wavelength as a function of the radiant exposure was studied. Figure 8.4 summarises the result of this investigation. These measurements provided further elucidation of the mechanism by which the optical bleaching of states occurs. Here a model described by Chen *et al.* (1970) and applied by Israeli *et al.* (1971) for the description of the excitation of thermoluminescence in KBr, proved useful. In these studies the population of thermoluminescence states in terms of the absorption of light in an arbitrary solid, containing a uniform density of charge trapping states and recombination centres, was considered. According to such a model, the relative optical bleaching response $\eta(x)$, at

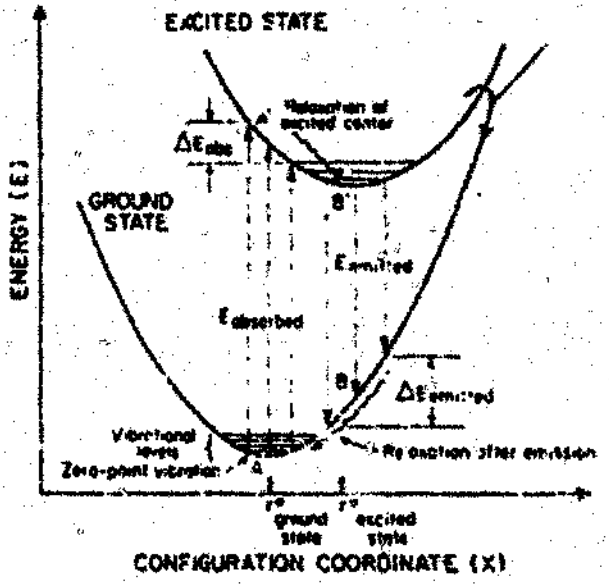

Figure 8.3: The configurational diagram showing the relationship between optical and thermal activation energies for a hypothetical defect centre.

relatively large values of the optical absorption coefficient, $\mu(\lambda)$, is determined by the following relationship:

$$I(x) = 1 - \left(\frac{1}{\mu L}\right)\int_{\alpha x \mu e^{-\mu L}}^{\alpha x \mu} d\left(\frac{e^{-x'}}{x'}\right) \qquad (8.2)$$

where x is the radiant exposure, α is a proportionality constant and L is the sample thickness. At low radiant exposures, the response is expected to be linear in the first approximation, and may be expressed in the following convenient form:

$$I(x) = \frac{\alpha \mu x}{L}\left(1 - e^{-\mu L}\right) \qquad (8.3)$$

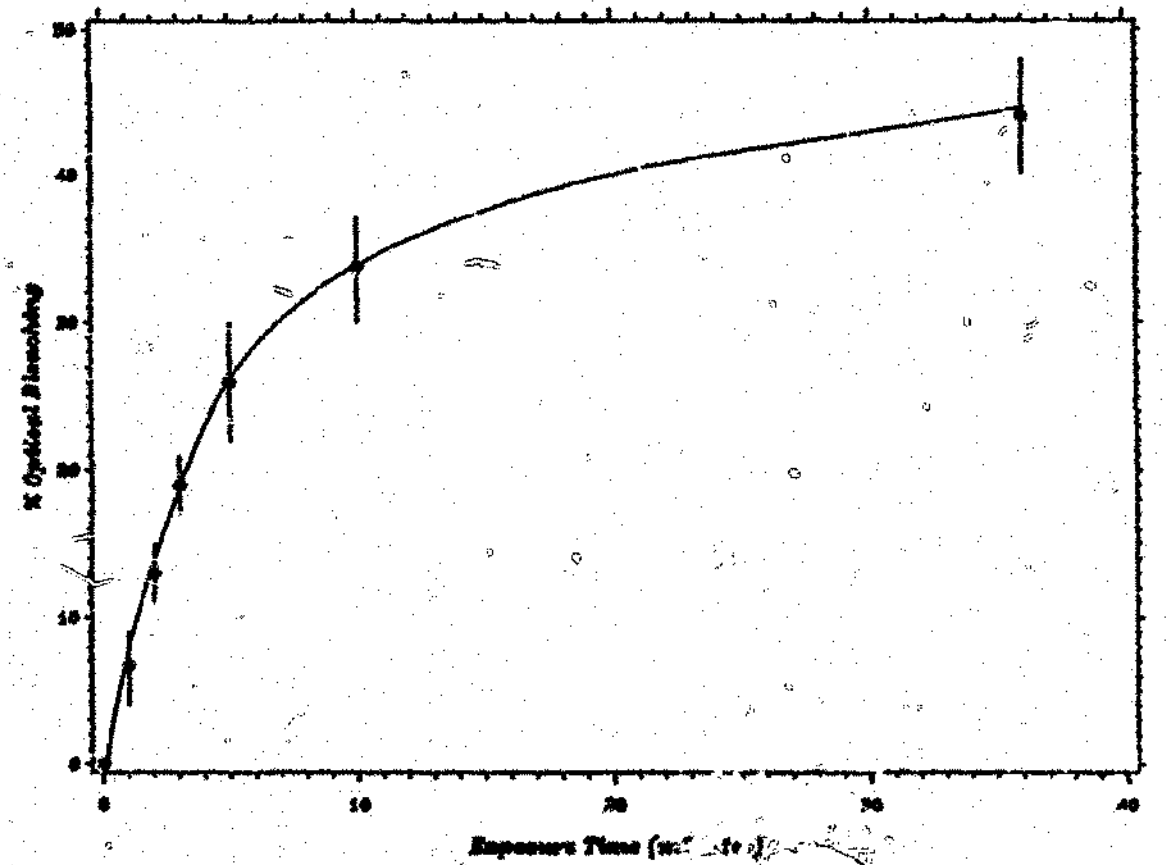

Figure 8.4: The optical bleaching response of the pre-cleared thermolu[illegible]nce glow curve as a function of the radiant exposure at 375 nm.

Although the spatial distribution of defect centres in these diamond may not be uniform, this model is believed to be a good first approximation to the true situation in these crystals. The assumption of a relatively high optical absorption coefficient in the derivation of the theoretical model was fulfilled by the choice of 375 nm as the optical bleaching wavelength. As can be appreciated from the inspection of the optical absorbance spectrum of these diamond (cf Appendix II), the optical absorption coefficient increases in magnitude on moving to the shorter wavelengths in the ultraviolet region of the spectrum. This result of the optical bleaching measurement with radiant exposure as illustrated in figure 8.4 shows an initial linear region with the tendency for saturation to set in at relatively low values of radiant exposure. These effects can be accounted for by the relatively short effective path length of ultraviolet light in the crystal. Such a dependence of the measurements is qualitatively similar to the form described by equation 8.2. From expression 8.3 it can be appreciated that the radiant exposure response is dependent on the sample thickness (L). In the case of the synthetic diamond crystals used in this study this effect could be neglected from crystal to crystal, as the dimensions of the crystals used in this study were constant to within a small standard deviation. The physical significance of these measurements is that the stimulating light photons liberate charge carriers which, because of the predominantly first order nature of the thermoluminescence process, then recombine at luminescence centres (cf Chapter 6). It is therefore expected that an RPL response to excitation light can be measured due to the radiative recombination of liberated charge carriers at luminescence centres. This formed the motivation for the measurement of the RPL response of the thermally accessible charge trapping states within the diamond crystal as a function of β and γ doses. Taking cognizance of the optical bleaching response as a function of wavelength (figures 8.1 and 8.2) the 404.7 nm Mercury line was chosen as an appropriate and easily available source of excitation wavelength with sufficient intensity.

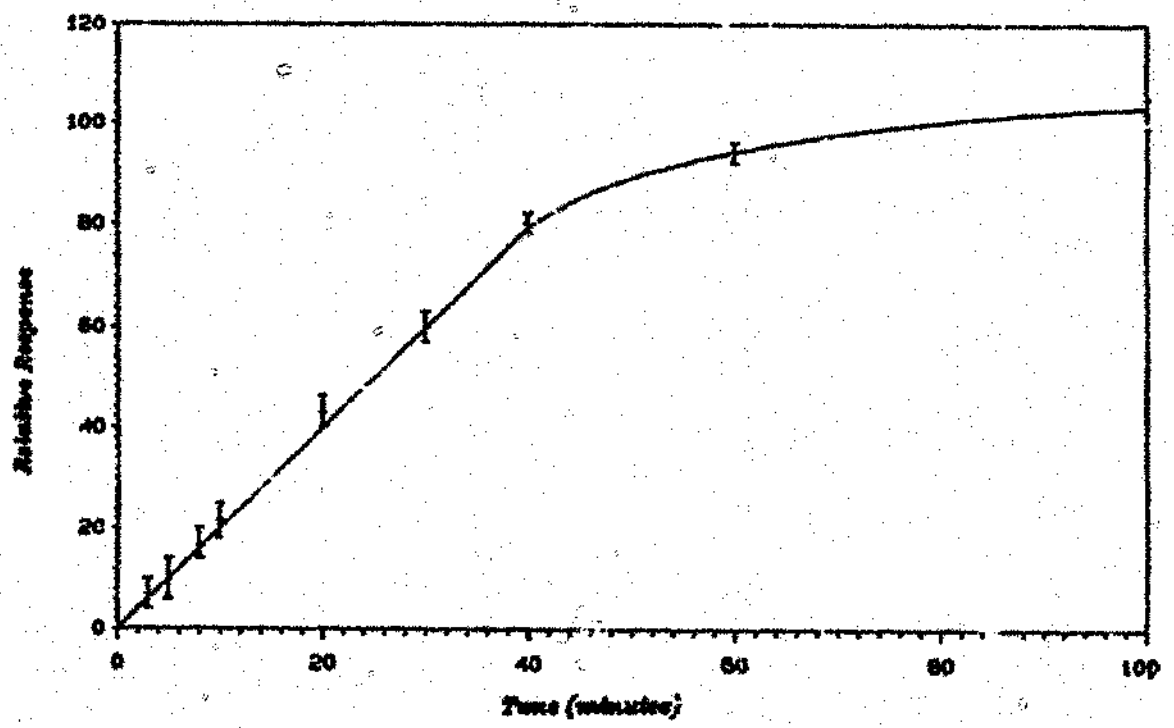

Figure 8.5: The radiant exposure response of the TLD diamond to illuminations at 250 nm. The integral thermoluminescence response when a readout cycle of ramping at 16°C s^{-1} to a maximum temperature of 450°C was instituted, is given as the *y*-ordinate.

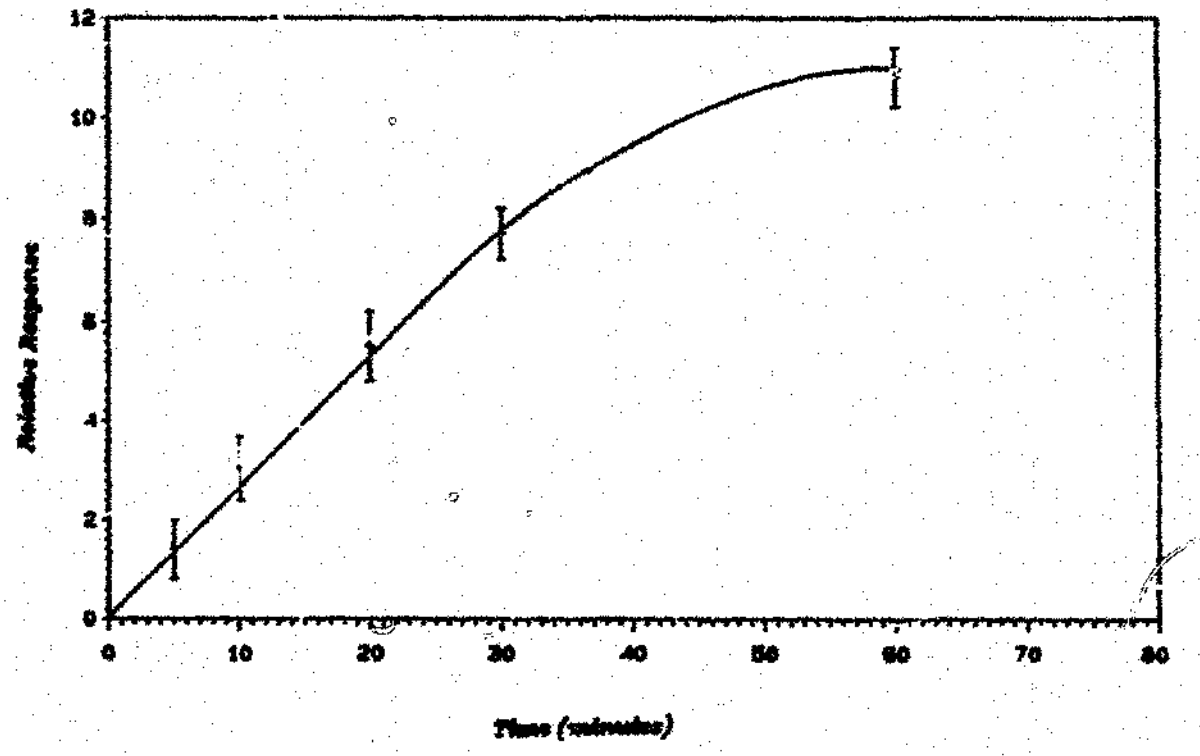

Figure 8.6: The radiant exposure response of the TLD diamond to illuminations at 250 nm. The integral thermoluminescence response when the usual pre-cleaning cycle (cf text) was instituted, is given as the *y*-ordinate.

8.2.3 The Intrinsic Radiant Exposure Response at 250 nm

The radiant exposure response of the TLD diamond to ultraviolet light was studied to determine the onset of band transitions in the diamond crystal not previously subjected to radiation treatment. This was done in order to exclude the superposition of such effects from the RPL measurements. It was found that light of 250 nm resulted in filling of thermoluminescence states in proportion to the radiant exposure. The radiant exposure response measurements (figures 8.5 and 8.6) were achieved by exploiting the second order diffraction component at the 500 nm setting of the Bausch & Loumb monochromator in conjunction with the use of a 252±10 nm bandpass filter. For this part of the study the diamond was subjected to illuminations of varying intervals, followed by a measurement of the integral thermoluminescence response. Depicted in figures 8.5 and 8.6 are the radiant exposure responses obtained from the integral glow measurement effected without and with the pre-cleaning cycle described earlier. This behaviour is believed to be consistent with the interpretation that light of 250 nm is capable of ionising hole centres above the valence band, resulting in the filling of thermoluminescence states. This effect is also thought to be responsible for the observed *'extension'* of the fundamental optical absorption band edge of these (cf Appendix II) and other Type I diamond (Kaiser and Bond, 1959). Further evidence for this postulate, rather than the postulate that the filling of thermoluminescence states is due to transitions from the valence band edge directly to energy levels responsible for the thermoluminescence spectrum is provided by the fact that the entire spectrum ranging from room temperature to 450°C is excited. If the thermoluminescence spectrum was selectively excited, the latter postulate would be more feasible. If it is assumed that the optical activation energy for the filling of thermoluminescence states is commensurate with the energy of a light photon of approximately 250 nm, the difference in the intrinsic energy gap for diamond (5.48 eV) and this optical activation energy provides an estimate of 0.53 eV for the position of the hole centre above the valence band. Energy levels of

this nature could possibly explain the quenching of luminescence observed and discussed in Chapter 6 for these synthetic diamond crystals.

The linearity of response of these diamond to ultra-violet radiant exposures suggests a practical application of this phenomenon for use as ultra-violet dosimeters, in which an interest has been shown (Mehta and Sengupta, 1978; Lakshmanan *et al.*, 1978) for biomedical research as well as personal dosimetry. For phosphors such as LiF use of the F-centre has been made for ultra-violet dosimetry. The phosphor is *'sensitised'* by applying a large initial γ dose, filling the both shallow and deep charge trapping states. The shallow traps are subsequently bleached by a normal thermoluminescence readout cycle, so that all but the deepest traps are emptied. As a dosimeter the radiant exposure response to ultraviolet light, which is demonstrated to empty the deep trapping states, thereby transferring the charge to shallower trapping states which are accessible by the thermoluminescence technique, is measured. A normal thermoluminescence readout can then provide a measurement of the radiation dose.

The application of the diamond TLD as an ultra-violet dosimeter appears to be more promising when it is considered that a sensitisation process is not necessary, thereby eliminating a step in the readout procedure. Of primary importance to the RPL study, is that special care had to be taken to ensure that the diamond samples are not exposed to light of wavelengths shorter than or equal to 250 nm. In this manner the superposition of the effects from light of these wavelengths with the RPL-signal could be eliminated.

8.2.4 Phototransference Measurements

In order to verify the existence of deep, thermally inaccessible charge trapping states the phototransference characteristics of the TLD diamonds were studied. For this part of the study the TLD diamond which had been annealed, β dosed and undergone a

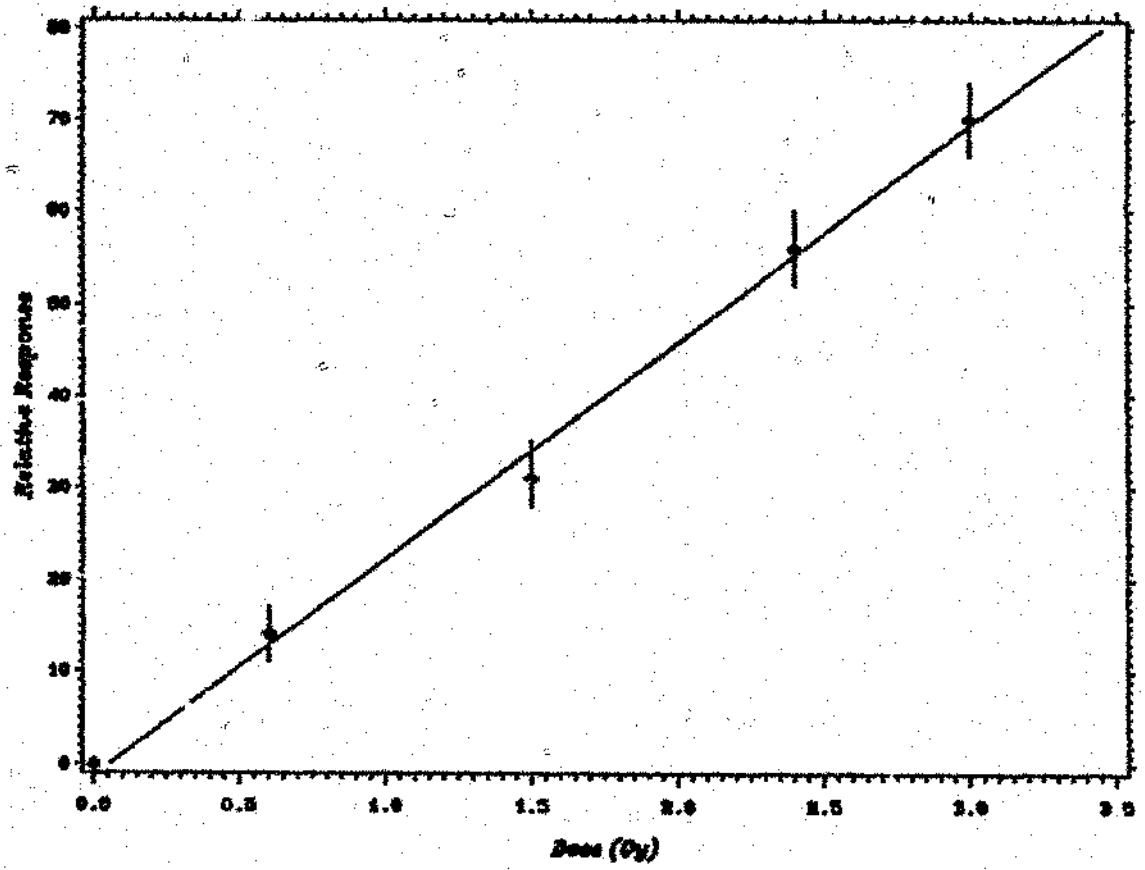

Figure 8.7. Phototransferred yield measured by thermoluminescence as a function of β particle dose delivered from a ^{90}Sr source.

normal thermoluminescence readout cycle, was subsequently illuminated with light of pre-determined wavelength from the Xenon lamp before the final thermoluminescence readout process was initiated. Positive results were obtained when a monochromator setting of [illegible] nm was used in order to make use of the overlapping second order component at 300±10 nm. The second order component had to be used as only monochromator settings in the 350-900 nm range were accessible. Figure 8.7 depicts the intensity of the thermoluminescence signal excited for a fixed radiant exposure with light of 300 nm, after the diamond sensor had been given the range of β doses shown. This behaviour gives an indication of the phototransference and bleaching properties of the deep charge trapping states situated in the forbidden band gap of these diamond. The phototransference of charge carriers is evidenced by the fact that thermally accessible peaks, previously emptied, can be thermally excited. In addition, repeated illuminations of the TLD appreciably decreased the thermoluminescence signal. Such presence of deep charge trapping states provides the possibility for the re-assessment of radiation doses, especially in instances where a second readout is required to confirm or repudiate initial measurements. This formed the motivation for the study of the RPL yield as a function of radiation dose due to excitation with the 296 nm Mercury line.

8.2.5 The Emission Spectrum

In order that a suitable choice of radiophotoluminescence emission response wavelength to light of 404 nm and 296 nm could be made, the emission spectra under excitation from these Mercury lines, were measured in the experimental arrangement of figure 2.7. As an additional requirement two further measurements of the emission spectra were undertaken. The cathodoluminescence spectra of the diamond crystals were measured in the experimental arrangement of figure 2.5 at ambient and liquid nitrogen temperatures in an attempt to excite all possible radiative transitions which can occur

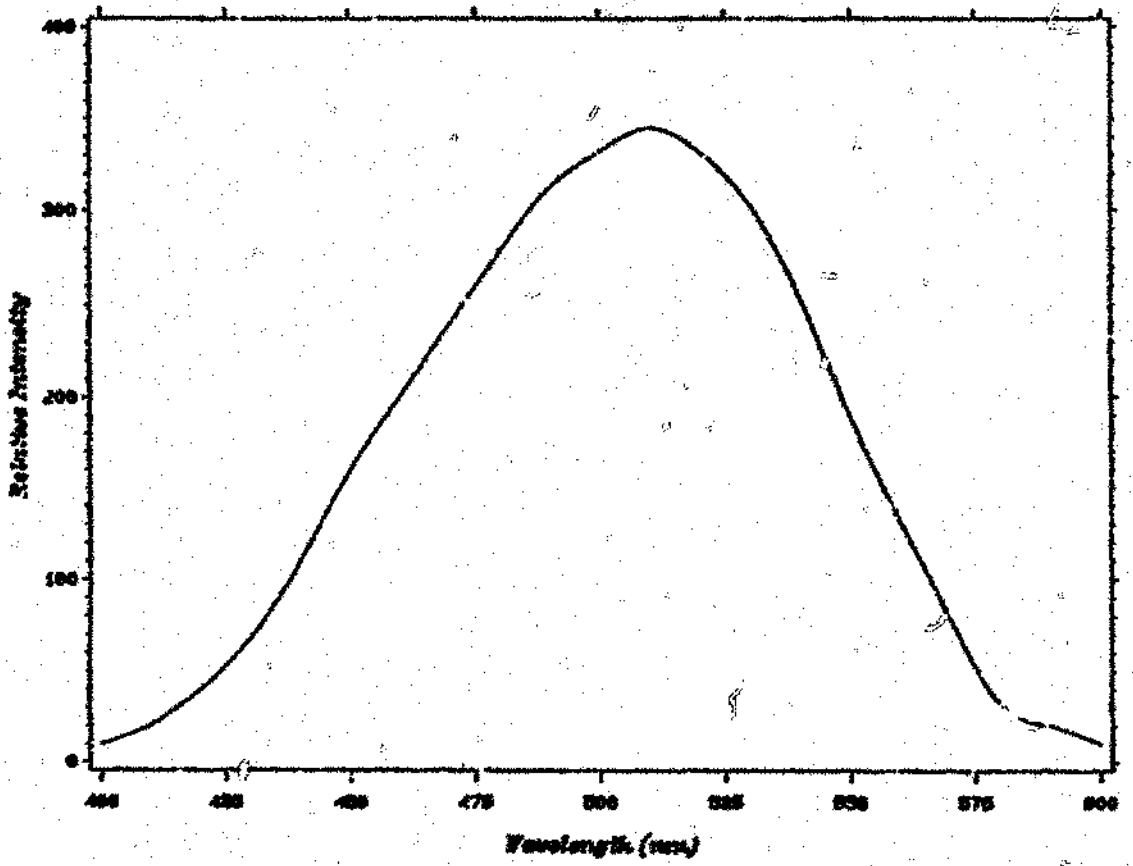

Figure 8.8: A typical emission spectrum of the synthetic TLD diamond.

in these synthetic diamond crystals. For these measurements the probe illustrated in figure 2.8 was used for the housing of the diamond which could then be subjected to electron beam energies ranging in value from 5 keV to 18 keV. The phosphorescence emission spectrum was also determined in the arrangement depicted in figure 2.5, for comparison.

In all emission spectra measurements the final data was derived by folding in the photomultiplier tube response and the relative absorbance response of these diamond in the relevant wavelength region. A typical absorbance spectrum utilised is given in Appendix II. This response was folded in to account for self-absorption of the stimulated light by the diamond crystal which is non-negligible in the ultra-violet end of the spectrum. The physical form of the emission spectra derived was found to be independent of the mode of excitation or temperature in the case where cathodoluminescence was performed at ambient and liquid nitrogen temperatures. Depicted in figure 8.8 is a response typifying the emission spectrum under either of the radiophotoluminescence, cathodoluminescence and phosphorescence excitation modes. This result shows a spectrum having a broad range of emission wavelengths ranging in magnitude from 400 nm to 580 nm with a maximum response at approximately 510 nm. This spectrum is similar to the band A cathodoluminescence reported for Type Ib synthetic diamond crystals (Collins, 1974). The suggested explanation of this spectrum is that it is due to donor-acceptor pair recombination at luminescence centres.

8.3 Results and Discussions

Taking cognizance of the results of the preliminary study, all radiophotoluminescence responses resulting from excitation wavelengths of 404 nm and 296 nm were measured with the bandpass filter closest to the maximum response in the emission spectrum viz. 526±10 nm. These responses are termed RPL-404 and RPL-296, respectively, throughout these discussions.

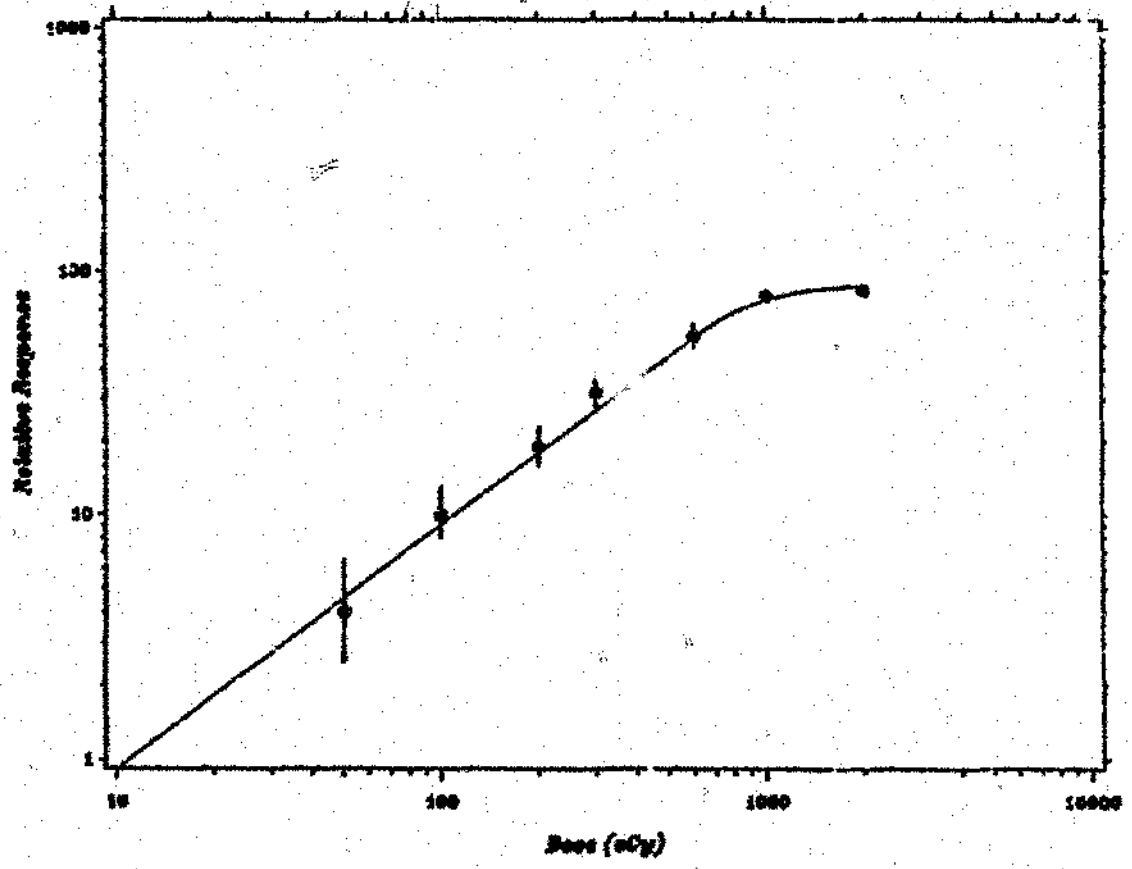

Figure 8.9: Radiophotoluminescence yield at 526 nm due to excitation with the 404.7 nm Mercury line as a function of β radiation dose.

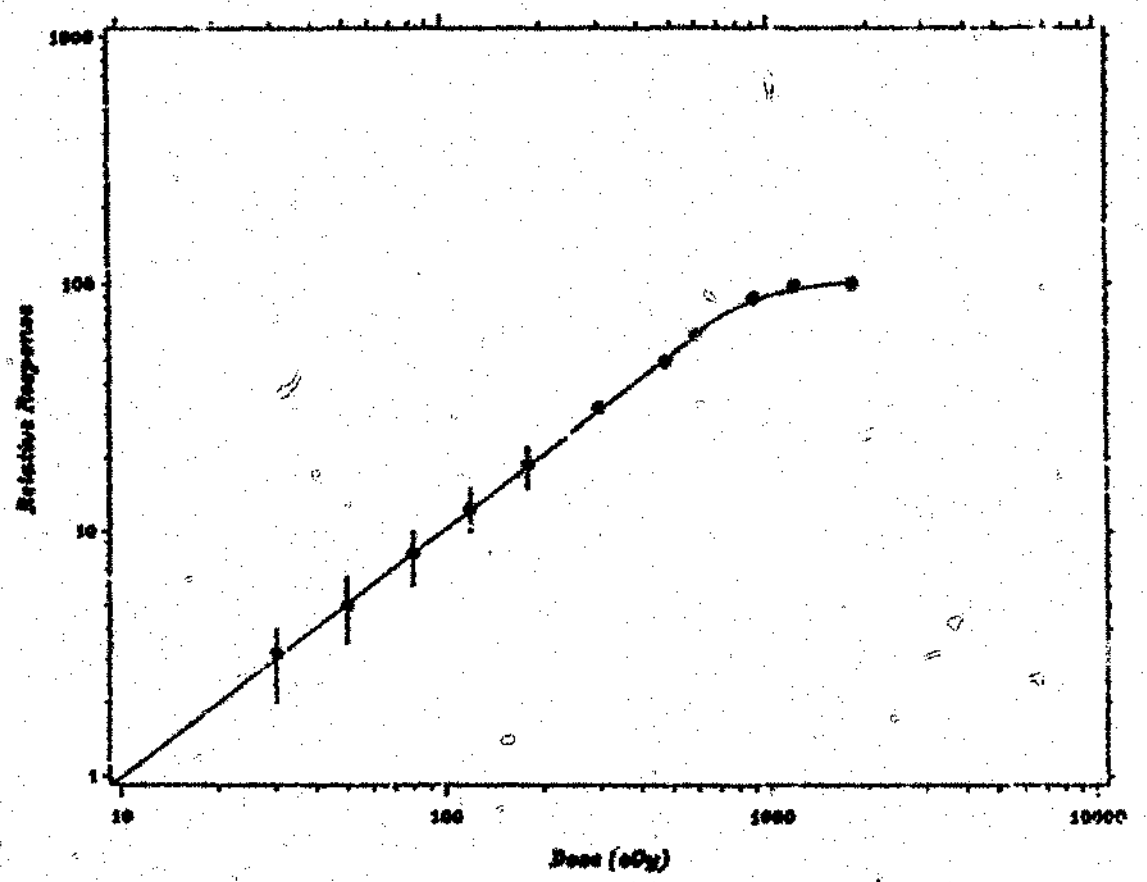

Figure 8.10: Radiophotoluminescence yield at 526 nm due to excitation with the 404.7 nm Mercury line as a function of γ radiation dose.

The results of the 404.7 nm photostimulated emission of the crystals, after ɣ and β pre-exposures is depicted in figures 8.9 and 8.10. The experimental procedure adopted for obtaining these results is as follows:

- The diamond TLD was irradiated by either of the ^{60}Co or the ^{90}Sr sources to the required radiation dose.

- The crystal was then mounted in the experimental arrangement of figure 2.11.

- The radiophotoluminescence yield was then measured after a delay of 10 minutes post-irradiation. This involved measuring the response at [illegible] nm, due to excitation with the 404.7 nm Mercury line, which was selected by an appropriate setting of the monochromator.

In order to exclude second order diffraction components a 320 nm high pass cut-off filter was superimposed at the exit monochromator slit. The introduction of a fixed 10 minute post-irradiation time delay was implemented for all RPL measurements to obviate any time dependent effects such as charge transfer processes. This procedure is justified by the measurements of the fading and build-up properties of the RPL-signal undertaken in the latter part of this study. Prior to the measurement of the RPL dosimetric responses of a given diamond crystal to varying β and ɣ radiations, a measurement of the background signal was made. For this, precautions were taken to ensure that the mounting of the unirradiated diamond crystal was identical to that used for subsequent RPL dose response measurements. The signal measured when the unirradiated diamond crystal was illuminated with the pre-selected wavelength was then taken to be the background signal. The principal component of this background signal is ascribed to the transmission of a small fraction of the excitation radiation that was scattered off the diamond and planchet, through the bandpass filter and on to the photomultiplier tube. The remaining contribution was sourced to intrinsic electronic noise.

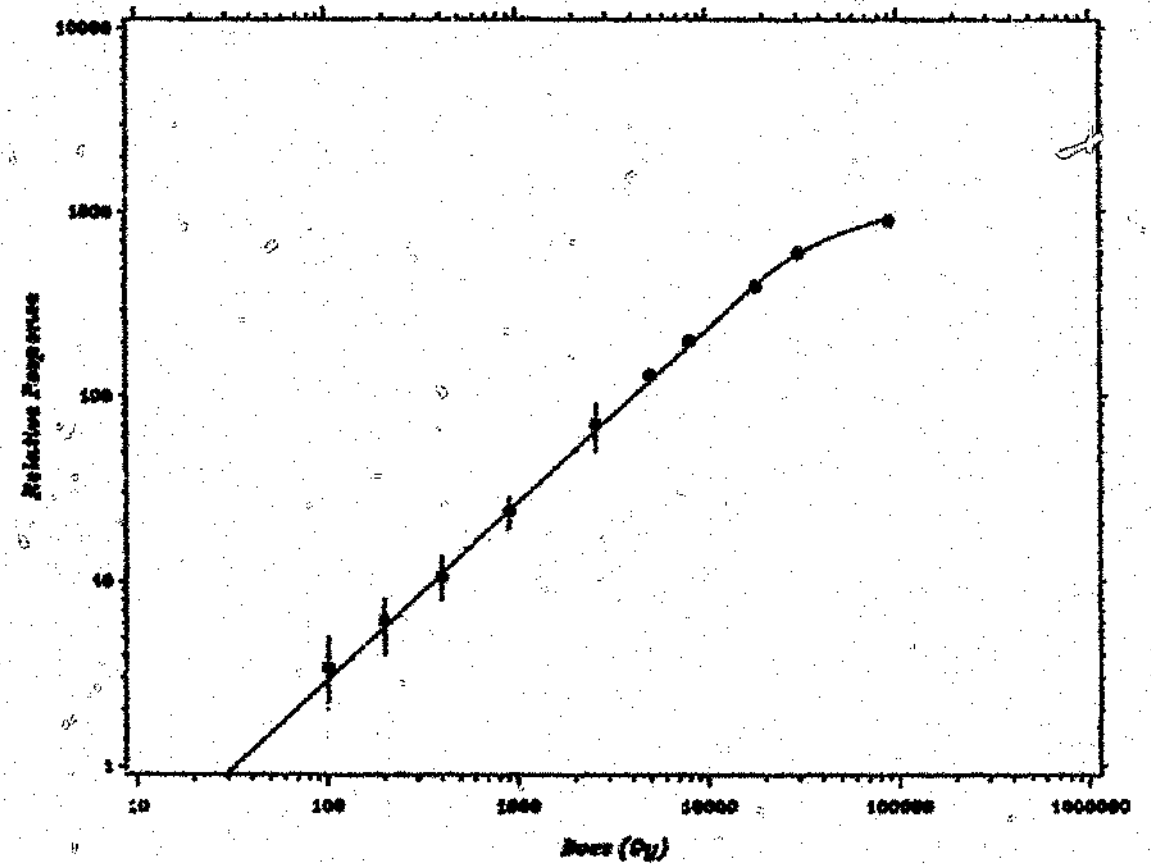

Figure 8.11: Radiophotoluminescence yield at 52[illegible] nm due to excitation with the 296 nm Mercury line as a function of γ radiation dose.

In the experiments involving the use of a custom built ^{60}Co facility (Kerr *et al.*, 1975) for γ irradiations, the dose rates and doses delivered to the samples were varied by changing the sample to source distance and the exposure times respectively. Exposure rates ranging in value from 2 R min^{-1} to 2200 R min^{-1} could be achieved using the system. An absolute calibration of the source exposure rate as a function of the distance from the source centre, using a Farmer Secondary Standard dosemeter, is given in Appendix III.

The relative responses of the diamonds to γ and β radiation doses as depicted in figures 3.9 and 3.10 are very similar in form. Linearity in responses from 0.3 to 10 Gy with saturation effects setting in at doses greater than 10 Gy are typical features. This response is primarily due to the depopulation of the thermally accessible charge trapping states. The same saturation effect at approximately 10 Gy was observed when a normal thermoluminescence readout process was utilized. An uncertainty of approximately 10 % in the dose determination is displayed explicitly on the figures and was derived by averaging a number of values for the RPL-signal.

In the second photostimulated study an excitation wavelength of 296 nm was used. The corresponding emission was again measured in the 526±10 nm region. The experimental procedure adopted for these measurements is as follows:

- The diamond crystal was irradiated at the ^{60}Co facility to high γ doses at an exposure rate of 2200 R min^{-1}.

- The thermally accessible charge trapping states were then bleached by performing a thermoluminescence readout cycle which involved ramping the temperature of the diamond TLD from room temperature to 450°C at 16°C s^{-1}.

- The crystal was then mounted in the experimental arrangement of figure 2.11.

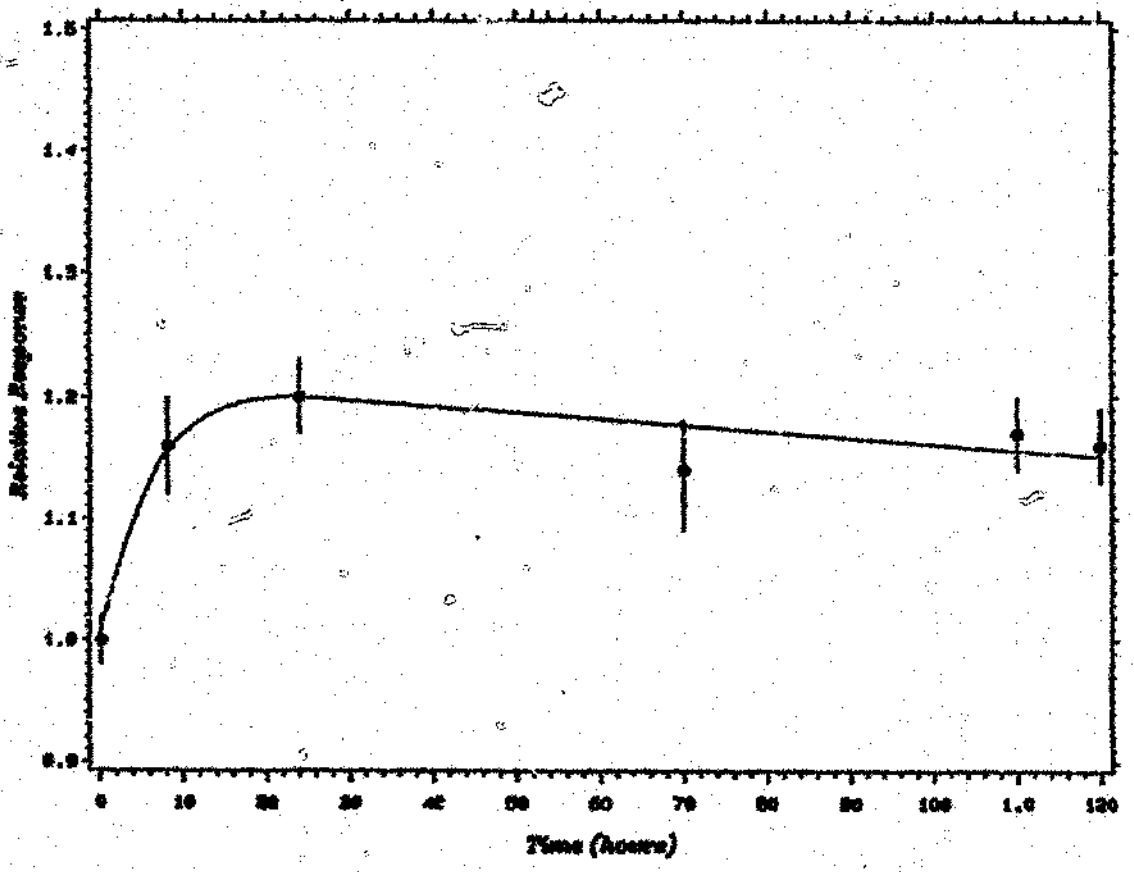

Figure 8.12: Stability characteristics of the 526 nm radiophotoluminescence response of the pre-irradiated diamond as a function of time. The excitation was carried out with the 404.7 nm Mercury line.

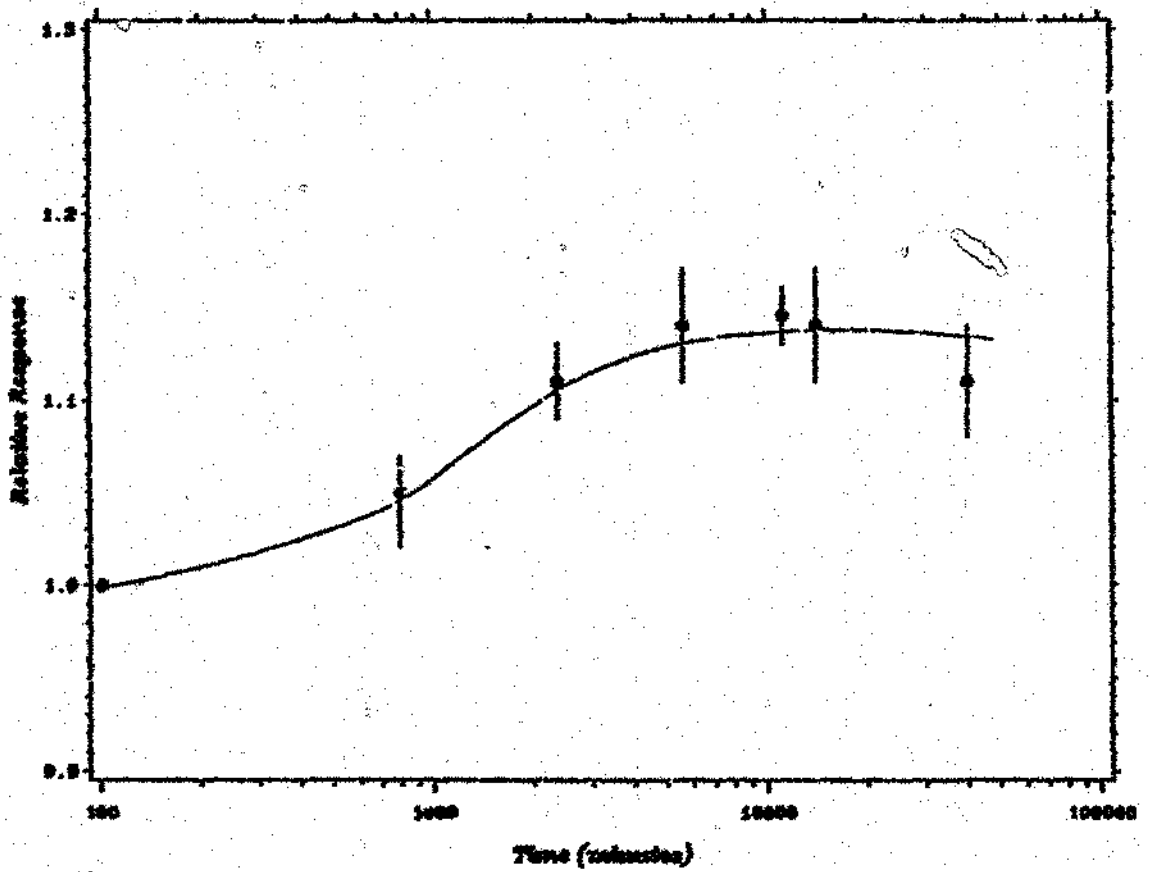

Figure 8.13: The long-term stability of the 526 nm radiophotoluminescence response of the pre-irradiated diamond crystal as a function of time. The excitation wavelength utilised was the 296 nm Mercury line.

- The 526 nm RPL yield obtained, after a delay of 10 minutes post-irradiation, with the 296 nm Mercury line was then measured.

A measurement of the background signal contribution was also carried out for subsequent correction. The result of these measurements is depicted in figure 8.11. It is clear from the figure that a minimum detectable dose of just under 100 Gy was achieved. Use of such a system allowed accurate assessment of radiation doses in the kGy range, with saturation effects only becoming relevant at approximately 20 kGy.

In order to gain further insight into the mechanism of radiophotoluminescence, as well as the usefulness of this technique in radiation dosimetry, two further sets of measurements were undertaken. These were respectively,

- The fading and build-up characteristics of the RPL-404 and RPL-296 signals.

- The bleaching response of the RPL-404 and RPL-296 signals as a function of the illumination dose.

The fading and build-up characteristics for the RPL-404 and RPL-296 are given in figures 8.12 and 8.13, respectively. Each of these measurements were performed on the same diamond crystal at the times following the initial radiation as indicated. These results show the very stable storage characteristics of the TLD diamond. A relatively fast build-up period in the first 10 hours post-irradiation, followed by a period in which the measured values are constant within a small margin, is a characteristic of figure 8.12. In the case of the deep charge trapping states, figure 8.13 also shows a gradual increase in the measured RPL-signal. An increase in signal of approximately 10 % in 24 hours is a typical feature of such measurement. At later times the response is constant to within 5%. Such initial build-ups in the [illegible] signal has been observed in magnesium-activated lithium fluoride (Levita *et al.*, 1976) and silver-activated glass (Schulman *et al.*, 1953)

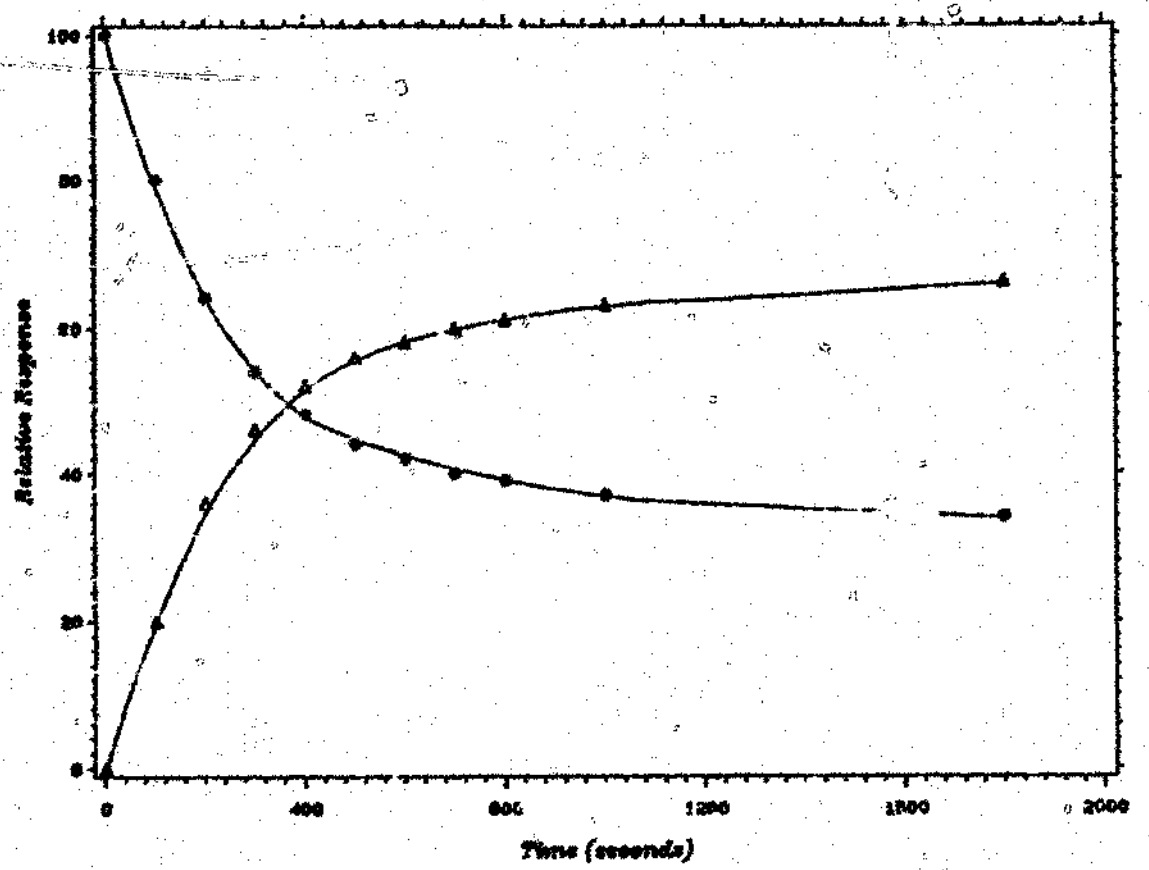

Figure 8.14: The result of optical bleaching of the deep charge trapping states by 236 nm Hg-lamp illumination.

and appears to be a typical feature of RPL time measurements. Solid state kinetic models which have been postulated to interpret such behaviour (Vogel and Becker, 1965) propose a period in which charge transfer processes are dominant factors influencing the observed behaviour. The initial build-up phase as depicted in both figures 8.12 and 8.13 suggest that a similar mechanism, as proposed in current models for other phosphors, occurs in the TLD diamond. This supports the preliminary measurements of the relative density of states performed in Chapter 6 which suggested that charge transfer processes, by a tunnelling mechanism, between defect centres are quite feasible.

The result of bleaching illumination by light of 404.7 nm and 296 nm on the magnitude of the RPL-404 and RPL-296 was also assessed. Depicted in figure 8.14 is the simultaneous measurement of the remnant RPL-signal with sustained 296 nm mercury lamp illumination (●). A reduction of the RPL-signal by approximately 35 % was obtained after a period of 30 minutes illumination. These results underline the conditions under which the RPL-signal may be preserved for later readout procedures. Also shown on the same set of axes, is a complementary function of the remnant RPL-signal viz. the relative bleaching efficiency. The bleaching efficiency is taken to be:

$$(100 - RPL_{remnant})\ \%$$

where $RPL_{remnant}$ is the normalised remnant RPL-signal. This result, depicted by the triangles in the figure, is in many respects similar to the bleaching response of figure 8.4. In particular, a relatively early saturation in the bleaching efficiency is observed. A similar interpretation may therefore apply to the bleaching response of figure 8.14, concerning the effective path length of the excitation light in the diamond crystal.

8.4 Conclusions

It has been shown that, due to deep charge trapping states in the band gap of the synthetic diamond crystal, such crystals demonstrate characteristic radiophotoluminescence responses. These responses include a time response with optical excitation, initiated post-irradiation, consistent with the form of optical bleaching spectra measured by thermoluminescence. The radiophotoluminescence study of the diamond crystals post-γ irradiation al revealed an enhanced high dose dosimetric response. Compared to the 10 Gy maximum measurable dose achievable by the thermoluminescence technique, as opposed to 20 kGy achievable by the radiophotoluminescence technique, a vast improvement in the dosimetric capability of the technique can be claimed for dose measurements in this range.

CHAPTER 9

Conclusions

9.1 Summary of Conclusions

This study has highlighted some of the solid state properties of the synthetic TLD diamond which make these crystals suitable for application as dosimeters in ultraviolet, γ and β radiation fields. Much of the research effort was devoted to properties relating to the phosphorescence decay spectra and the characteristic optical excitation spectra of these crystals.

The investigation of the solid state dosimetric properties of diamond crystals having characteristic thermoluminescence spectra was initiated in Chapter 5. This study yielded accurate and consistent values for empirical parameters such as the thermal activation energy, with the associated frequency factor and kinetic order parameter for the Fe-free synthetic diamond crystals. The estimates of the activation energy derived by initial rise analysis and general order full curve analysis were found to differ in magnitude and these differences were ascribed to the occurrence of a thermal quenching process.

The resolution of the composite glow spectrum of the TLD diamond was accomplished in Chapter 6, taking cognizance of the analysis of Chapter 5. The principal results of this analysis concern the relative density of states for thermally stimulated processes. Thermal activation energies ranging in value from 0.5 to 2.1 eV were derived by the technique of general order curve fitting. The density of the states having such activation energies was found to follow an exponential dependence in the range of values from 0.7 to 1.5 eV. Initial rise analysis undertaken, confirmed the presence of a thermal quenching mechanism for activation energies greater than 1.2 eV for these crystals. These estimates were used in the comparison of optical and thermal activation energies.

Results which further corroborate those obtained in Chapter 6 refer to the isothermal decay spectra measured at elevated temperatures. These measurements

which probe the recombination kinetics of the intermediate charge trapping states and are the subject of Chapter 7, show that the theoretical form of these spectra, viz. proportional to t^{-1}, is consistent with decay from a distribution of levels. Also included in this section is the study of the kinetic parameters describing the decay of luminescence from shallow trapping states which are thermally unstable at ambient temperatures. The well-defined exponential-type decay in conjunction with the favourable temperature dependence of these kinetic parameters suggested a dosimetric application for these crystals in the phosphorescence mode.

An in-depth study of these diamond under optical excitation undertaken in Chapter 8 yielded results which suggested the modality subsequently employed in the radiophotoluminescence study. Important results of this section include the determination of the optical bleaching spectra as a function of radiation wavelength which show that the thermally accessible charge trapping states can be depopulated by light in the UV-visible range. An interpretation of the physical process of optical bleaching has also been provided in the determination of the bleaching response as a function of illumination exposure at 375 nm. The theoretical form describing the recombination of charge carriers, previously liberated by optical means, locally at luminescence centres (as is the case in first order processes) was demonstrated to be qualitatively similar to the measured response. The establishment of phototransference of charge to thermally accessible charge trapping states in these diamond provided a further means of probing the properties of deeper, thermally inaccessible charge trapping states. A linear response describing charge carriers transferred optically and measured by thermoluminescence as a function of β radiation dose, was achieved when an excitation wavelength of 296 nm was used. This motivated a detailed study of these deep charge trapping states by the radiophotoluminescence technique. Ancillary to this part of the study is the ratio of E_{opt}/E_{max} which was determined to be 1.5. This supported the postulate that these diamond crystals fall into the class of Stokes-type phosphors.

The main result of Chapter 8 relates to the dose response of the synthetic diamond crystals to radiation dose when the readout was effected by optical means. The radiophotoluminescence dose response measurement undertaken at an excitation wavelength of 304 nm exhibits a response to γ and β dose which is linear in the dose range less than 10 Gy and is similar to the thermoluminescence dose response. The radiophotoluminescence dose response obtained when optical stimulation at 296 nm was effected showed a marked enhancement in the maximum dose measurable. In this mode, γ radiation doses up to 20 kGy were linearly measured. The illumination bleaching response of the charge trapping states also displayed a dependence on the radiant exposure which was very similar to those undertaken for the thermally accessible charge trapping states at 375 nm, therefore suggesting a similar mechanism for optical excitation and subsequent radiative recombination.

9.2 Ideas for Future Research

Investigations initiated for the fulfilment of this dissertation and which appear promising for future research include the development of a dosimetric system based on the radiophosphorescent properties of the synthetic diamond. Such a system would incorporate a small diamond crystal attached to a thin optical fibre for measurement of radiation fields *in situ* and *in vivo*. The luminescence from the diamond can be either measured directly or stored for subsequent computational analysis.

The completion of the measurement of the absolute response of the diamond crystal under ultraviolet exposure to wavelengths shorter than 250 nm could suggest useful fields of application. This latter-mentioned aspect is prescribed by the maximum absolute exposure which results in saturation of the thermally accessible charge trapping states. A possible feature which could be utilised to extend the range of dosimetric exposures of these crystals, refers to the use of the phototransference phenomenon. By priming the diamond crystal with a large γ pre-exposure dose and subsequently emptying the thermally accessible charge trapping states by a normal thermoluminescence

readout, the remaining activated deep charge trapping states could be utilised for dosimetry. Radiant exposure from incident light in the 300 nm wavelength region could then be measured by the phototransference of deep charge carriers to the shallower, thermally accessible charge trapping states. Such a measurement would be based on the final response derived by means of a normal thermoluminescence readout process.

Appendix I

The non-linear set of equations to be solved for the parameters describing the glow curve, after Horowitz *et al.* (1986), are given by:

$$\sum_{k=1}^{n} \epsilon_k \exp\{1 + W(x_k - x_0) - \exp(W(x_k - x_0))\} = \sum_{k=1}^{n} \epsilon_k \frac{P^k}{I_m} = 0 \qquad (I.1)$$

$$\sum_{k=1}^{n} \epsilon_k (x_k - x_0)\{1 - \exp\{W(x_k - x_0)\}\} P^k = 0 \qquad (I.2)$$

$$\sum_{k=1}^{n} \epsilon_k W\{\exp\{W(x_k - x_0)\} - 1\} P^k = 0 \qquad (I.3)$$

$$\epsilon_k = P^k - Y^k_{exp} \quad \text{is the residual}$$

All the variables above are as defined in the text of Chapter 5. This defines a set of three non-linear equations *in* three unknowns, viz. I_m, W and x_0, which can be solved by the Levenburg-Marquardt algorithm, given the data set $(x_k; Y^k_{exp})$.

Appendix II

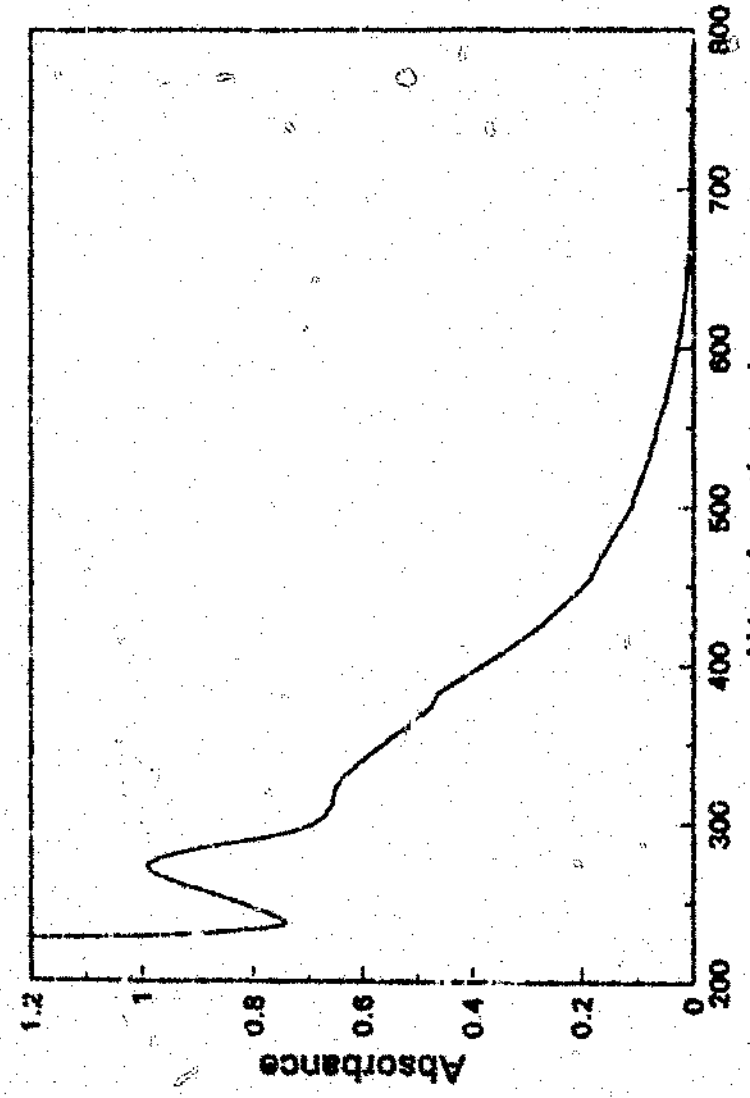

A typical optical absorbance spectrum of the TLD diamond of low nitrogen concentration.

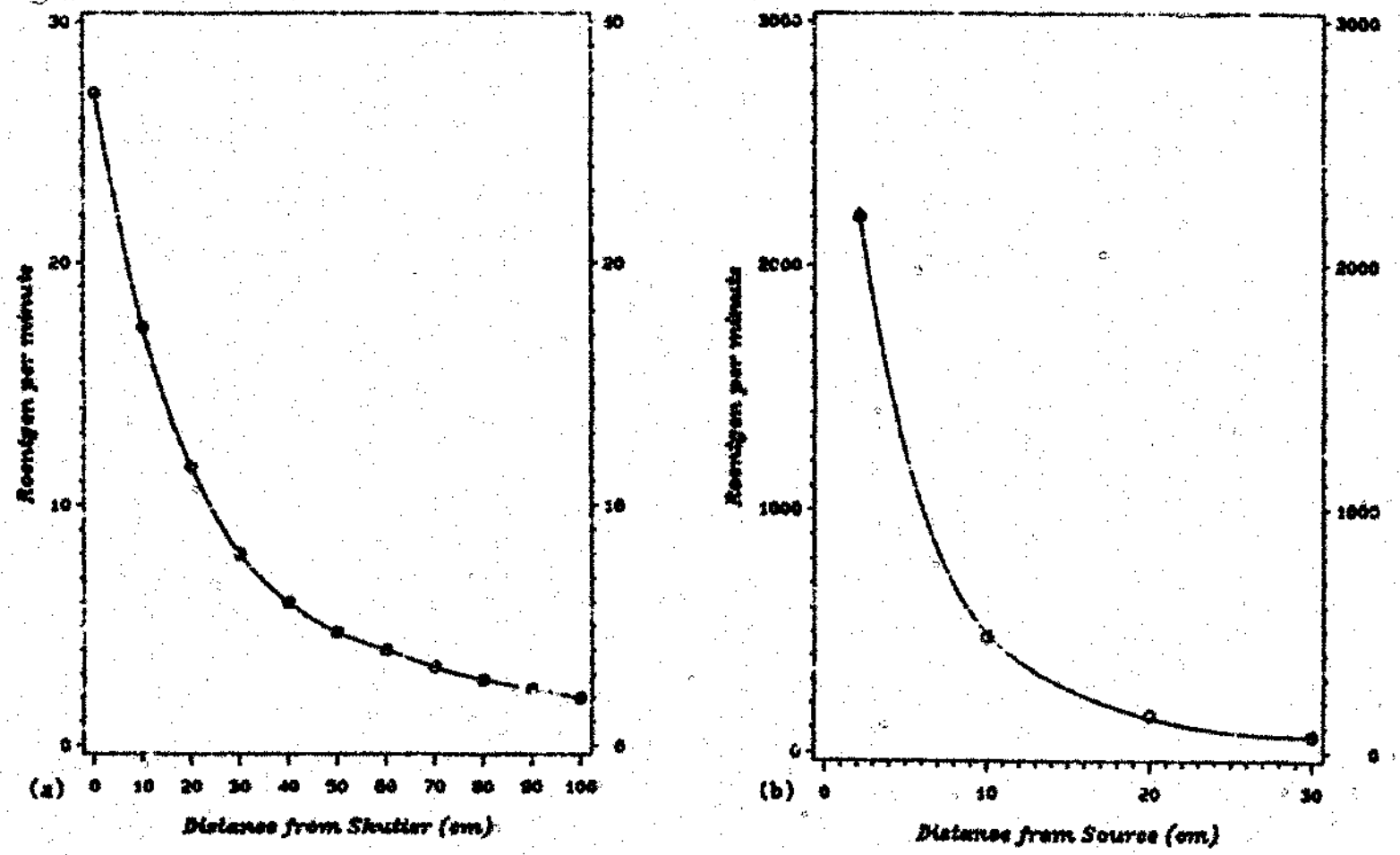

The ^{60}Co calibration curves acquired on the 15/01/92. (a) The dose rates attainable when the source is in the withdrawn position. (b) The dose rate attainable when the source is out of the enclosure. (cf Kerr *et al.*, 1975)

Appendix IV

Papers presented at Conferences

S. Araikum, T. L. Nam and R. J. Keddy, "Dosimetry Based on the Photostimulated Luminescence of Diamond" 32nd Annual Congress of SAAPMB, Midrand 11-13 March 1992

S. Araikum, T. L. Nam and R. J. Keddy, "Radiophotoluminescence Response of Synthetic Diamond to High Radiation Dose" SAIP Conference, Johannesburg, 1-3 July 1992

S. Araikum, T. L. Nam and R. J. Keddy, "Thermally and Optically Stimulated Luminescence in Synthetic Diamond" Diamond Conference, Cambridge, 5-8 July 1992

S. Araikum, T. L. Nam and R. J. Keddy, "Radiation Dosimetry Based on the Radiophosphorescence of Synthetic Diamond" 33rd Annual Congress of SAAPMB, Bloemfontein, 8-10 March 1993

S. Araikum, T. L. Nam and R. J. Keddy, "Radiation Dosimetry via the Radiophotoluminescence of Synthetic Diamond" Materials Research Society Conference, San Francisco, 12-16 April 1993

Patents

B. L. Jones, T. L. Nam, S. Araikum and R. J. Keddy, "Radiation Probe", U. K. Patent Application No. 92/05458, 1992

T. L. Nam, S. Araikum and R. J. Keddy, "Diamond Phosphorescence Probe", Provisional Patent Application No. 93/1478, 1993

Papers for Publication

S. Araikum, T. L. Nam and R. J. Keddy, "Radiation Dosimetry Based on the Radio-photoluminescence of Synthetic Diamond", Accepted for publication in Radiation Physics and Chemistry, 1993

References

Adirowitch E. I. (1956) *J. Phys. Rad.* 17, 1705

Avouris Ph. and Morgan T. N. (1981) *J. Chem. Phys.* 74, 4347

Boyle R. (1663) *Register of the Roy. Soc.* 213

Bull C. and Garlick G. F. J. (1950) *Proc. Phys. Soc. Lond.* 63, 1283

Chen R. (1969a) *J. Appl. Phys.* 40, 570

Chen R. (1969b) *J. Electrochem. Soc.* 116, 1254

Chen R., Israeli M. and Kristianpoller N. (1970) *Chem. Phys. Lett.* 7, (2), 171

Chen R. and Kirsh Y. (1981) *Analysis of thermally stimulated processes* Pergamon Press, Oxford

Chen R., Kristianpoller N., Davidson Z. and Visocekas R. (1981) *J. Lumin.* 23, 293

Collins A. T. (1974) *Industrial Diamond Review* 34, 131

Curie M. (1904) *Radioactive substances* (English translation of doctoral thesis presented to the Faculty of Science, Paris) Greenwood Press, Westpoint (1961)

Daniels F., Boyd C. A. and Saunders D. F. (1953) *Science* 117, 343

Fillard J. P., Gasiot J. and Manifacier J. C. (1978) *Phys. Rev.* B18, 4497

Garlick G. F. J. and Gibson A. F. (1948) *Proc. Phys. Soc.* 60, 574

Gobrecht H. and Hofmann D. (1966) *J. Phys. Chem. Sol.* 27, 509

Halperin A. and Braner A. A. (1960) *Phys. Rev.* 117, 408

Halperin A., Braner A. A., Ben-Zvi A. and Kristianpoller N. (1960) *Phys. Rev.* 117, 416

Hildebrand F. B. (1956) *Introduction to Numerical Analysis* McGraw-Hill, New York, p.379

Horowitz Y. S., Moscovitch M. and Wilt M. (1986) *Nucl. Instr. Meth.* A244, 556

IMSL MATH LIBRARY (1987) *Non-linear Equations* 776

Israeli M. and Kristianpoller N. (1971) *Phys. Stat. Sol.* B45, K29

Johnson P. D. and Williams F. E. (1952) *J. Chem. Phys.* 20, 124

Jorge M., Garbow B. and Hillstrom K. (1980) *User Guide for MINPACK-1*, Argonne National Labs Report ANL, Argonne, Illinois

Kaiser W. and Bond W. L. (1959) *Phys. Rev.* 107, 966

Keddy R. J., Nam T. L. and Burns R. C. (1987) *Phys. Med. Biol.* 32, (6), 751

Kerr D. S. M., Sellschop J. P. F., Keddy R. J. and Nam T. L. (1975) *Int. J. Appl. Radiat. Isot.* 26, 533

Kittel C. (1986) *Introduction to Solid State Physics* John Wiley & Sons, New York

Kivits P. and Hagebeuk H. J. L. (1977) *J. Lumin.* 15, 1

Lakshmanan A. R., Chandra B. and Bhatt R. C. (1978) *Nucl. Instrum. Meth.* 153, 581

Levita M., Schlesinger T. and Friedland S. S. (1976) *IEEE Transactions on Nuclear Science* NS-23, 1

Levy P. W. (1979) *PACT* 3, 466

Marquardt D. (1963) *SIAM Journal on Applied Mathematics* 11, 431

May C. E. and Partridge J. A. (1964) *J. Chem. Phys* 40, 1401

McKeever S. W. S. (1985) *Thermoluminescence of Solids* Cambridge University Press, Cambridge

Medlin W. L. (1961a) *Phys. Rev.* 122, (3), 837

Medlin W. L. (1961b) *Phys. Rev.* 123, (2), 502

Mehta S. K. and Sengupta S. (1978) *Phys. Med. Biol.* 23, 471

Nahum J. and Halperin A. (1963) *J. Phys. Chem. Solids* 24, 823

Nam T. L., Karfunkel U., Keddy R. J. and Every A. G. (1991) *Radiation Effects and Defects in Solids* 116, 233

Nicholas K. H. and Woods J. (1964) *Br. J. Appl. Phys.* 15, 783

Randall J. T. and Wilkins M. H. F. (1945a) *Proc. Roy. Soc. Lond.* 184, 366

Randall J. T. and Wilkins M. H. F. (1945b) *Proc. Roy. Soc. Lond.* 184, 390

Schulman J. H., Schurchiff W., Ginther R. J. and Attix F. H. (1953) *Nucleonics* 11, (10), 52

Seitz F. (1938) *J. Chem. Phys.* 6, 150

Shenker D. and Chen R. (1972) *J. Comput. Phys.* 10, 272

Simon W. (1970) *Phys. Med. Biol.* 15, (2), 355

Sunta C. M. and Bapat V. N. (1982) *PACT* 6, 252

Thorn G. W , Adams R. D., Braunwald E., Isselbacher K. J. and Peterdorf R. G. (1977) *Harrison's Principles of Internal Medicine* (8th*Ed.*) McGraw-Hill, Tokyo, p.53

Wiedemann E. and Schmidt G. C. (1895) *Ann. Phys. Chem. Nueue Folge* 54, 604

Wintle A. G. (1975) *Geophys. J. Roy. Astr. Soc.* 41, 107

Author: Araikum Shawn.
Name of thesis: Thermally and optically stimulated luminescence in synthetic diamond.

PUBLISHER:
University of the Witwatersrand, Johannesburg
©2015

LEGALNOTICES:

Copyright Notice: All materials on the University of the Witwatersrand, Johannesburg Library website are protected by South African copyright law and may not be distributed, transmitted, displayed or otherwise published in any format, without the prior written permission of the copyright owner.

Disclaimer and Terms of Use: Provided that you maintain all copyright and other notices contained therein, you may download material (one machine readable copy and one print copy per page)for your personal and/or educational non-commercial use only.

The University of the Witwatersrand, Johannesburg, is not responsible for any errors or omissions and excludes any and all liability for any errors in or omissions from the information on the Library website.